Príprava a vlastnosti progresívnych keramických materiálov

odborný seminár

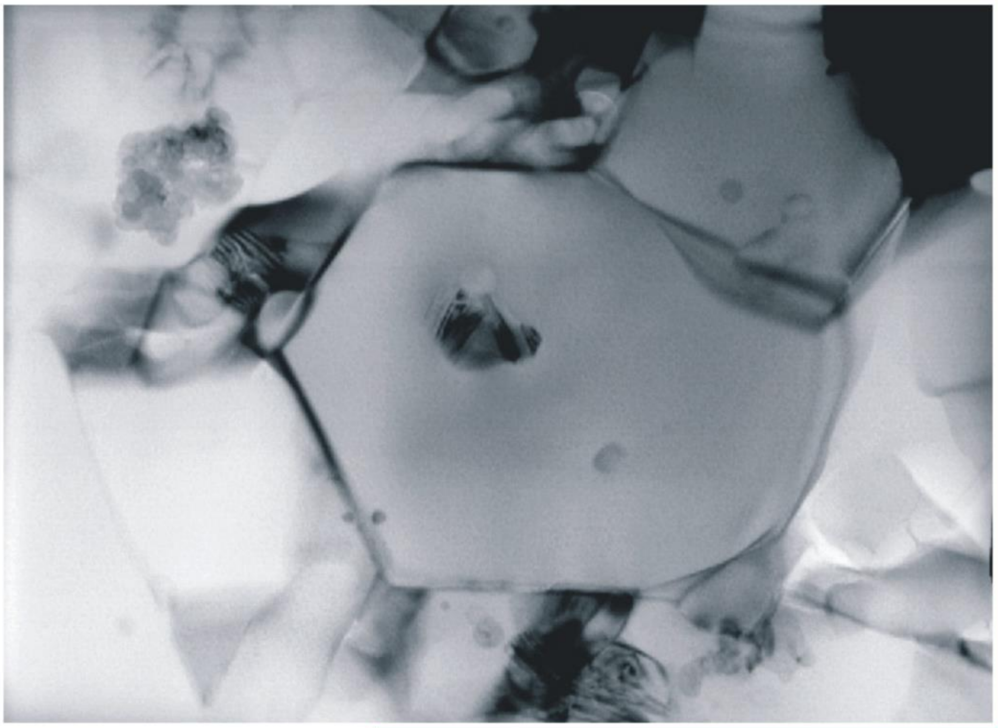

zborník rozšírených abstraktov

18.-19. november, 2013
Ružín, Slovensko

USPORIADATELIA

Ústav anorganickej chémie Slovenská akadémia vied

Slovenská silikátová vedecko-technická spoločnosť

Odborní garanti

prof. Pavol Šajgalík, RNDr., DrSc.
prof. Ján Dusza, RNDr., DrSc.
doc. Dušan Galusek, PhD.

Organizačný výbor

doc. Miroslav Hnatko, PhD.
Anna Jurová - SSiVTS

Termín konania: 18. – 19. November 2013

Miesto konania: penzión Lesanka na Ružíne pri Košiciach

Edited by: Jana Valúchová

ISBN 978-80-971499-4-9

PREDSLOV

Pokročilé keramické materiály sú triedou materiálov, ktoré nachádzajú stále viac aplikácií v priemyselnej praxi. Nie sú to len ich výnimočné mechanické vlastnosti, ktoré ich predurčujú na použitie v strojárskych aplikáciách, ale čoraz viac sa využívajú ich fyzikálne vlastnosti. Sú to predovšetkým optické, elektrické a tepelné vlastnosti, ktoré sa dosahujú manipulovaním štruktúry samotných bazálnych zlúčenín alebo modifikovaním mikroštruktúry keramických telies z nich zložených.

Pracovníci Oddelenia konštrukčnej keramiky Ústavu materiálového výskumu SAV v Košiciach, pracovníci Spoločného pracoviska VILA Ústavu anorganickej chémie SAV, Fakulty chemickej a potravinárskej technológie STU a Trenčianskej univerzity Alexandra Dubčeka v Trenčíne a pracovníci Oddelenia keramiky Ústavu anorganickej chémie SAV sa stretli v penzióne Lesanka, Ružín už po piaty raz. Vzájomne sa informovali o dosiahnutých výsledkoch výskumu od posledného stretnutia a vypočuli si prezentácie, predovšetkým doktorandov, ktorí sú vychovávaní na týchto pracoviskách. Úroveň prezentácií bola vysoká a v diskusii odzneli námety na budúcu spoluprácu týchto skupín.

Komplementarita všetkých troch skupín týkajúca sa návrhu zloženia a prípravy materiálov ako aj merania ich vlastností sa pri vhodnej spätnej väzbe prejavuje v synergii dosiahnutých výsledkov. Takýmto iteračným cyklom a vzájomným ovplyvňovaním sa jednotlivých skupín boli pripravené mnohé materiály s vynikajúcimi vlastnosťami a vzniklo mnoho kvalitných prác publikovaných v špičkových časopisoch alebo prezentovaných na najvýznamnejších podujatiach na svete z oblasti keramických materiálov.

Tohtoročnej konferencie sa zúčastnilo 30 účastníkov a prezentovalo svoje výsledky v 18 orálnych vystúpeniach.

prof. RNDr. Pavol Šajgalík, DrSc.

OBSAH

OBSAH

OPOTREBENIE KOMPOZITOV Si_3N_4/GRAFÉN PRI IZBOVEJ A ZVÝŠENÝCH TEPLOTÁCH

WEAR DAMAGE OF SI_3N_4/GRAPHENE COMPOSITES AT ROOM AND ELEVATED TEMPERATURES

Ján Balko[1], Pavol Hvizdoš[1], Csaba Balázsi[2]

1Ústav materiálového výskumu, Slovenská akadémia vied, Košice, SK

2Bay Zoltán Nonprofit Ltd for Applied Research, Institute for Materials Science and Technology, Budapest, HU

ABSTRACT

Tribological properties such as coefficient of friction and wear rate of silicon nitride based composites with admixed two kinds of graphene platelets are measured by pin-on-disc technique in dry sliding conditions. The wear tracks are observed by scanning electron microscopy and mechanisms of wear and damage are identified. It is shown that addition of carbon phases does not lower the coefficient of friction. Graphene platelets seem to be integrated into the matrix very strongly and they do not participate in lubricating processes. Their presence in higher volume fractions leads to reduced wear rates. The best performance at room temperature offer materials with 3wt% of graphene platelets, which have the highest wear resistance due to enhanced fracture toughness. With increasing temperature, particularly above 500°C wear rates increase.

Keywords: *friction coefficient, wear rate, silicon nitride, graphene multilayers*

ÚVOD

Materiály na báze nitridu kremičitého boli vyvinuté ako materiály pre vysoko teplotné aplikácie z dôvodu jeho vysokej pevnosti a húževnatosti pri zvýšených teplotách [1]. V posledných desaťročiach boli študované spôsoby ako znížiť krehkosť a zvýšiť húževnatosť týchto materiálov. V poslednom období boli dosiahnuté určité úspechy prídavkom grafénových multivrstiev[2]. Do dnešného obdobia však existuje málo štúdií ktoré by sa zaoberali tribológiou týchto materiálov, z pohľadu koeficientu trenia a špecifického opotrebenia. Cieľom tohto príspevku je preskúmať vplyv prídavku rôznych druhov grafénových platničiek na tribologické správanie a mechanizmy poškodenia kompozitov s matricou Si_3N_4.

EXPERIMENTÁLNA ČASŤ

Experimentálny materiál bol vyrobený v MFA Budapešť a jeho základ tvorí zmes komerčne dostupných práškov: Si_3N_4 (Ube , SN - ESP) s 6 % Y_2O_3 (HC Starck , trieda C) a 4 % Al_2O_3 (Alcoa , A16), ktoré boli použité ako spekacie prísady. Ako prídavky grafénu boli použité dva komerčne dostupné prášky: xGnP-M-5 – veľkosť častice 5μm (výrobca xG Sciences), Angstron N006-010-P – veľkosť častice 14 μm. Práškové zmesi boli zmiešané s grafénom a spoločne mleté. Následne boli spekané metódou žiarového izostatického lisovania (HIP) po dobu 3h pri tlaku 20MPa a teplote 1700 °C[3]. Označenie a mechanické vlastnosti materiálov sú v tabuľke 1.

Tabuľka 1 Označenie a základné mechanické vlastnosti materiálov[4]

Materiál	wt% C	Typ grafénu	HV5 [GPa]	K_{IC} [$MPa.m^{-1/2}$]	Označenie
Si_3N_4	0	----	15.4 ± 0.4	6.9 ± 0.4	M
Si_3N_4+ x5μm	1	graphene - xG5μm	14.6 ± 0.2	7.8 ± 0.4	1G
Si_3N_4+1Angstron	1	graphene - Angstron	14.6 ± 0.6	8.9 ± 0.4	1A
Si_3N_4+ x5μm	3	graphene - xGn5μm	7.7 ± 0.1		3G
Si_3N_4+3Angstron	3	graphene - Angstron	8.1 ± 0.2		3A

Tribologické merania boli realizované na zariadení High Temperature Tribometer THT (CSM instruments) metódou ball-on-dics pri nasledujúcich podmienkach: dráha 300 m, rýchlosť 0,1 m/s, zaťaženie 5 N, guľôčka Si_3N_4 s priemerom 6 mm (Spheric Trafalgar Ltd.). Testy boli vykonané pri teplotách: 25, 300, 500, 700 °C, na vzduchu.

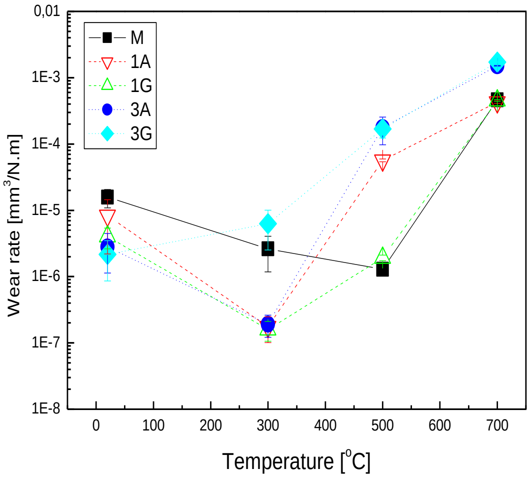

Obr. 1 Špecifické opotrebenie pri rôznych teplotách.

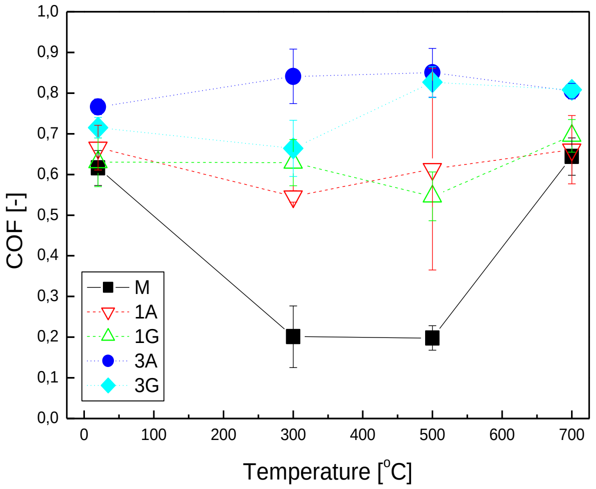

Obr. 2 Koeficient trenia pri rôznych teplotách.

Na obr. 1 je znázornený teplotný priebeh špecifického opotrebenia. Materiál 3G ukázal závislosť rastúceho opotrebenia s teplotou. U ostatných materiálov špecifické opotrebenie rástlo od teploty 300 °C. EDX analýzy potvrdili zvýšený obsah kyslíka v povrchových vrstvách. To naznačuje vznik vrstvy oxidov kremíka v zóne kontaktu. V prípade monolitného materiálu to viedlo k zníženiu koeficientu trenia v teplotnom intervale 300 – 500 °C až na hodnoty blízke 0,2. Na obr. 2 je znázornená teplotná závislosť koeficientov trenia. Koeficient trenia materiálov s prídavkom 1% grafénu sa pohybuje v intervale 0,6 – 0,7. U materiálov 3% prídavkom 0,7 – 0,8.

ZÁVER

Z nameraných hodnôt koeficientu trenia vyplýva, že prídavok grafénových multivrstiev neprispieva k jeho zníženiu. Pri meraniach vykonávaných pri teplote 700 °C podiel grafénu klesol a teda aj koeficienty trenia kompozitov sú veľmi podobné referenčnému monolitu. Špecifické opotrebenie je pri izbovej teplote podobné pre všetky materiály a má stúpajúcu tendenciu s rastom teploty z dôvodu postupného oslabovania štruktúry.

POĎAKOVANIE

Práca bola realizovaná s podporou projektov NanoCEXmat II: ITMS No: 26220120035; NanoCEXmat I: ITMS No: 26220120019; a CEKSIM: ITMS No: 26220120056; ktoré sú podporované z Operačného programu "Výskum a vývoj" financovaný prostredníctvom Európskeho fondu regionálneho rozvoja a projektu APVV s číslom 0161-11.

LITERATÚRA

[1] Riley F.L.: Silicon Nitride and Related Materials, Journal of the American Ceramics Society, 83, 245-65 (2000).
[2] Jones M.I., Hyuga H. Hirao K., Yamauchi Y.: Tribology of silicon based nitride ceramics, Journal of the Australian Ceramic Society, 48(1), 21-37 (2012).
[3] Balázsi C.: Silicon Nitride Composites with Different Nanocarbon Additives, Journal of the Korean Ceramic Society, 49(4), 352-362 (2012).
[4] Kvetková L., Duszová A., Hvizdoš P., Dusza J., Kun P., Balázsi C.: Fracture toughness and toughening mechanisms in graphene platelet reinforced Si3N4 composites, Scripta Materialia 66, 793– 796 (2012)

VPLYV ORIENTÁCIE ZŔN NA ICH TVRDOSŤ V SYSTÉME WC-9CO

EFFECT OF GRAIN ORIENTATION ON THEIR HARDNESS IN WC-9CO SYSTEM

Marek Bľanda[1,2]*, Tamás Csanádi*[1]*, Annamária Duszová*[1]*, Pavol Hvizdoš*[1]*, Ján Dusza*[1]*,*
Marek Faryna[3]*, Jerzy Morgiel*[3]

1 Ústav materiálového výskumu, Slovenská akadémie vied, Watsonova 47, 040 01 Košice, SK

2 Materiálovotechnologická fakulta STU v Trnave, Bottova 25, 917 02 Trnava, SK

3 Institute of Metallurgy and Materials Science of Polish Academy of Sciences, Reymonta 25, 30 059 Krakow, PL

ABSTRACT

The mechanical properties of WC-9Co hardmetal were investigated by nanoindentation method. The crystallographic orientation of WC grains was investigated using EBSD analyses. Grains with basal and prismatic planes on the polished surface were identified. Indentation tests were performed with maximum applied load of 10 mN to determine the hardness values. Their evaluation was performed according to Oliver&Pharr method. The results deriving from nanoindentation test show significantly higher hardness on basal planes ($H_{IT}=37 \pm 2.1$ GPa) than the prismatic planes ($H_{IT}=27 \pm 2.4$ GPa) and of binder phase ($H_{IT}=7 \pm 1.4$ GPa).

Keywords: *nanoindentation, hardness, grain orientation, basal and prismatic planes*

ÚVOD

Spekané karbidy majú široké uplatnenie v priemysle hlavne ako rezné nástroje. Je to dôsledok ich výborných mechanických vlastností, hlavne vysokou pevnosťou, tvrdosťou a dobrou oteruvzdornosťou. Najčastejšie používaným pojivom pre spekané karbidy je kobalt v rôznych objemových podieloch. Zrná karbidu volfrámu majú hexagonálnu štruktúru, kde bazálne roviny majú obyčajne tvar zrezaného trojuholníka a prizmatické roviny sú charakteristické obdĺžnikovým alebo štvorcovým tvarom (Obr. 1). To priviedlo niektorých autorov [1-5] k štúdiu mechanických vlastností v závislosti od orientácie WC zŕn. Následné indentačné štúdie potvrdili výrazný vplyv orientácie zŕn na mechanické vlastnosti WC zŕn. Vo väčšine prípadov sa ukazuje, že bazálne orientované WC zrná majú výrazne vyššiu tvrdosť ako prizmaticky orientované zrná [2-5], avšak výsledky niektorých autorov [1] viedli k opačnému záveru.

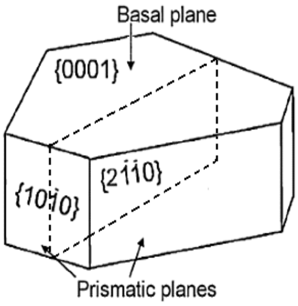

Obr. 1 Bazálne a prizmaticky orientované roviny WC zrna

Našim cieľom bolo tento fakt preskúmať, prispieť k potvrdeniu toho či onoho záveru. Ďalším cieľom bolo zmapovať zmenu mechanických vlastností v závislosti od postupnej zmeny orientácie WC zŕn od bazálnej k prizmatickej.

EXPERIMENT

Pre tento experiment bol vybraný spekaný karbid s 9 % objemovým prídavkom kobaltu (WC-9Co). Výrobca uvádza veľkosť zŕn 3 – 25 µm a tvrdosť 9,82 GPa (zaťaženie 30 Kg).

Povrch vzorky bol pripravený leštením. Finálna fáza leštenia bola realizovaná vibračným leštením (dosiahnutá drsnosť < 5 nm) a následne bola vykoná EBSD analýza rastrovacím elektrónovým mikroskopom (Philips XL 30) na IMMS v Krakove. Na EBSD analýzu boli vybrané štyri oblasti na vzorke. Nanoindentačné meranie bolo realizované za použitia Nanoindentoru Agilent G200 v štandardnom móde zaťaženie-odľahčenie s Berkovičovým typom indentoru. Pred meraním sme si vybrali jednu oblasť na vzorke, kde bola vykonaná EBSD analýza a vytvorili sme v tejto oblasti matricu 20x20 vpichov s maximálnym zaťažením 10 mN, rýchlosťou zaťaženia 20 mN/min a výdržou 5 s na maximálnom zaťažení.

VÝSLEDKY A DISKUSIA

Výsledky hodnôt tvrdosti zo všetkých 400 vpichov sú uvedené na Obr. 2. Štatisticky sme dostali veľmi veľký rozptyl hodnôt tvrdosti od 5 GPa až po 38 GPa. Z toho grafu nie je možné určiť akú tvrdosť majú typické bazálne a prizmaticky orientované roviny.

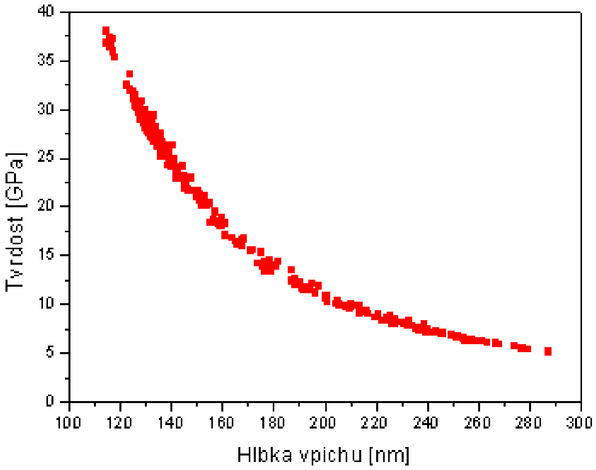

Obr. 2 Závislosť indentačnej tvrdosti na hĺbke vpichu

Následne sme pomocou SEM nasnímali všetky vpichy a ku každému sme priradili zodpovedajúcu hodnotu tvrdosti. EBSD analýzou sme určili orientáciu jednotlivých zŕn. Potom sme si legendu pre EBSD analýzu (Obr. 3) rozdelili na 8 typických oblastí (farieb) a pre každú sme vybrali niekoľko zŕn. V týchto zrnách sú uhly medzi bazálne a prizmaticky orientovanými rovinami nasledovné: od (0001) k (2-1-10) 1- 0-10°, 2 – 10-40°, 4 – 40-80°, 6 – 80-90° a od (0001) k (10-10) 3 – 10-40°, 5 – 40-80°, 8 – 80-90°. Hodnoty tvrdosti sme štatisticky vyhodnotili a vytvorili závislosť tvrdosti na orientácii zŕn (Obr. 4). Pre porovnanie sme pridali typickú hodnotu tvrdosti pre kobaltovú fázu. Hodnoty tvrdosti pre bazálne orientované zrná boli 37 ± 2,1 GPa a pre prizmaticky orientované zrná 27 ± 2,4 GPa. Pre kobaltovú fázu boli hodnoty tvrdosti 7 ± 1,4 GPa.

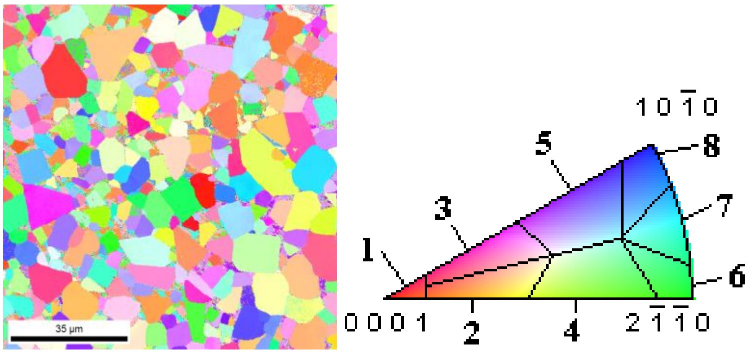

Obr. 3 EBSD mapa s legendou

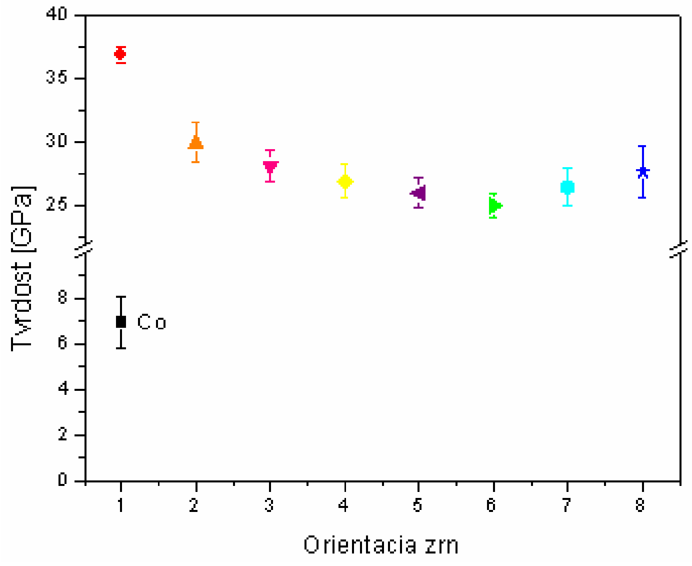

Obr. 4 Závislosť indentačnej tvrdosti na orientácii WC zŕn

ZÁVER

Experimentálne merania systému WC-9Co potvrdili, že bazálne orientované zrná majú výrazne vyššiu tvrdosť ako prizmaticky orientované WC zrná, a to približne o 10 GPa. Z tohto zistenia vyplýva, že ak by bolo možné usporiadať mikroštruktúru tak, že bazálne orientované WC zrná by tvorili funkčný povrch rezného nástroja, bolo by možné zvýšiť jeho tvrdosť až 1,5 násobne.

POĎAKOVANIE

Táto práca bola realizovaná s podporou projektov APVV-0161-11, NanoCEXmat II: ITMS No: 26220120035, NanoCEXmat I: ITMS No: 26220120019 a CEKSIM: ITMS No: 26220120056.

LITERATÚRA

[1] Bonache, V., Rayón, E., Salvador, M.D., Busquets, D.: Nanoindentation study of WC-12Co hardmetals obtained from nanocrystalline powders: Evaluation of hardness and modulus on individual phases, Mater. Sci. Eng. A 527, 2935-2941 (2010).
[2] Cuadrado, N., D. Casellas, D., Llanes, L., Gonzalez, I., Caro, J.: Effect of crystal anisotropy on the mechanical properties of WC embedded in WC-Co cemented carbides, Proceedings Euro PM2011-Hard materials, Vol.2. (2011)
[3] Duszová, A., Halgaš, R., Bľanda, M., Hvizdoš, P., Lofaj, F., Dusza, J., Morgiel, J.: Nanoindentation of WC-Co hardmetals, J. Eur. Ceram. Soc. 33 2227-2232 (2013).
[4] Luyckx, S.B., Nabarro, F.R.N., Wai, S-W., James, M.N.: The anisotropic work hardening of WC crystals, Acta Metall. 40 1623-1627 (1992).
[5] Roebuck, B., Klose, P., Mingard, K.P.: Hardness of hexagonal tungsten carbide crystals as a function of orientation, Acta Mater. 60 6131-6143 (2012).

ŠTÚDIUM MONOKRYŠTÁLOV WC VO WC-Co KOMPOZITOCH POUŽITÍM NANOINDENTÁCIE A AFM TECHNÍK

INVESTIGATION OF WC MONOCRYSTALS IN WC-Co COMPOSITE USING NANOINDENTATION AND AFM TECHNIQUES

Tamás Csanádi[1], *Marek Bľanda*[1,2], *Annamária Duszová*[1], *Pavol Hvizdoš*[1] *and Ján Dusza*[1,2]

[1]*Institute of Materials Research, Slovak Academy of Sciences, Watsonova 47, Košice, Slovak republic*

[2]*Faculty of Materials Science and Technology, Slovak University of Technology, Paulínska 16, Trnava, Slovak republic*

ABSTRACT

Elastic and plastic properties of WC-9%Co hardmetal were investigated by nanoindentation and the resulted hardness values were checked by means of atomic force microscope (AFM) at room temperature. Two crystallographic planes were investigated, namely the basal and prismatic planes, on which nanoindentation tests were performed with different applied load from 1 mN to 50 mN.

The results determined by nanoindentation show higher indentation hardness on basal planes (H_{IT}=28.9±0.1 GPa) than on prismatic ones (H_{IT}=21.9±0.1 GPa) over 10 mN load. For loads below 10 mN the results for H_{IT} were inconsistent. The corresponding indents were checked by AFM and correct values of hardness were found. It is pointed out that below 50 nm contact depth the applied built-in contact area-contact depth function is not appropriate and a new corrected contact area-contact depth function is proposed, thus the resulting recalculated hardness values are in good agreement with the AFM measurements.

Keywords: *nanoindentation, hardmetal, basal plane, prismatic plane, AFM*

INTRODUCTION

Cemented carbides are widely used as machining tools because of their excellent mechanical properties [1]. One of the most commonly used hardmetal is the tungsten carbide-cobalt composite. For more than fifty years, several indentation studies on tungsten carbide single crystals have shown considerable anisotropy depending on the orientation of the facets [2-5]. Even though a number of experimental and theoretical studies have been carried out on WC-Co cemented carbides [6-9] concerning the description of the elastic and plastic behaviour, these measurements could have given an account of only the common effect of the deformation of WC particles and the cobalt binder during microindentation. After the development of nanoindentation technique it has been possible to investigate both tungsten carbide and cobalt phases individually, but until now only few studies exist in this field from only very shallow indentation region [10,11] or from relatively deep penetration region [12]. Moreover, the results are contradictory. Bonache and his colleagues made the very first paper [10], where the differently orientated WC grains and the cobalt binders have been investigated and it was claimed that the prismatic facets are harder than the basal ones. These results are inconsistent with the earlier studies [2-5] and with some recent papers [11,12] on WC single crystals grains, where the opposite was experienced.

This paper addresses this problem in order to reveal the real anisotropic behaviour of elastic and plastic deformation induced by nanoindentation in wide range of depth.

EXPERIMENTAL

In this paper, tungsten carbide-cobalt composite was investigated containing 9 vol.% of cobalt (WC-9Co). In brief, the WC grain size was 3-25 μm and the Vickers macrohardness (*HV*30) was around 982. The sample was prepared properly for nanoindentation and its surface was checked by scanning electron microscope (SEM). Additional details about the microstructure and the sample preparation can be found elsewhere [11].

The nanoindentation tests were carried out on Nanoindentation Tester NHT-TTX made by CSM Instruments (Switzerland) at room temperature. Indentations were performed using Berkovich indenter on the basal and prismatic planes. The orientations of facets were checked by means of electron backscattered diffraction technique (EBSD). Due to the relatively big WC particle size, it was possible to perform all of the indentations in the same grain but at distances large enough from each other to avoid the influence of the crystal orientation and to minimize the effect of the mutual stress fields on hardness. Two indentations were made with the same load in each grain applying single loading-unloading cycles using 1 mN, 2 mN, 3 mN, 5 mN, 10 mN, 25 mN and 50 mN loads.

Atomic force microscopy (AFM) investigations were performed on the indents to study the resulting cross profiles and to verify the reliability of the calculated hardness values by nanoindentation technique in the shallow depth regime.

RESULTS AND CONCLUSIONS

NANOINDENTATION MEASUREMENTS

The results determined by nanoindentation show considerable indentation size effect (ISE), but over 10 mN load the hardness can be considered constant and its value is significantly higher on basal planes (*H*=28.9±0.1 GPa) than on prismatic ones (*H*=21.9±0.1 GPa),see in Fig. 1a. These results are in good agreement with some recent papers, where similar WC-Co composites were investigated [11,12]. In the latter paper [12] the hardness values are slightly lower, 25.6 GPa for basal and 17.2GPa for prismatic planes, which can be explained by ISE, because of the higher applied load. The former paper [11], in which much lower loads were used, reports higher hardness 40.4 GPa and 32.8 GPa on both basal and prismatic planes, respectively. The deviance from our measurement can be also explained by the indentation size effect. It is clearly seen in Fig. 1a that our measurements coincide with those results in the low applied load region over 5 mN. However, according to the paper by Bonache et al. [10], in the very shallow depth regime (below 30 nm) which corresponds to the region of lower loads than 5 mN the opposite behaviour was experienced. According to our measurements in this force region a sudden drop-off can be observed in the tendency of hardness (Fig. 1a), therefore first we had to analyse and clarify the physical background of this behaviour.To this end, careful AFM studies were carried out on each indent in the whole range of applied loads from 1 mN up to 50 mN.

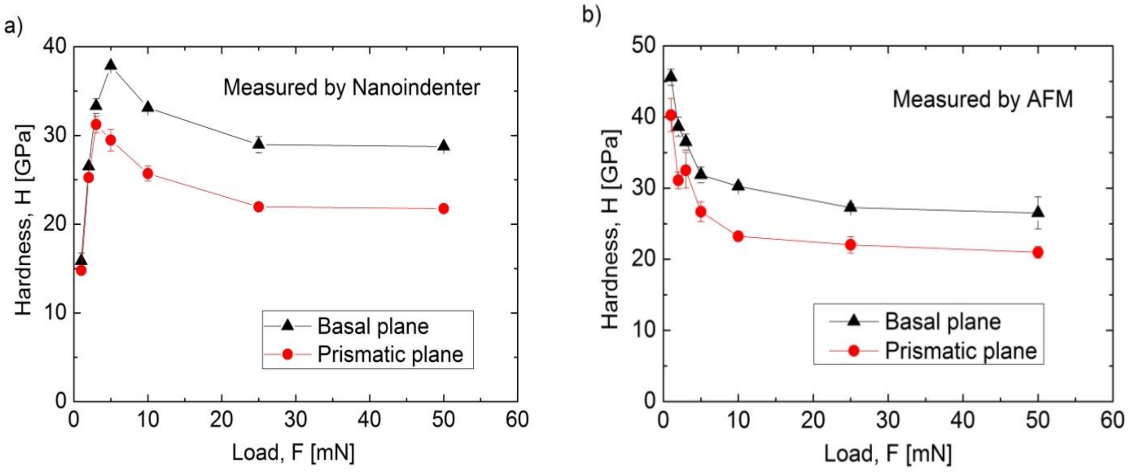

Fig.1. Hardness values of basal and prismatic planes obtaining from a) nanoindentation, b) AFM.

AFM MEASUREMENTS

Using AFM cross profiles, the contact projected areas were calculated and then the hardness values were evaluated. This calculation is based on that the projected contact area remains constant during unloading [13]. The results show a strong indentation size effect and higher harness values corresponding to the basal plane than the prismatic one in the whole investigated depth regime, as it is shown in Fig. 1b. These results are inconsistent with those published by Bonache et al. [10], but they are in good agreement with some other recent nanoindentation studies on WC-Co composites [11,12] and many earlier microindentation investigations on WC single crystals [2-5].

However, the experienced drop-off behaviour below 5 mN is still an open question in spite of the fact that the nanoindentaion machine has been carefully calibrated. To ascertain the origin of it, calibration data on fused silica has been precisely analysed. The fitting procedure of contact area function revealed that original built-in function was not appropriate in the whole depth range in spite of the fact that the best fits were used. This is summarized briefly in the following section, suggesting a new area calibration function.

NEW CONTACT AREA FUNCTION

The routine machine calibration is based on individual single cycle indentations on fused silica using loads from 0.1 mN to 100 mN. The contact area values were calculated by Oliver Pharr method assuming that the Young modulus of fused silica is constant in the whole investigated load region. Finally it was plotted as function of the contact depth and was fitted using the built-in contact area functions (Eq. 1) to obtain the best fit.

$$A(h_c) = 24.5h_c^2 + a_1h_c + a_2h_c^{1/2} + a_3h_c^{1/4} + a_4h_c^{1/8} + a_5h_c^{1/16} + a_6h_c^{1/32} + a_7h_c^{1/64} + a_8h_c^{1/128} \qquad (1)$$

In spite of the best fit was used, the above function (Eq. 1) was not able to fit properly the calculated area values in the shallow depth regime. This observation requires the definition of a new contact area function which fits properly the whole analysed load or depth region. It can be shown that the $A(h_c)$ function deviates from the parabolic behaviour but adequately can be fitted by the following simple power-law function (Eq. 2) with 1.8 exponent instead of 2.

$$A(h_c) = 85.1h_c^{1.8} \qquad (2)$$

Using this new contact area function the resulting hardness values for both basal and prismatic planes are in good agreement with the AFM measurements in the whole investigated depth region (see in Fig. 2).

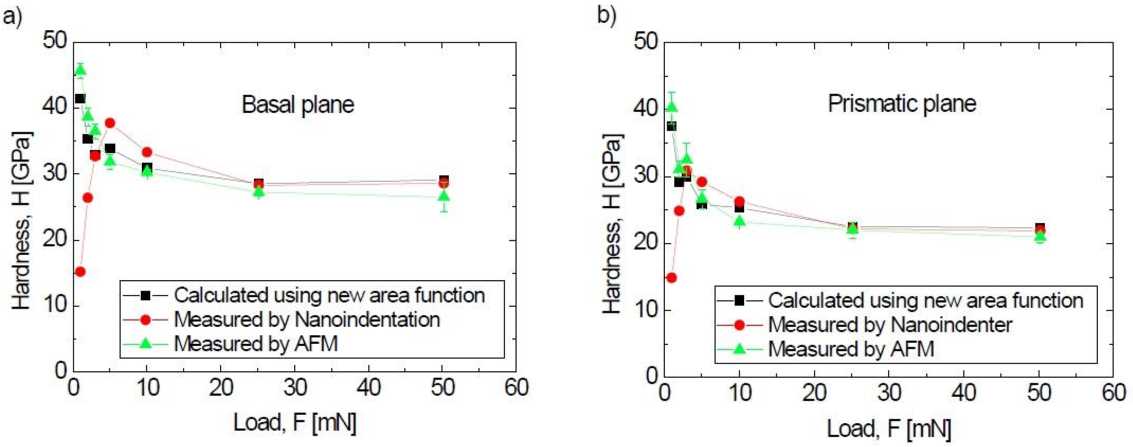

Fig. 2. Hardness values of a) basal and b) prismatic planes derived from nanoindentation, AFM measurement and calculated by the new contact area function.

ACKNOWLEDGEMENTS

This work was realized within the frame of the projects NanoCEXmat II: ITMS No: 26220120035; NanoCEXmat I: ITMS No: 26220120019; and CEKSIM: ITMS No: 26220120056; which are supported by the Operational Program “Research and Development” financed through European Regional Development Fund and projects of APVV with number 0161-11.This work was also supported by Agilent Technologies.

REFERENCES

[1] Exner, H.E.: Physical and chemical nature of cemented carbides, Int. Met. Rev. 4, 149-173 (1979).
[2] Takahashi, T., Friese, E.J.: Determination of the slip systems in single crystals of tungsten monocarbide, Phil. Mag. 12, 1-8 (1965).
[3] French, D.N., Thomas, D.A.: Hardness anisotropy and slip in WC crystals, Trans. Metall. Soc. AIME 233, 950-952 (1965).
[4] Hibbs, M.K., Sinclair,R.: Room-temperature deformation mechanisms and the defect structure of tungsten carbide, Acta Metall. 29, 1645-1654 (1981).

[5] Luyckx, S.B., Nabarro, F.R.N., Wai, S-W., James, M.N.: The anisotropic work hardening of WC crystals, Acta Metall. 40, 1623-1627 (1992).
[6] Nabarro, F.R.N., Luyckx,S.B.: The theory of the strength of tungsten carbide-cobalt compacts, Trans. J. Int. Met. 9, 610-615 (1968).
[7] Jayaram, V., Sinclair, R., Rowcliffe, D.J.: Intergranular cracking in WC-6%Co: An application of the von Mises criterion, Acta Metall. 31, 373-378 (1983).
[8] Roebuck, B., Almond, E.A.: Deformation and fracture processes and the physical metallurgy of WC-Co hardmetals, Int. Mater. Rev. 33, 90-110 (1988).
[9] Rowcliffe, D.J., Jayaram, V., Hibbs, M.K., Sinclair, R.: Compressive deformation and fracture in WC materials, Mater. Sci. Eng.A 105-106, 299-303 (1988).
[10] Bonache, V., Rayón, E., Salvador, M.D., Busquets, D.: Nanoindentation study of WC-12Co hardmetals obtained from nanocrystalline powders: Evaluation of hardness and modulus on individual phases, Mater. Sci. Eng.A 527, 2935-2941 (2010).
[11] Duszová, A.,Halgas, R., Blanda, R., Hvizdoš, P., Lofaj, F., Dusza, J., Morgiel, J.: Nanoindentation of WC-Co hardmetals, J. Eur. Ceram. Soc. 33, 2227-2232 (2013).
[12] Cuadrado, N., Casellas, D., Llanes, L., Gonzalez, I., Caro, J.: Effect of crystal anisotropy on the mechanical properties of WC embedded in WC-Co cemented carbides, Proceedings Euro PM2011-Hard materials, Vol.2. (2011).
[13] Oliver, W.C., Pharr, G.M: An improved technique to determine hardness and elastic modulus using load and displacement sensing indentation experiments, J. Mater. Res. 7, 1564-1583 (1992).

PRÍPRAVA PÓROVITEJ KERAMIKY NA BÁZE NITRIDU KREMIČITÉHO REPLIKAČNOU METÓDOU PRE BIOAPLIKÁCIE

PREPARATION OF POROUS SILICON NITRIDE BASED CERAMICS BY THE REPLICA METHOD FOR BIOAPPLICATION

M. Domanická,[a] *K. Bodišová,* [a] *Z. Lenčéš,* [a] *Z. Vilčeková,* [b] *M. Kašiarová,* [b] *M. Hnatko,* [a] *P. Šajgalík* [a]

a Institute of Inorganic Chemistry, Slovak Academy of Science, Dúbravská cesta 9, 842 36 Bratislava, Slovakia

b Institute of Materials Research, Slovak Academy of Sciences, Watsonova 47, 04353 Košice, Slovakia

ABSTRACT

Porous silicon nitride ceramics having properties similar to the human trabecular bone has been sintered and characterized in order to develop a material applicable as bone substitute. At first, human trabecular bone was characterized especially in term of pore structure which is, besides the non-toxicity, the most critical for acceptation of the substitute. The pore network of highly porous trabecular bone is formed by interconnected large pores of approximately 300 – 1000 µm. Similar pore structure of silicon nitride-based ceramics was attained by the replica method with polyurethane sponge as pore forming agent. Porous ceramics were prepared in two ways, namely as air-sintered silicon nitride and sintered reaction-bonded silicon nitride. The materials were characterized using the same methods as for the bone samples. Both types of the materials fulfilled the microstructural requirements for bioapplications, moreover their non-cytotoxicity was proved by measuring yellow tetrazolium MTT proliferation assay using human fibroblast cell line.

Keywords: *porosity, mechanical properties, silicon nitride, biomedical applications*

INTRODUCTION

Progress in orthopedic surgery is inevitably related to the development of new biomaterials appropriate as bone substitutes in terms of structure, mechanical and biological properties. General requirements involve specially high chemical inertness in corrosive body fluids, high wear resistance, sufficient mechanical properties and biocompatibility.

In the process of development of the new biomaterials for tissue replacement must be taken into account structure and properties of the tissue, which has to be replaced. If the properties of new material significantly differ from the host tissue, the material will cause dynamic changes of the host tissue after implantation. Silicon nitride based ceramics fulfill all mentioned conditions and it represent a promising alternative to metals or polymers [1].

This work is focused on preparation and characterization of porous silicon nitride with properties similar to the human trabecular bone. The prepared porous ceramics were characterized using the same methods as for bone samples – density measurement, SEM, XRD analysis, XRD-micro-tomography and mercury porosimetry. Also the mechanical properties as hardness (H), elastic modulus (E) and compressive strength (σ) of prepared materials have been measured and the obtained values were compared with the values of bone samples.

EXPERIMENTAL

The silicon nitride-based samples were prepared by replica method using polyurethane sponge as pore-forming agent by two different methods. In the first one, suspension with 35 vol. % of Si3N4 powder (Yantai, Tomley Hi-Tech Ind. & Tra. Co., Ltd., D90=10.0 µm, O < 1.5%) was prepared. The polyurethane sponges (Bulpren S, average pore size 0,48 mm,) were dipped into slurry and compressed while submerged, to fill all the cells in the sponge and achieve good wetting between sponge and slurry. The impregnated sponge was then passed through rollers to remove the excess suspension. After drying the sponge was burnt out at 600 °C for 1 h on air (heating rate: 1 °C·min-1).

Then the sintering at 1250 °C on air was performed. These samples are depicted as air-sintered silicon nitride (ASSN) [2].

In the second method sintered reaction bonded silicon nitride (SRBSN) samples were prepared. Suspension with 48 vol. % of powder mixture consisting of silicon (grade 4D, d_{50}= 7 μm, Sicomill, Vesta Ceramics AB, Ljungaverk, Sweden) and α-Si3N4 (SN-E10, Ube Ind., Japan) in a weight ratio of 4:1 was prepared in deionised water. The polyurethane sponges (Bulpren S, average pore size 0,62 mm) were impregnated with the slurry and the excess of suspension was removed by roll-press processing. After drying, the sponge was burnt at the same conditions as in the first method. The nitridation of Si-based porous structure was carried out at 1400°C for 3 h followed by sintering at 1750 °C for 2 h in nitrogen atmosphere.

The results show that the mechanical properties of air-sintered silicon nitride ($H = 0.46 \pm 0.07$ GPa; $E = 11.4 \pm 0.9$ GPa; $\sigma = 3.2 \pm 1.8$ MPa) are very close to the values measured for bone ($H = 0.51 \pm 0.03$ GPa; $E = 11.2 \pm 0.9$ GPa; $\sigma = 4.7 \pm 1.6$ MPa) contrary to reaction bonded silicon nitride ceramics ($H = 6.3 \pm 2.3$ GPa; $E = 92.1 \pm 21.3$ GPa; $\sigma = 5.95 \pm 0.4$ MPa). However mechanical properties can be modified by changing of sintering regime.

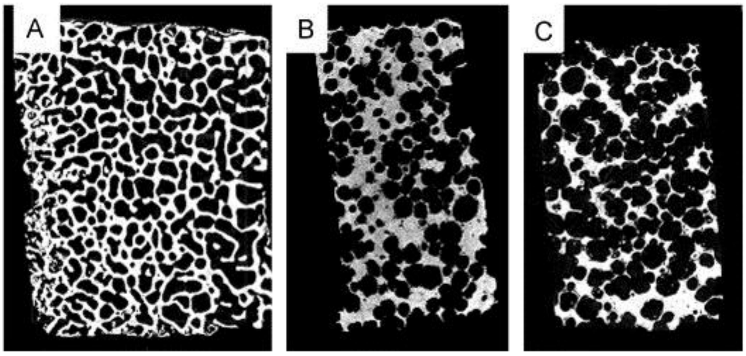

Obr. 1 Sections from XRD microtomography of bone (64 vol% pores)—(A), air-sintered Si3N4 (65 vol% pores)—(B), SRBSN (73 vol% pores)—(C).

CONCLUSION

Porous silicon nitride-based ceramics with structure similar to the trabecular bone structure consisting of interconnected macroporous network was prepared using replica method. The mechanical properties of air-sintered silicon nitride were very close to the bone properties. In the case of sintered reaction-bonded silicon nitride the preparation method requires decrease the hardness and Young's modulus values. The non-cytotoxicity of porous silicon nitride-based ceramic materials was confirmed by MTT proliferation test.

ACKNOWLEDGEMENT

This work was supported by the Slovak Grant Agency APVV Project No. APVV-0500-10. This work is the result of the project Competence center for new materials, advanced technologies and energy ITMS 26240220073, supported by the Research and Development Operational Program funded by the European Regional Development Fund.

REFERENCES

[1] Fung YC. Biomechanics: mechanical properties of living tissues, 2nd ed. New York: Springer, 1993.

[2] Bodišová K., Kašiarová M., Domanická M., Hnatko M., Lenčéš Z., Varcholová Nováková Z., Vojtaššák J., Gromošová S., Šajgalík P. Porous silicon nitride ceramics designed for bone substitute applications. In *Ceramics Internation* 39 [7] (2013) p. 8355–8362.

VPLYV KYSLÝCH NÁPOJOV NA MIKROMECHANICKÉ VLASTNOSTI ĽUDSKEJ ZUBNEJ SKLOVINY

EFFECT OF ACIDIC BEVERAGES ON THE MICROMECHANICAL PROPERTIES OF HUMAN TOOTH ENAMEL

P. Gaalová[1], D. Galusková[1], D. Galusek[1], J. Kováč[3], D. Kováč[3]

[1]Vitrum Laugaricio – Joint Glass Center of the Institute of Inorganic Chemistry, SAS

Alexander Dubček University of Trenčín, and Faculty of Chemical and Food Technology, Slovak University of Technology, Študentská 2, 911 50 Trenčín,Slovakia

[3]Comenius University of Bratislava, Faculty of Medicine, Vajanského nábrežie, 811 02

Bratislava-Staré Mesto, Slovakia

ABSTRACT

The influence of corrosion in acid beverages (white wine, pH~3.5) on micromechanical properties of human teeth was studied. Simultaneously, the effect of fluorine-containing mouthwash Elmex (pH~4.4) and of artificial saliva (Biothene, pH~5.3) in terms of their protective action against corrosion, and the recovery of mechanical properties through fluoridation and re-calcification was studied. The influence of the solutions on Vickers hardness of dental enamel was monitored on the basis of results from the tests carried out under dynamic conditions. The dynamic tests were performed at temperature corresponding to the temperature of human body (37°C). The polished surfaces of human enamel were exposed to corrosion solution from 10 to 60 minutes, the hardness testing was performed in 10 minutes intervals at the load of 0.2 N. The measurements confirmed a significant deterioration of microhardness with prolonged exposure to white wine. The Vickers hardness decreased from 347 HV0.2 in uncorroded specimens to 186 HV0.2 in samples corroded for 60 minutes in white wine. Significant recovery of Vickers hardness was observed after 60 minutes exposition time in the Elmex fluoridation solution, with the increase from 186 to 372 HV0.2 (*Fig. 1*). Similar effect was observed in the artificial saliva Biothene solution, with observed hardness increase from 186 to 320 HV0.2 (*Fig. 2*). Healing of corrosion-induced defects by the action of both the Elmex and Biothene solutions was observed by SEM, and associated with observed increase of hardness.

Keywords: *human tooth enamel, microhardness, corrosion, recovery*

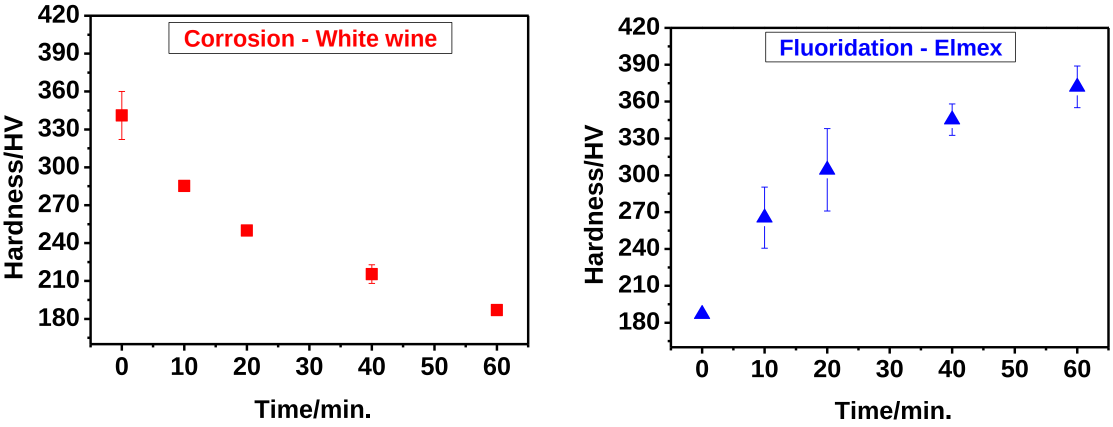

a) *b)*

Fig. 1: Variation of enamel surface microhardness as a function of the exposure time,

a) Corrosion White wine, b) Fluoridation Elmex

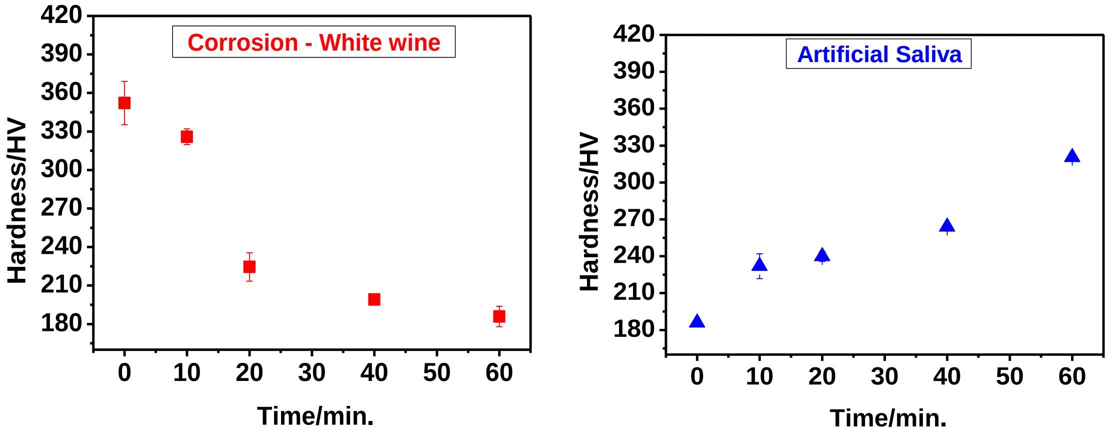

a) *b)*

Fig. 2: Variation of enamel surface microhardness as a function of the exposure time, a) Corrosion White wine, b) Artificial saliva

ACKNOWLEDGMENT

The financial support of this work by the grant VEGA 1/0206/11, and the grant APVV 0218-11 is gratefully acknowledged. This publication was created in the frame of the project "Centre of excellence for ceramics, glass, and silicate materials" ITMS code 262 201 20056, based on the Operational Program Research and Development funded from the European Regional Development Fund.

PREDBEŽNÉ ŠTÚDIUM Mn^{2+} DOPOVANÝCH SKIEL V SÚSTAVE Y_2O_3–Al_2O_3–SiO_2

PRELIMINARY STUDY OF Mn^{2+}-DOPED GLASSES IN THE SYSTEM Y_2O_3–Al_2O_3–SiO_2

K. Haladejová, R. Klement, A. Prnová, D. Galusek

Vitrum Laugaricio – Centrum kompetencie pre výskum skla, spoločné pracovisko UACH SAV, TnUAD a FCHPT STU, Študentská 2, SK-91150 Trenčín

ABSTRACT

In recent years, rare-earth ions doped yttrium aluminum garnet ($Y_3Al_5O_{12}$, YAG) has been widely applied as a luminescent material due to its excellent mechanical properties, transparency, thermal conductivity and chemical stability. YAG represents a host matrix with very good structural compatibility. Y^{3+} and Al^{3+} in the structure of YAG can be replaced by various other cations with different valency and size within a suitable range. Many previous works investigated the effect of host substitution on the luminescence properties of usual luminescent centres in YAG. It is common that only one cation is substituted in YAG, however it is also possible that two or more different cations are co-doped into YAG at the same time. Trivalent rare-earth ions (e.g. La^{3+},Gd^{3+},Tb^{3+}, Nd^{3+} and others) can be used to replace Y^{3+}. The boron family elements (e.g. B^{3+}, Ga^{3+}) can be used to replace Al^{3+} homogeneously. When only one kind of cation is built into the YAG structure, trivalent cations are optimal because both substituted and replaced cations have the same valence. It is not suitable to use only one type of divalent or tetravalent cation for replacement of Y^{3+} or Al^{3+}: the content of a substituent must be small for the sake of charge balance, otherwise new phases appear, which destroy the single garnet structure of the material.

The YAG phase as a host doped by various cations (e.g. Ce^{3+}), has been widely used for preparation of phosphors for LED applications, especially white light emitting diodes (LEDs). However, red emission deficiency still persists in these phosphors.

In the present work we report on the results of preliminary study of photoluminescence properties of Mn^{2+} doped glasses and their crystalline counterparts in the systems Y_2O_3–Al_2O_3 and Y_2O_3–Al_2O_3–SiO_2 as potential candidates for efficient red light emitting phosphors. The glasses were prepared in the form of glass microspheres with composition derived from Y_2O_3–Al_2O_3 eutectic (76.8 mol. % Al_2O_3, 23.2 mol. % Y_2O_3), and modified by the addition of 5, 10, 15 and 20 mol. % of SiO_2. The doping level of Mn^{2+} was maintained at 0.5 mol. %. The effect of SiO_2 content on the red emission of prepared phosphors was studied in detail.

Keywords: *Photoluminescence, Mn^{2+} doped glasses, aluminate/low silica aluminosilicate glasses, LED, red phosphors*

ACKNOWLEDGEMENT

The financial support of this work by the bilateral project (Slovakia–Taiwan) SAS-NSC JRP 2012/14 is gratefully acknowledged. This work was carried out in the frame of the project „Centre of Excellence for Ceramics, Glass and Silicate Materials“, ITMS code 262 201 20056, based on the Operational Program Research and Development funded from the European Regional Development Fund.

ELEKTRICKÁ A TEPELNÁ VODIVOSŤ Al_2O_3-MWCNTS KOMPOZITOV

ELECTRICAL AND THERMAL CONDUCTIVITY OF ALUMINA-MWCNTS COMPOSITES

Ondrej Hanzel, Jaroslav Sedláček, Pavol Šajgalík

Institute of Inorganic Chemistry, Slovak Academy of Sciences

ABSTRACT

Alumina – multi-wall carbon nanotubes composites were studied with respect to obtain the homogeneous distribution of nanotubes within the alumina matrix. New approach comprises stabilization of alumina/CNT dispersion with subsequent freezing has been used, which resulted in formation of homogenous mixture. The ceramic composites were prepared by hot pressing at 1550°C using these mixtures. Microstructural analysis, electrical conductivity measurements as well as thermal diffusivity measurements has been used for observation of distribution of nanotubes within composites. Electrical conductivity, as an indicator of homogeneity of conductive network distribution, increases from 6 to 1140 S/m when compared the conventional process and approach presented in this work at the same volume fraction of MWCNTs 10 vol. %. Moreover, homogeneous distribution of CNTs resulted in refinement of microstructure measured with respect to the average grain size of alumina particles (~1µm) compared to conventional powder mixing by only ball milling (~ 5µm) at the same MWCNTs loading.

Keywords: *Al_2O_3, carbon nanotubes, freeze granulation, microstructure, electrical conductivity*

INTRODUCTION

Alumina ceramics, one of extensively utilised structural ceramics, have great potential to be used in many special applications where low density, high hardness, chemical inertness and good high-temperature properties are required. However, alumina is a brittle material with poor fracture toughness and low thermal and electrical conductivity and thermal shock resistance. Carbon nanotubes (CNTs) have excellent mechanical properties. Therefore, they are attractive candidates for reinforcement of various materials. Except their reinforcing effect, they have extraordinary thermal and electrical conductivity and thus can improve also functional properties of alumina ceramics. However, CNTs tend to agglomerate due to the attractive van der Waals forces and thus have a detrimental effect on the mechanical and functional properties of composites. To avoid these problems it is necessary to ensure the homogeneous distribution CNTs in ceramic matrix. In order to reach homogenous distribution of CNTs in alumina matrix the novel approach of processing has been used. This approach comprises acid treatment of CNTs, their homogenous dispergation and freeze drying of this state.

EXPERIMENT

Multi-wall carbon nanotubes (MWCNTs) with outer diameter of 8 – 15 nm and length of 50 µm (Chengdu Organic Chemicals Co. Ltd., China) were stirred in a mixture of concentrated sulphuric and nitric acids. Afterwards, the CNTs were filtered from this mixture and thoroughly washed by distilled water to be acid-free and then finally dried at 80° C overnight. Water based dispersion of as treated MWCNTs have been prepared with addition of stabilizing agent of sodium dodecyl sulphate (SDS, Alfa Aesar GmbH, Germany). Alumina powder (Martoxid MR-70) was added into the stabilized dispersion of MWCNTs in order to prepare mixtures with various content of nanotubes in the range of 2,5 to 10 vol. %. Obtained dispersions were rapidly frozen in liquid nitrogen (LS-2, PowderPro AB, Sweden) and subsequently lyophilised (Unicryo MC2L, UniEquip Laborgerätebau- und Vertriebs GmbH, Germany) to dry the granulate. Alumina-CNTs composites were then densified at 1550°C for 1 hour and load of 30 MPa under inert atmosphere of argon.

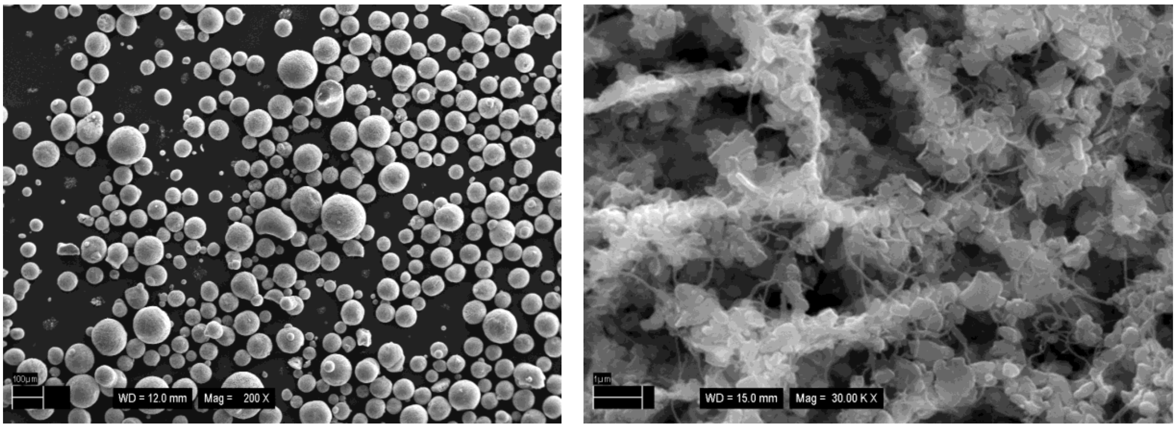

Figure 1. Granulated alumina/CNT composite powder and detail of granule surface with distribution of MWCNTs and alumina grains

Raman spectra of raw as well as acid treated MWCNTs were recorded using Micro-Raman spectrometer (Horiba HR800, Germany) equipped with an Ar laser (irradiation wavelength 633 nm). Zeta potential of MWCNT and alumina dispersions has been measured at various pH in the range of 2 to 11 (Zetasizer Nano Malvern Instruments Ltd., United Kingdom). Densities of ceramic composites were measured using Archimedes method by weighing in water. Scanning electron microscopy (EVO 40HV, Carl Zeiss, Germany) was used for microstructural analysis of prepared powder mixture as well as final composite bodies; grain size of alumina matrix was estimated by the linear interception method. Microstructural evolution and MWCNTs distribution within the alumina matrix was compared with composite counterparts prepared by conventional powder processing and densified under the same condition. Electrical resistivity was measured by 4-point method using compensated RLC bridge.

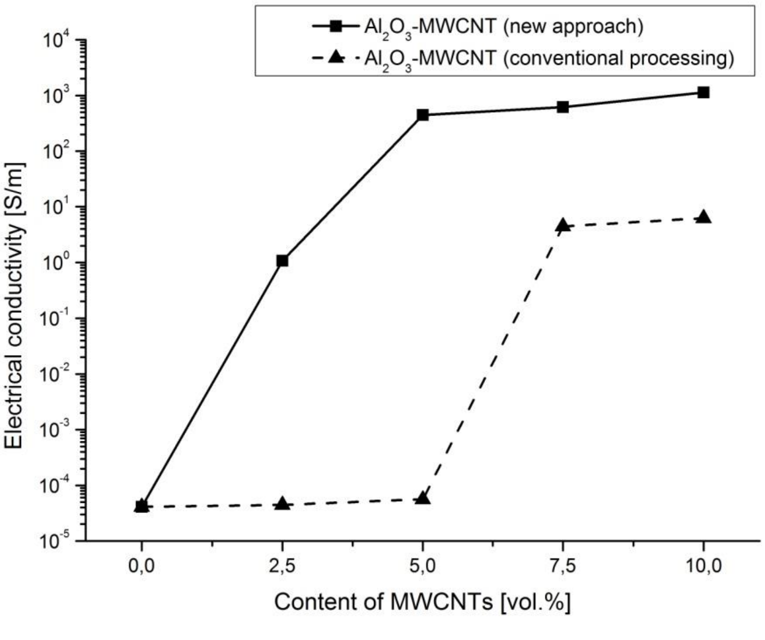

Figure 2: Comparison of electrical conductivity of alumina-CNT composites prepared by conventional process and new approach

CONCLUSION

Multi-wall carbon nanotubes are attractive materials for reinforcement (strength and toughness) and also improvement functional properties of ceramics. The most important prerequisite for improvement mechanical and functional properties of ceramics is uniform distribution of carbon nanotubes in ceramic matrix. This work focuses on new approach for preparation of alumina composites with homogeneously distributed MWCNTs. This approach results in a granulated powder in which MWCNTs were homogeneously distributed and individually isolated and thus to more homogeneous ceramic composites. The preliminary results of microstructural evolution and electrical properties seem to be very promising. From comparison of fracture surfaces of composites prepared by conventional and this new process is clearly seen significant differences in microstructure, especially in the distribution of nanotubes, grain size and presence of agglomerates. Electrical conductivity, as indicator of creation conductive network, increases significantly also due to the better distribution. Thermal conductivity decreases with increasing content of MWCNTs in alumina matrix. More investigation in thermal properties of alumina-MWCNTs will be necessary in order to better understanding of this behaviour.

ACKNOWLEDGEMENT

This work was supported by the Slovak Grant Agency VEGA Project No. 2/0036/10. This work is the result of the project Competence center for new materials, advanced technologies and energy ITMS 26240220073, suported by the Research and Development Operational Program funded by the European Regional Development Fund.

LAMINÁRNA KERAMIKA - KONTAKTNÁ PEVNOSŤ A TVORBA TRHLÍN

LAMINAR CERAMICS - CONTACT STRENGTH AND CRACK FORMATION

Lucia Hegedűsová, Ján Dusza

Institute of Materials Research, Slovak Academy of Sciences, Watsonova 47, Košice, SR

ABSTRACT

The paper deals with the determination of contact strength of laminar composite ceramics by opposite rollers and spheres. Results of the single-cycle contact tests are compared with those of the standard bending test. Parameters of the Weibull analysis which is considered for the determination of strength of ceramic materials are presented.

Keywords: *contact test, microstructure, cone cracks*

INTRODUCTION

Conventional tests for determination of strength of ceramics describe failure behaviour related to a simple stress state which is mostly uniaxial with insignificant gradients. Considering practical applications, mechanical loading leads to an inhomogeneous multi-axial stress state which can be simulated, regarding laboratory measurements, by contact line or point loading. The contact line/point is induced by two opposite rollers and spheres. Weibull analysis is commonly used for describing the values of the bending strength results which are characterized by the characteristic strength σ_0 and the Weibull parameter *m* which is the measure of the scatter in strength values. The Fett's theory [1] which defines relationships between parameters of the Weibull analysis for the four-point bending test ($\sigma_{0,\mathrm{bend}}$, m_{bend}) and single-cycle contact test using rollers ($\sigma_{0,\mathrm{cont,r}}$ $m_{\mathrm{cont,r}}$) is derived as

$$m_{bend} \approx 2\, m_{cont,r}\,, \quad \sigma_{0,bend} \approx \sigma_{0,cont,r}\ . \tag{1}$$

The characteristic strength $\sigma_{0,\mathrm{bend}}$ and $\sigma_{0,\mathrm{cont,r}}$ results from experimental values of σ_{bend} and $\sigma_{\mathrm{cont,r}}$, respectively, defined as [2]

$$\sigma_{bend} = \frac{3P(S_1 - S_2)}{2tW^2}\,, \quad \sigma_{cont,r} = \frac{1.96P}{tW}\,. \tag{2}$$

S_1 and S_2 represent outer and inner spans, respectively. *W* and *t* are dimensions of a sample along directions parallel and perpendicular to a direction of the applied force *P* at failure, respectively.

Finally, the stress $\sigma_{\mathrm{cont,s}}$ along with the Young's modulus *E* have the forms [2]

$$\sigma_{cont,s} = \frac{1-2\nu_m}{3\pi}\left[\frac{6PE^2}{R^2}\right]^{1/3}, \frac{1}{E} = \frac{1-\nu_s^2}{E_s} + \frac{1-\nu_m^2}{E_m}\,, \tag{2}$$

where E_s, ν_s and E_m, ν_m are the Young's modulus, the Poisson's ratio for the spheres and a ceramic material, respectively. The paper deals with the determination of contact strength of laminar composite ceramics by opposite rollers and spheres. Results of the single-cycle contact tests are compared with those of the standard bending test, and an analysis concerning the Fett's theory is presented.

EXPERIMENTAL PROCEDURE AND RESULTS

An experimental material is represented by Al2O3-ZTA laminar composite ceramics which is made by tape casting followed by binder burn-out and sintering, where ZTA=60vol.%Al2O3+40vol.%ZrO2. This 9-layered material of five layers of Al2O3 and four layers of ZrO2.was prepared at the Institute of Science and Technology for Ceramics, Faenza, Italy. The bending test was applied at S1 = 40, S2 = 20 (mm). The single-contact mode by rollers of a standard hardened steel was performed in such way that the load P increased to a value of failure of specimens, where D = 3 mm is a diameter of the rollers, L = 10-15 mm is length of specimens, and W = 3 mm, t =

4 mm. The contact modes by standard hardened steel spheres with the radius R = 2.5 mm were applied to specimens with the dimensions W = 3 mm, t = 4 mm, L = 25 mm, at a loading range of 0-5 kN.

RESULTS AND DISCUSSION

Microstructure of the materials was studied by scanning electron microscopy of polished and etched samples. Microstructure of the ZTA layer (see Fig.1) consists of relatively large Al_2O_3 grains and small ZrO_2. grains as dark and bright phases with size of 1 μm and 0.3 μm, respectively, where both phases exhibiting equiaxed shapes are uniformly dispersed throughout the ZTA layer with thickness of 529 μm. The Weibull characteristics for the investigated material are as follows: $\sigma_{0,\mathrm{bend}}$ = 650 MPa, m_{bend} = 19.8; $\sigma_{0,\mathrm{cont,r}}$ = 715 MPa, $m_{\mathrm{cont,r}}$ = 7.9; $\sigma_{\mathrm{cont,s}}$ = 3453.3 Mpa, $m_{\mathrm{cont,s}}$ = 21.6; $\sigma_{0,\mathrm{cont,r}} / \sigma_{0,\mathrm{bend}}$ = 1.1, $m_{\mathrm{bend}} / m_{\mathrm{cont,r}}$ = 2.5.

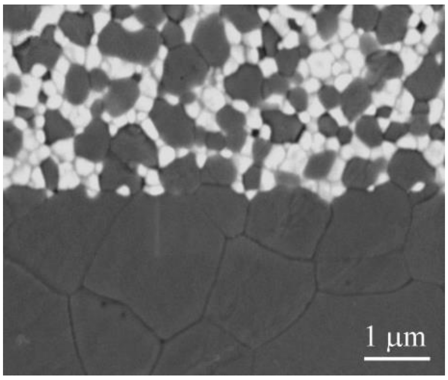

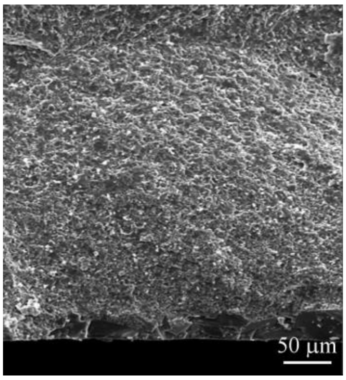

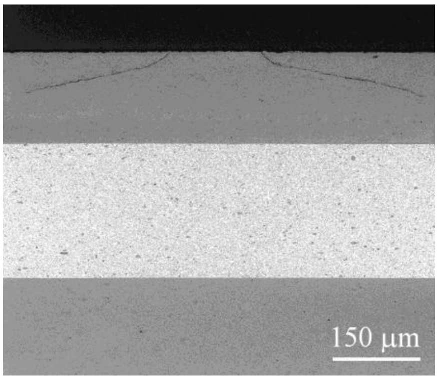

Fig. 1 SEM micrograph of microstructure of the Al_2O_3*-ZTA interface.*

Fig. 2 SEM micrograph of a large processing flaw in the ZTA layer.

Fig. 3 SEM micrograph of a cross-section view with a cone crack induced by the single-cycle contact test using spheres.

Fig.2 shows a fracture surface of Al2O3-ZTA loaded by rollers of the single-cycle contact test along with a large processing flaw in the ZTA layer. Such flaws along with the large grains of Al_2O_3 in the Al_2O_3 layer might be assumed to be a reason of a deviation from the Fett's theory regarding the ratio $m_{\mathrm{bend}}/m_{\mathrm{cont}}$ in contrast to the ratio $\sigma_{0,\mathrm{cont,r}} / \sigma_{0,\mathrm{bend}}$ which corresponds to the Fett's theory. Additionally, due to the difference $\alpha_{\mathrm{Al2O3}} < \alpha_{\mathrm{ZTA}}$ in thermal expansion coefficients, the Al_2O_3 and ZTA layers are loaded by compressive and tensile thermal stresses acting in a plane of a layer, respectively. These stresses in each layer exhibit a significant distribution along the plane normal. This distribution might be assumed to be also a reason of the deviation from the Fett's theory.

Fig.3 shows SEM micrographs of a cross-section view of Al_2O_3-ZTA with a cone crack which is formed during the single-cycle contact test by spheres. The cone crack as a reason of failure and strength degradation of the material exhibits a perpendicular course below the contact surface, followed by a linear course.

CONCLUSIONS

Results of this paper concerning the Al_2O_3-ZTA laminar composite ceramics are as follows. The characteristic strength by the Weibull analysis of the bending test and contact test by rollers are in an agreement with the Fett's theory. The disagreement of the Weibull moduli of these tests with the Fett's theory is assumed to be caused by (1) the presence of large processing flaws; (2) much greater grains in the Al_2O_3 layer than those in the ZTA layer; (3) a significant distribution of thermal stresses, where the distribution is related to a normal of a plane of the Al_2O_3-ZTA layers. The contact test by spheres in a single-cycle mode induces a single cone crack.

ACKNOWLEDGEMENT

This work was realized within the frame of the projects NanoCEXmat II: ITMS No: 26220120035; NanoCEXmat I: ITMS No: 26220120019; and CEKSIM: ITMS No: 26220120056; which are supported by the Operational Program "Research and Development" financed through European Regional Development Fund and project APVV-0161-11.

LITERATURE

[1] Fett T., Munz D.: Influence of stress gradients on failure in contact strength tests with cylinder loading, Eng. Fract. Mech., 69, 1353-1361 (2002).
[2] Fett T., Ernst E., Munz D.: Contact Strength Measurements of Bars under Opposite Sphere Loading, J. Mater. Sci. Lett., 21, 1955-1957 (2002).

VPLYV PODMIENOK DEPOZÍCIE NANOKOPOZITNÝCH WC-C POVLAKOV NA ICH NANOTVRDOSŤ A TRIBOLOGICKÉ VLASTNOSTI

INFLUENCE OF DEPOSITION CONDITIONS OF NANOCOMPOSITE WC-C COATINGS ON THEIR NANOHARDNESS AND TRIBOLOGICAL PROPERTIES

Peter Horňák[1]*, Milan Ferdinandy*[1]*, František Lofaj*[1,2]

Ústav materiálového výskumu SAV, Watsonova 47, Košice

Materiálovotechnologická fakulta STU v Bratislave, Paulínska 16, Trnava

ABSTRACT

The aim of the present contribution is to investigate the influence of deposition conditions of PECVD WC-C coatings on their mechanical properties. The additional gasses including Ar, C_2H_2, H_2, N_2, N_2+SiH_4 influenced the indentation hardness (H_{IT}) and coefficient of friction (COF) of WC-C coatings. The highest hardness of WC-C coatings of around 28 GPa was obtained with Ar addition. The lowest COF of around 0.12 was obtained with C_2H_2 addition. Addition of N_2+SiH_4 mixture increased H_{IT} to 27 GPa and simultaneously decreased COF from 0.71 to 0.35 in comparison with additional gasses.

Keywords: *WC/C coatings, PECVD, nanohardness, coefficient of friction*

ÚVOD

Karbid volfrámu je pre svoju vysokú tvrdosť s nízkym koeficientom trenia široko používaným materiálom v aplikáciách pre rezné nástroje, vrtáky prípadne tvárniace zariadenia. WC povlaky je možné pripravovať magnetrónovým naprašovaním z terčov volfrámu alebo karbidu volfrámu [1], alebo depozíciou pomocou metódy PECVD (Plasma Enhanced Chemical Vapour Deposition) z karbonylu volfrámu [2,3]. Optimalizáciou podmienok depozície a prídavných plynov je možné dosiahnuť ďalšie zlepšenie vlastností povlakov. Reaktívne procesy takto umožňujú zabudovať do povlaku v procese depozície prídavné prvky, alebo regulovať ich množstvo. Tým vieme ovplyvňovať štruktúru aj mechanické vlastnosti nanesených povlakov a vybrať na základe podmienok depozície požadované mechanické vlastnosti pre konkrétnu aplikáciu a použitie. Cieľom príspevku je objasniť vplyv prídavných plynov (C_2H_2, Ar, H_2, N_2, N_2+SiH_4) na tvrdosť a koeficient trenia WC/C povlakov deponovaných metódou PECVD. Získané dáta boli použité na optimalizáciu podmienok depozície nanokompozitných WC/C povlakov.

EXPERIMENT

Povlaky WC_x-C ($x \approx 0.8$) boli nanášané metódou PECVD na oceľové podložky z materiálu C45. Ako prekurzor bol použitý hexakarbonyl volfrámu $W(CO)_6$ bez a s prídavnými plynmi (acetylén, vodík, argón, dusík a zmes 1,4 % silánu v dusíku). Depozičný tlak v komore bol v intervale 1 – 6 Pa, záporné predpätie na vzorke bolo 0 až -5 kV. Indentačná tvrdosť (H_{IT}) bola meraná nanoindentorom NTH, CSM Instruments s Berkovichovým diamantovým hrotom v sínusovom móde s maximálnou zaťažujúcou silou 50 mN. Koeficient trenia bol meraný metódou „pin-on-disc“ na tribometri CSM Instruments. Ako protikus bola použitá oceľová gulička 100Cr6 so zaťažujúcou silou 0,5 N, rýchlosťou pohybu guličky 10 cm/s a dĺžkou dráhy do 200 m.

VÝSLEDKY A DISKUSIA

Optimalizáciou bola pripravená séria WC-C povlakov. Cieľom tejto optimalizácie bolo dosiahnutie najvyššej tvrdosti WC-C povlakov. Tabuľka 1 sumarizuje optimalizované vzorky WC-C povlakov pripravených len z pár karbonylu a následne aj s prídavnými plynmi, s ohľadom na dosiahnutú tvrdosť a koeficienty trenia.

Tabuľka 1. Porovnanie WC-C povlakov optimalizovaných s ohľadom na tvrdosť.

Číslo vzorky	Plyn v komore [Pa]	Tlak plynu [Pa]	Tlak $W(CO)_6$ [Pa]	Celkový tlak [Pa]	H_{IT}	COF
#1	-	-	3	3	16,5±0,4	0,71±0,06
#2	Ar	1	1	2	28,5±0,8	0,82±0,08
#3	C_2H_2	1	1	2	14,6±0,5	0,12±0,05
#4	H_2	2	2	4	15,7±1,1	0,85±0,07
#5	N_2	2	2	4	19,7±0,8	0,71±0,11
#6	$SiH_4 + N_2$	1	1	2	26,9±0,9	0,35±0,07

Tvrdosť vzoriek pripravených len z pár karbonylu je na úrovni 16,5 GPa, čo je približne zhodné s tvrdosťou dosiahnutou pridávaním dodatočných plynov. Vzorky s prídavkom acetylénu (14,6 GPa) a vodíka (15,7 GPa) sú mierne pod touto hodnotou, vzorka s prídavkom dusíka (19,7 GPa) vykazuje mierne vyššiu tvrdosť. Najvyššiu, takmer dvojnásobnú tvrdosť dosahuje povlak nanášaný s prídavkom argónu. Získané výsledky sú porovnateľné s autormi Mrabet a spol. [4], ktorí vo svojej publikácii uvádzajú porovnávací prehľad hodnôt tvrdostí a koeficientov trenia WC/C povlakov čerpajúc z viac ako šestnástich literárnych zdrojov. Abad a kol. [5] dosiahli priemernú tvrdosť WC/C povlakov deponovaných pomocou magnetrónového naprašovania v rozmedzí 16 až 25 GPa, čo je v úplnej zhode s nami pripravenými povlakmi.

Z výsledkov optimalizácie depozičných procesov uvedených v tabuľke 1 je zrejmé, že hodnoty koeficientov trenia sú pre procesy s čistým karbonylom, prípadne s prídavným vodíkom, dusíkom a argónom v intervale 0,71 – 0,85. Koeficient trenia bol približne 0,12 v dôsledku zvýšeného množstva uhlíka z acetylénu. Ten síce spôsobil významné zníženie koeficientu trenia, ale aj zníženie hodnoty tvrdosti (14,6 GPa). Silán v zmesi s dusíkom spôsobuje nepatrné zníženie tvrdosti oproti povlakom pripravených s argónom z 28,5 GPa na 26,9 GPa, ale dochádza aj k zníženiu koeficientov trenia až na hodnotu 0,35.

ZÁVER

Výsledky práce ukazujú, že najvyššia hodnota indentačnej tvrdosti WC/C povlakov 28,5 GPa bola získaná depozíciou pri pridávaní argónu. Prídavok zmesi silánu v dusíku spôsobuje zvýšenie tvrdosti na 26,9 GPa oproti H_{IT} na úrovni 19,7 GPa v prípade čistého dusíka a k poklesu koeficientu trenia z 0,7 na 0,4. Tento pokles pravdepodobne súvisí s prítomnosťou kremíka v povlaku, ktorý ovplyvňuje mechanizmus opotrebenia pri tribologických skúškach. Ďalšie prídavné plyny (Ar, N_2, N_2+SiH_4) zvyšujú hodnoty tvrdosti WC-C povlakov v porovnaní s povlakmi pripavenými len s čistým karbonylom (16,5 GPa) na hodnoty 28,5 GPa, 19,7 GPa a 26,9 GPa. Najnižšia hodnota koeficientu trenia COF (0,12) bola získaná depozíciou s pridaním acetylénu (C_2H_2). Toto spôsobuje prítomnosťou väčšieho množstva uhlíka v povlaku, ktorý svojím mazacím účinkom spôsobuje pokles COF.

POĎAKOVANIE

Táto práca bola realizovaná s podporou projektov NanoCEXmat II: ITMS č: 26220120035; NanoCEXmat I: ITMS č: 26220120019; a CEKSIM: ITMS č: 26220120056; ktoré sú podporované z operačného programu “Výskum a vývoj” financovaného z Programu Európskeho regionálneho rozvoja a projektov APVV-0161-11, APVV 0520-11 a VEGA 2/0108/11.

LITERATÚRA

[1] F. Lofaj et al.: Nanohardness vs. friction behavior in magnetron sputtered and PECVD W-C coatings, Key Eng. Mat. 586 (2014), 35-38

[2] F. Lofaj et al.: Nanoindentation, AFM and tribological properties of thin nc-WC/a-C coatings, J. Eur. Cer. Soc. 32 (2012) 2043-2051

[3] F. Lofaj et al.: Transfer film in a friction contact in the nanocomposite WC-C coatings, J. Austr. Cer. Soc. 49[1] (2013), 34-43

[4] S.El Mrabet et. al.: Identification of the wear mechanism on WC/C nanostructured coatings, Surf. Coat. Technol. 206 (2011), 1913-1920
[5] M.D. Abad, M.A. Munoz-Márquez et.al.: Tailored synthesis of nanostructured WC/a-C coatings by dual magnetron sputtering, Surf. Coat Technol. 204 (2010), 3490-3500

LUMINOFOR NA BÁZI $LaSi_3N_5$ DOPOVANÝ PRVKY VZÁCNÝCH ZEMIN

RARE EARTH-DOPED LANTHANUM SILICON NITRIDE-BASED PHOSPHORS

Monika Hrabalová [1], Zoltán Lenčéš [1], Adriana Czímerová [1], Pavol Šajgalík [1]

[1]Institute of Inorganic Chemistry, Slovak Academy of Sciences, Dúbravská cesta 9, 845 36 Bratislava, Slovakia

ABSTRACT

The aim of this work was the preparation of lanthanum silicon nitride-based phosphors doped with lanthanoides (Eu, Ce, Sm) which activate the luminescence. Ternary silicon nitride ($LaSi_3N_5$) was prepared by nitridation of LaSi and Si. The dopant elements, i.e. europium, cerium and samarium were added in a form of oxides in amount from 1 to 6 mol%. The starting powder mixture composed of $LaSi/Si/Si_3N_4/Eu_2O_3$ was nitrided in graphite resistance furnace at 1390°C and afterwards annealed in gas pressure furnace at 1650°C for 4 hours. The $LaSi_3N_5$:Eu phosphors emit light in the green-yellowish region with a maximum at 560 nm. The highest intensity of photoluminescence was observed for the phosphor with 4 % of added europium. The $LaSi_3N_5$:Ce phosphors show emission in the blue region with maximum photoluminescence intensity at 417 nm. The $LaSi_3N_5$:Sm phosphors emit light in the orange-red region. The photoluminescence intensity decreased with higher molar concentration of samarium and maximum photoluminescence intensity was observed for phosphors doped with 2% of samarium.

Keywords: *Lanthanum silicon nitride, nitridation, luminescence, phosphors*

INTRODUCTION

The grid-based electric lighting consumes worldwide about 3 TWh of electricity, amount close to 20% of total electricity consumption. Moreover, the demand for lighting is increasing rapidly in countries with large population like China, India or Brazil. Except of large energy consumption lighting is one of the biggest causes of greenhouse gas emissions [1,2]. For this reason a considerable attention is given to the research focused on the development of efficient and economical light sources. One of the alternatives is the efficient white LED, preferably with warmer (more yellow-red) light, with a colour close to daylight. Except of the sulfides (CaS:Eu, SrS:Eu, etc.), garnet and non-garnet oxide-based phosphors, also the nitride and oxynitride-based phosphors are intensively studied. The majority of these phosphors are Eu^{2+} or Ce^{3+}-doped silicon based compounds, due to the high covalency of the crystal lattices and strong crystal fields of the host lattices [3]. Generally they have a superior chemical and thermal stability.

There is still a demand on efficient red and green phosphors prepared by cost-effective synthesis route. This work deals with the preparation of europium, cerium and samarium doped $LaSi_3N_5$ phosphors by nitridation of metal silicide and silicon-based starting powder mixtures.

EXPERIMENTAL PROCEDURE

The starting powder compositions for the synthesis of $LaSi_3N_5$ ternary nitride were calculated according to the equations used in our previous works [4,5]. In the general equation for the synthesis of $LaSi_3N_5$:

$$LaSi + (2\text{-}3x)\ Si + x\ Si_3N_4 + (5/2\text{-}2x)\ N_2 = LaSi_3N_5, \qquad (1)$$

the optimized ratio of reactants was $x = 0.55$.

The europium content in $LaSi_3N_5$ phosphors was calculated according to the following reactions:

$$(1\text{-}z)\ LaSi_3N_5 + z/2\ Eu_2O_3 + z\ Si_3N_4 = La_{1\text{-}z}Eu_zSi_3N_{5\text{-}z}O_{3/2z} \qquad (2)$$

The europium content was in the range of $z \in \langle 0.01; 0.06 \rangle$ with a step of 0.01. Similar reaction was used also for the calculation of samarium content.

The cerium content in $LaSi_3N_5$ phosphors was calculated according to the following equations:

$$(1\text{-}z)\ LaSi_3N_5 + z\ CeO_2 + z\ Si_3N_4 = La_{1-z}Ce_zSi_3N_{5-z}O_{2z} \qquad (3)$$

The cerium content was in the range of $z \in \langle 0.01; 0.06\rangle$ with a step of 0.01.

For the synthesis of $LaSi_3N_5$-based phosphors the following starting powders were used: LaSi (High Purity Chemicals, Japan), Si (grade 2C, SicoMill, Vesta Ceramics, Sweden), α-Si_3N_4 (grade SN-E10, Ube Industries, Ltd, Yamaguchi, Japan), Eu_2O_3, CeO_2 and Sm_2O_3 (99,99%, Treibacher Industries AG, Austria).

The powder mixtures were homogenized in agate mortar in a dry state. From the powders pellets were pressed (diameter 8 mm) with a pressure of 100 MPa. The tablets were placed in a BN crucible without powder bed, and afterwards nitrided in a graphite resistance furnace (Centorr, USA). The nitridation was performed up to the temperature of 1390°C with a dwell time for 4 hours. After the nitridation the crushed samples were additionally annealed in a gas pressure furnace at 1650°C (samples $LaSi_3N_5$:Eu) under nitrogen pressure of 1.5 MPa for 4 hours and at 1700 °C (samples $LaSi_3N_5$:Ce and $LaSi_3N_5$:Sm) under nitrogen pressure of 4.0 MPa for 5 hours. Phase composition was determined by XRD analysis (D8-Discover, Bruker, Madison, WI, CuKα radiation). Photoluminescence spectra of the powders were investigated by a fluorescence spectrometer (Fluorolog 3-11, ISA/Jobin Yvon-SPEX, Longjumeau, France).

RESULTS AND DISCUSION

According to the results of DTA/TG measurements the nitridation condition of $LaSi_3N_5$-based phosphors was optimized. Due to the presence of iron impurity in the silicon powder, the eutectic temperature of silicon and silicide (LaSi) and the added dopant (Eu_2O_3, CeO_2 and Sm_2O_3) three exothermic peaks were observed during the DTA-TG analysis of the starting powder mixture in N2 atmosphere. The exothermic peaks were accompanied by weight gain, i.e. nitridation of silicon and respective silicide. To avoid the melting of silicon or silicide due to the exothermic reaction a short dwell time, or slow heating rate was applied close to the observed exothermic peaks. By the application of these nitridation steps a full conversion of silicon and silicide to $LaSi_3N_5$ was achieved. The nitrided product had a grey colour, while after additional annealing at higher temperature the colour was yellowish for all samples.

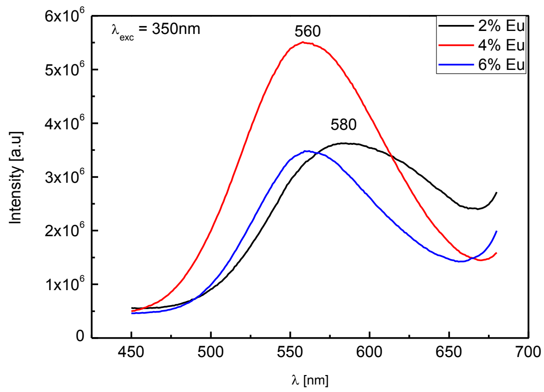

's.

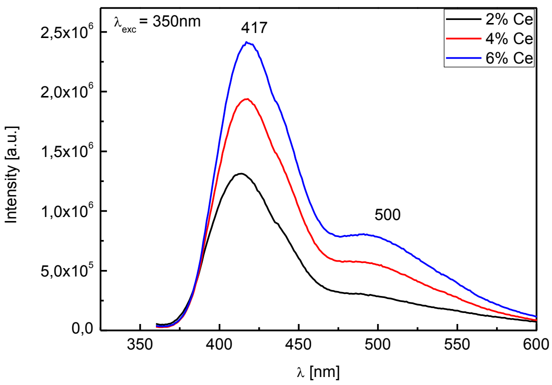

Figure 1 shows the emission spectra of Eu-doped $LaSi_3N_5$ phosphor. These phosphors emit green-yellowish light after excitation with 350 nm UV light. Maximum photoluminescence intensity was observed for the phosphor with 4% Eu from the tested compositions. The small red shift is visible for phosphors doped with 2% Eu.

Figure 2 shows the emission spectra of $LaSi_3N_5$ phosphors doped with several molar concentration of cerium after excitation wavelength 350 nm. Contrary to the previous phosphors, these phosphors emit light in the violet-blue region. Maximum intensity at 417 nm was obtained for phosphors doped with 6 mol% of cerium. The photoluminescence intensity increased with increasing molar concentration of cerium.

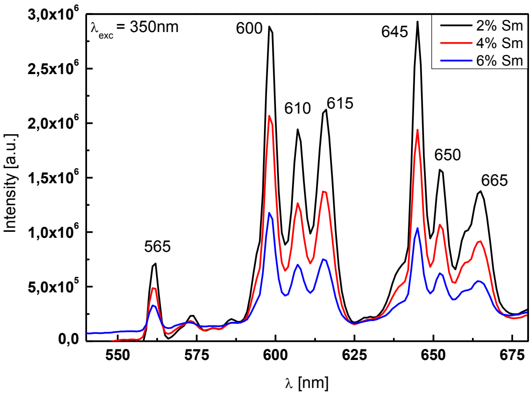

Fig.3. Emission spectra of $LaSi_3N_5$: Sm phosphors.

Figure 3 shows the emission spectra of $LaSi_3N_5$ doped with several molar concentration of samarium. These phosphors emit light in the orange and red region. The highest intensity was obtained for 2 mol% of samarium with a maximum at 645 nm. The photoluminescence intensity decreased with higher molar concentration of samarium, i.e. concentration quenching was observed.

CONCLUSION

By the nitridation of $LaSi/Si/Si_3N_4$ starting powder mixtures doped with Eu_2O_3, CeO_2 and Sm_2O_3 additives $LaSi_3N_5$-based phosphors were prepared. The photoluminescence measurements showed that the $LaSi_3N_5$:Eu-based phosphors emit green light with maximum PL intensity at 560 nm. Phosphors $LaSi_3N_5$ doped with cerium show emission in the violet-blue region with maximum PL intensity at 417 nm. In these phosphors the PL intensity increased with increasing molar concentration of cerium. On the other hand the $LaSi_3N_5$-based phosphor with samarium dopant emits light in the orange and red region with a maxima at 600 nm and 645 nm, respectively. The maximum PL intensity was obtained for the phosphor doped with 2 mol% of samarium. The PL intensity decreased with higher molar concentration of samarium.

ACKNOWLEDGEMENT

This work was financially supported by the projects 7th FP Marie Curie Initial Training Network "Functional Nitrides for Energy Applications (FUNEA)" and VEGA-2/0178/10.

REFERENCES

[1] P.A. Janeway, "Lighting in the Solid State" Am. Ceram. Soc. Bull., **85** 17-20 (2006).
[2] C.J. Humphreys, "Solid State Lighting" Mat. Res. Soc. Bull., **33** 459-70 (2008).
[3] R.J. Xie, N. Hirosaki, Sci. Technol. Adv. Mater., **8** 588-600 (2007).
[4] Z. Lenčéš, K. Hirao, Y. Yamauchi, S. Kanzaki, "Reaction Synthesis of Magnesium Silicon Nitride Powder" J. Am. Ceram. Soc., **86** 1088-93 (2003).
[5] Z. Lenčéš, L. Benco, J. Madejová, Y. Zhou, L. Kipsová, K. Hirao, "Reaction Synthesis and Characterization of Lanthanum Silicon Nitride" J. Eur. Ceram. Soc., **28** 1917-22 (2008).
[6] Z. Lenčéš, M. Hrabalová, A. Czímerová, P. Šajgalík, Y. Zhou, K. Hirao: "Luminescent Properties of Europium-Doped Lanthanum Silicon Nitride Phosphor ", J. Korean Ceram. Soc., **49** 325-327 (2012).

POROVNANIE NANOTVRDOSTI A TRENIA POVLAKOV NA BÁZE WC A CrN

COMPARISON OF NANOHARDNESS AND FRICTION BEHAVIOUR OF WC AND CrN COATINGS

Petra Hviščová[1], *Michal Novák*[1,2] , *František Lofaj*[1,2]

[1]*Ústav materiálového výskumu SAV, Watsonova 47 Košice*

[2] *Materiálovo technologická fakulta STU, Bottova 25, Trnava*

ABSTRACT

The nanohardness and coefficient of friction of DC magnetron sputtered Cr-N and W-C coatings deposited from Cr and WC targets, respectively, in the reactive atmospheres with various fractions of reactive gases were investigated to determine the influence of pressure, reactive gas content and negative bias. The hardness was measured by nanoindenter G200 (Agilent) and the coefficient of friction (COF) by nanotribometer NTR2 (CSM

Instruments). In the case of 50 vol.% of N_2 added into Ar atmosphere under working pressure of 0,5 Pa and negative bias of -30 V, CrN coating hardeness increased from 11-14 GPa for pure Cr coating up to ~ 27 GPa. The highest hardness of W-C coatings was 28 GPa (at 0,25 Pa and 2% of C_2H_2). The COF values of W-C coatings were slightly lower (0.25-0.45) than those measured for CrN coatings (0.3-0.5).

Keywords: *nanohardness, friction coefficient, DC magnetron sputtering, CrN, WC*

ÚVOD

WC a CrN povlaky sa v súčasnosti stávajú veľmi využívanými v priemyselných aplikáciách, najmä kvôli ich odolnosti voči opotrebeniu a zvýšenej tvrdosti. CrN povlaky dosahujú relatívne vysokú tvrdosť (20 – 25 GPa), dobrú adhéziu k podložke a dobrú koróznu odolnosť. Aj napriek tomu, že dosahujú lepšie vlastnosti ako TiN_x povlaky, sú podstatne menej študované [1-5]. Štruktúra, fázové zloženie, veľkosť zŕn, textúra a ich vlastnosti závisia od množstva obsahu dusíka privádzaného do komory počas depozície, teploty podložky a privádzaného záporného predpätia. V závislosti na obsahu dusíka, CrN povlaky môžu pozostávať z niekoľkých fáz Cr, β-Cr_2N, c-CrN a/alebo zmesi týchto fáz a dosahujú tvrdosť 21 – 23 GPa [6-9]. Druhou skúmanou skupinou povlakov sú WC povlaky, ktoré sa vyznačujú vysokou tvrdosťou (~ 40 GPa), prípadne nízkym koeficientom trenia (~ 0,2). Jedným zo spôsobov ako dosiahnuť takéto vlastnosti WC povlakov je vytvoriť nanokompozitnú štruktúru pozostávajúcu z veľkého množstva nanokryštalitov WC v amorfnej matrici z uhlíka alebo DLC [10, 11]. V prípade DC magnetrónového naprašovania dostávame podstechiometrické WC_{1-x} povlaky a preto je nutné pridávať uhlík z reaktívnych plynov. Napríklad Czyzniewski a kol. [12, 13] použili pre tvorbu WC/a-C:H povlakov reaktívne naprašovanie a ako reaktívny plyn pridávali acetylén. Dosiahli tvrdosť až 45 GPa a súčasne pomerne nízky koeficient trenia (~ 0,18). Cieľom práce bolo stanoviť vplyv celkového tlaku, dodatočných reaktívnych plynov a biasu na dosahovanú tvrdosť a koeficient trenia WC a CrN povlakov.

EXPERIMENTÁLNA ČASŤ

Povlaky boli nanášané v zariadení Cryofox Discovery 500 DC magnetrónovým naprašovaním pri konštantnom výkone (WC – 150 W, CrN – 700 W). WC povlaky boli naprašované z WC terča v čistej Ar atmosfére pri tlaku 0,25 – 1,2 Pa, alebo pridaním reaktívnych plynov C2H2, N2, N2+SiH4 a ich kombináciou pri konštantnom tlaku 0,5 Pa a dobe depozície 20 minút. Množstvo reaktívnych plynov bolo od 1 – 5 % z celkového prietoku plynov privádzaných do komory a záporné predpätie privádzané na podložku bolo 0 - -300 V. CrN povlaky boli nanášané z Cr terča pri tlaku 0,2 – 1,2 Pa s 20 % reaktívneho dusíka. Vplyv obsahu dusíka bol stanovený zo série vzoriek pripravených s variabilným prietokom od 0 – 70 % z celkového prietoku plynov. Záporné predpätie bolo v intervale 0 - -300 V. Tvrdosť povlakov bola meraná nanoindentorom Agilent G 200 použitím CSM módu pre tenké povlaky s maximálnou hĺbkou penetrácie 600 nm, konštantnou rýchlosťou zaťažovania 0,05 s-1 a frekvenciou 45 Hz. Koeficient trenia bol meraný pomocou NTR 2 CSM Instruments so zaťažením 300 mN, polamplitúdou 1 mm, rýchlosťou pohybu 3 cm/s a dĺžkou dráhy 1 m (250 cyklov).

VÝSLEDKY A DISKUSIA

Tlak v komore je jedným z parametrov, ktoré ovplyvňujú tvrdosť povlakov. Z literatúry je známe, že optimálnym tlakom pre DC magnetronové naprašovanie WC povlakov je z hľadiska dosahovania zvýšenej tvrdosti tlak do 0,7 Pa. Závislosť tvrdosti na tlaku v komore je zobrazená na obr. 1. Z danej závislosti jasne vyplýva, že s rastúcim tlakom v komore klesá tvrdosť WC povlakov. Najvyššia tvrdosť WC povlakov (20,5 GPa) bola dosiahnutá pri tlaku 0,25 Pa. V prípade CrN povlakov majú hodnoty tvrdosti klesajúci charakter nad 0,7 Pa, pri ktorom bola nameraná najvyššia tvrdosť CrN povlakov ~22 GPa. Pridaním 20 % dusíka do pracovnej atmosféry počas depozície došlo k nárastu tvrdosti (18 – 22 GPa) oproti čistému Cr povlaku, ktorého tvrdosť bola na úrovni 11 – 14 GPa.

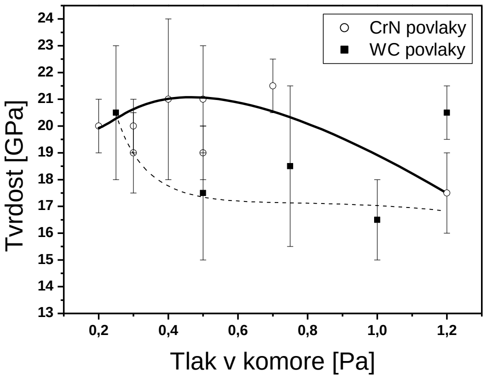

Obr. 1. Vplyv tlaku v komore na tvrdosť povlakov.

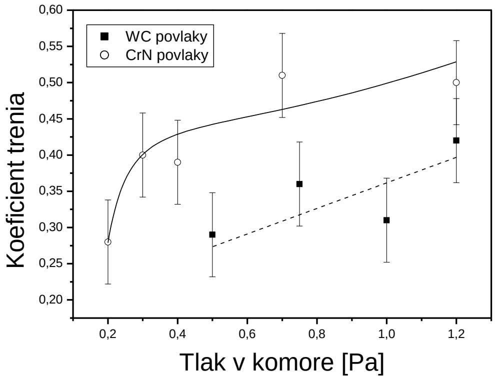

Obr. 2. Závislosť CoF na tlaku v komore.

Obr. 2 zobrazuje závislosť koeficientu trenia na pracovnom tlaku v komore, z ktorej vyplýva nárast koeficientu trenia s rastúcim tlakom. CoF WC povlakov bol na úrovni 0,27 – 0,4 a CoF CrN povlakov dosahoval hodnoty 0,27 – 0,5. Mierny pokles CoF WC povlakov oproti CrN povlakom môže byť spôsobený prítomnosťou voľného uhlíka, ktorý má lubrikačný efekt. Obr. 3 znázorňuje porovnanie závislostí tvrdosti jednotlivých sérií CrN a WC povlakov od druhu napúšťaného reaktívneho plynu a biasu. Najvyššia tvrdosť 28 GPa bola nameraná na vzorke WC 19 pripravenej pri tlaku 0,25 Pa s pridaním 2% acetylénu. Následný pokles na ~ 15 GPa pri tlaku 0,5 Pa, je v zhode s predchádzajúcimi výsledkami, keď s rastúcim tlakom v komore klesala aj tvrdosť WC povlakov. Pridanie dusíka a zmesi dusíka so silánom (SiH_4) viedlo k zvýšeniu tvrdosti povlakov až na 20,6 GPa. To možno vysvetliť pravdepodobne tvorbou karbidov kremíka a dusíka avšak je potrebné povlaky dodatočne analýzovať. Dopovanie kremíkom sa prejaví na zvýšenej tvrdosti v prípade ak je zároveň pridávaný aj acetylén. Vplyv biasu sa v prípade WC povlakov pripravených pri daných podmienkach výrazne neprejavil. V prípade CrN povlakov však malo záporné predpätie pozitívny vplyv na dosahovanú tvrdosť, ktorá sa zvýšila z 22 GPa až na 27 GPa.

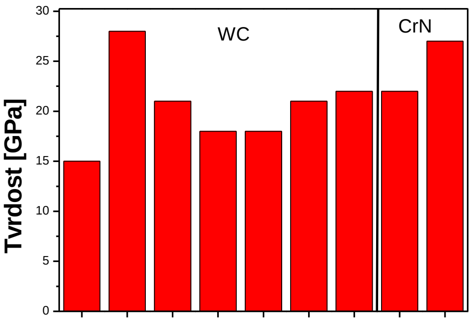

Obr. 3. Závislosť tvrdosti na podmienkach depozície.

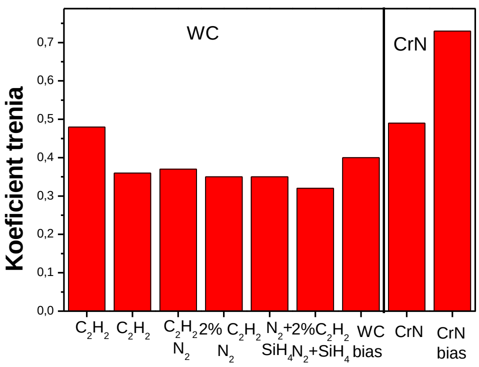

Obr. 4. Vplyv depozičných podmienok na CoF.

Koeficient trenia (obr. 4) WC povlakov dosahoval takmer vo všetkých prípadoch hodnotu ~ 0,35. CrN povlaky mali koeficient trenia o niečo vyšší (~ 0,5) a v prípade biasovaných vzoriek až 0,7. Takýto vysoký koeficient trenia môže byť spôsobený agresívnym abrazívnym mechanizmom opotrebenia tvrdými nitridickými fázami.

ZÁVER

Najvyššia tvrdosť dosiahnutá pri DC magnetrónovom naprašovaní CrN povlakov bola nameraná 27 ± 1 GPa (0,6 Pa, 700W, 50% N_2, -300 V) a koeficientom trenia 0,68. Pre WC povlaky to bolo 28 ± 1,5 GPa (0,25 Pa, 150 W, 2% C_2H_2) s koeficientom trenia ~ 0,35. Z hľadiska hodnôt tvrdosti a koeficientu trenia, ktoré sú požadované pri aplikáciach tenkých povlakov môžeme konštatovať, že WC povlaky sú vhodnejšie, nakoľko obvykle dosahujú vyššiu hodnotu tvrdosti a nižší koeficient trenia ako CrN povlaky.

POĎAKOVANIE

Práca bola realizovaná za podpory projektov: NanoCEXmat II (ITMS č. 26220120035); NanoCEXmat I (ITMS č. 26220120019); a CEKSIM (ITMS č. 26220120056); ktoré sú podporované z Operačného programu "Výskum a vývoj" financovaného prostredníctvom Európskeho Regionálneho Fondu pre podporu vývoja a projektov APVV č. 0520-10 a projektu VEGA č. 2/0108/11.

LITERATÚRA

[1] Liu B.: Corros. Sci. 43, 1953 (2001)
[2] Baba K., Hatata R.: Surf. Coat Technol. 66, 368 (1994)
[3] Ibrahim M. A. M., Korablov S. F., Yoshimura M.: Corros. Sci. 44, 298 (2002)
[4] Navinsek B., Panjan P., Milosev I.: Thin Solid Films 281 – 282, 298 (1997)
[5] Sant S. B., Gill K. S.: Surf. Coat. Technol. 68 – 69, 152 (1994)
[6] Ehisarian A. P., Hovsepian P. E., Hultman L., Helmersson U.: Thin Solid Films 457, 222 (2004)
[7] Foriés E., Escobar Galindo R., Sánchez O., Albella J. M.: Surf. Coat. Technol. 200, 6047 (2006)
[8] Wei G., Scharf T. W., Zhou J. N., Huang F., Weaver M. L., Barnard J. A.: Surf. Coat. Technol. 146/147, 357 (2001)
[9] Lin J., Moore J. J., Mishra B., Sproul W. D., Rees J. A.: Surf. Coat. Technol. 201, 4640 (2007)
[10] Radic N., Grzeta B., Milat O., Ivkov J., Stubicar M.: Thin solid films 320 (1998) 192
[11] Voevodin A. A., O'neill J. P., Zabinski J.S.: Surf. Coat. Technol. 116-119 (1999) 34
[12] Czyzniewski, A.: Thin Solid Films 433 (2003) 180
[13] Czyzniewski A., Precht W.: J. Mat. Proc. Technol. 157-158 (2004) 274

SAMARIUM-DOPED $LaSi_3N_5$: COMPUTED ELECTRONIC STRUCTURE AND BAND GAPS

Ismail A.M. Ibrahim,[a] *Zoltán Lenčéš,*[a] *Ľubomír Benco,*[a,b] *Pavol Šajgalík* [a]

[a]*Institute of Inorganic Chemistry, Slovak Academy of Sciences, Dúbravská cesta 9,*

845 36 Bratislava, Slovakia

[b]*Computational Materials Physics, Vienna University and Center for Computational Materials Science, A-1090, Vienna, Austria*

ABSTRACT

First-principles density-functional theory (DFT) calculations are performed using Vienna Ab initio Simulation Package (VASP) to enhance the understanding of the electronic structure of the stoichiometric $LaSi_3N_5$ and Sm-doped $LaSi_3N_5$. Electronic structure and band gaps are calculated in 2×1×2 super-cell with 144 atoms using the more precise screened Coulomb hybrid functional HSE06. Both La^{3+}/Sm^{3+} and La^{3+}/Sm^{2+} substitutions were calculated. The stoichiometric $LaSi_3N_5$ is an insulator with band gap value of 4.78 eV. The calculated band gap of Sm^{III}-doped $LaSi_3N_5$ is 2.01 eV in good agreement with the experimental value of 2.12 eV. However, the calculated electronic transition will be from *p* band of N and Si to unoccupied Sm spin-up 4*f* states that does not match up with the experimentally observed $4f^N \rightarrow 4f^{N-1}5d$ transition. The calculated band gap of Sm^{II}-doped $LaSi_3N_5$ is 1.43 eV and the calculated electronic transitions are from occupied Sm spin-up 4*f* states to La 5*d*, La 4*f*, or Sm 5*d* states in good agreement with the experimentally observed electronic transitions from Sm 4*f* states to La 5*d* states.

Keywords: *electronic structure; band gap; silicon nitride; plain DFT; hybrid functional HSE06*

INTRODUCTION

Development of efficient and economic luminescence materials has received a great attention. Samarium activated nitride compounds have attracted considerable interest due to their excellent efficient luminescence properties.The crystalline structure and the high thermal and chemical stability of lanthanum silicon nitride ($LaSi_3N_5$) allow its application for conversion phosphors in solid state lighting. Most of UV chip-based commercially available white LEDs adopt a wavelength range from 390 to 410 nm for pumping phosphors. Recently a tendency emerged to shift the excitation wavelength of phosphors to around 400 nm. The calculation of the influence of the dopant on the band gap of the host lattice is a useful tool for reducing the number of necessary experiments for the development of phosphors with required excitation wavelength range. In this work, the optical properties of Sm-doped $LaSi_3N_5$ are complemented with *ab initio* DFT calculations of the electronic structure and band gap of stoichiometric $LaSi_3N_5$ and Sm-doped $LaSi_3N_5$

RESULTS

The electronic structure of stoichiometric $LaSi_3N_5$ calculated using HSE06 is shown in Fig. 1. The valence band is composed of N *p*-orbitals and Si *p*-orbitals. The bottom of the conduction band consists of La 5*d* states at 4.78 eV. The calculated band gap is 4.78 eV. This value compares well with the experimental value of 4.5 eV.

In case of Sm^{III}-doped $LaSi_3N_5$, the calculated electronic structure is displayed in Fig. 2. The Sm spin-up 4*f* states are splitted to occupied and unoccupied states resulted from the configuration of Sm^{3+} [Xe] f^5. The occupied states are shifted down to -5 eV and the unoccupied states are located at ~2.0 eV. In this case, the valence band is still composed of N *p*-orbitals and Si *p*-orbitals. The bottom of the conduction band consists of unoccupied Sm spin-up 4*f* states. The possible electronic transitions will be from N and Si *p* bands to unoccupied Sm spin-up 4*f* states that does not match up with the experimentally observed $4f^N \rightarrow 4f^{N-1}5d$ transition. The calculated band gap is 2.01 eV, this value is in good agreement with the experimental value of 2.12 eV.

In order to have a good explanation to the electronic transition of Sm-doped $LaSi_3N_5$ that observed experimentally, we investigated the doping scheme of Sm^{II}-doped $LaSi_3N_5$. The calculated electronic structure is displayed in Fig. 3. The Sm spin-up 4f states are also split to occupied and unoccupied states resulting from the configuration of Sm2+ [Xe] f6. The occupied states are located at the Fermi level and the unoccupied states are shifted up to ~5 eV. It is observed that the unoccupied Sm spin-down 4f states are located out of the presented scale. In this case, the top of the valence band will be compose of occupied Sm spin-up 4f states. The bottom of the conduction band consists of La 5d, La 4f, and Sm 5d states, so the possible electronic transition will be from occupied Sm spin-up 4f states to La 5d, La 4f, or Sm 5d states. This is in good agreement with the experimentally observed electronic transitions from Sm 4f states to La 5d states. The calculated band gap is 1.43 eV, smaller than for SmIII-doped LaSi3N5 (2.01 eV) and the experimental value of 2.12 eV.

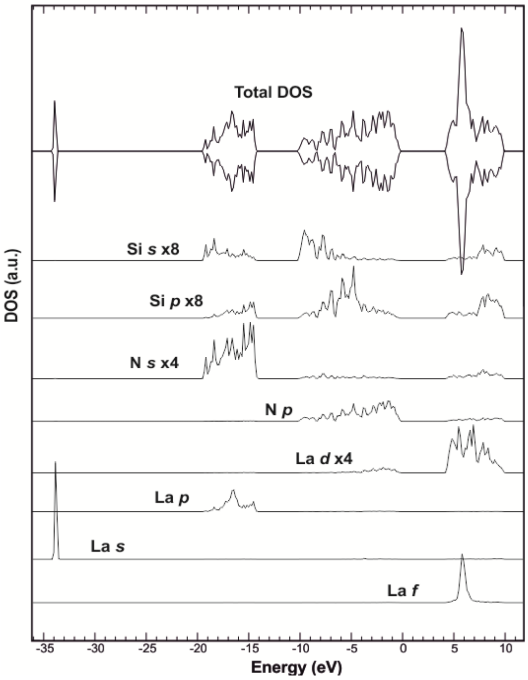

Fig. 1. Total DOS of the stoichiometric $LaSi_3N_5$ and Si-, N-, and La-projected orbital calculated by HSE06.

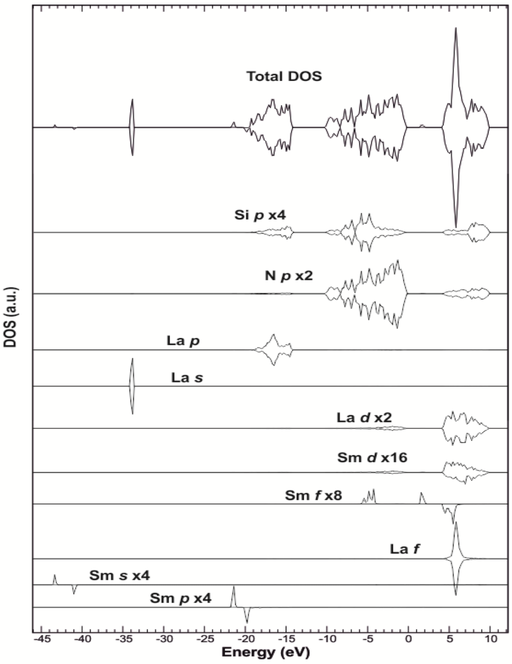

Fig. 2. Total DOS of Sm^{3+}-doped $LaSi_3N_5$ and La-, and Sm-projected orbital calculated by HSE06.

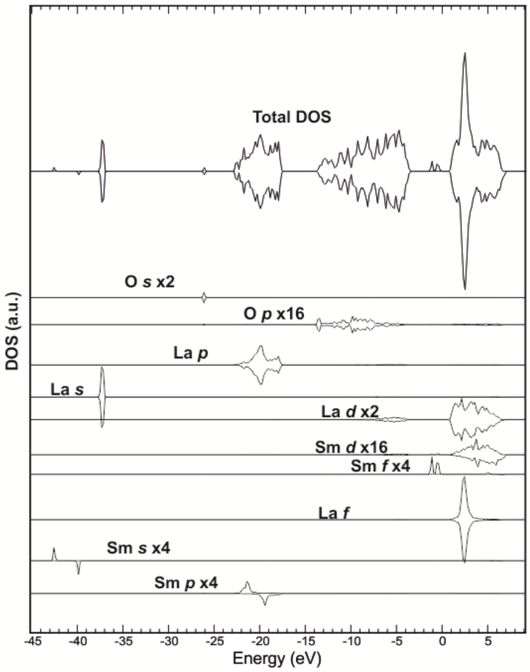

Fig. 3. Total DOS of Sm^{2+}-doped $LaSi_3N_5$ and La-, O- and Sm-projected orbital calculated by HSE06.

CONCLUSION

The electronic structure and band gaps of the stoichiometric $LaSi_3N_5$ and Sm-doped $LaSi_3N_5$ are calculated using HSE06. The stoichiometric $LaSi_3N_5$ is an insulator with band gap value of 4.78 eV separating the occupied states of the *p*-band and the unoccupied La states (4*f* and 5*d* orbitals). The calculated band gap of Sm(III)-doped $LaSi_3N_5$ is 2.01 eV. This value is in good agreement with the experimental value of 2.12 eV. The calculated electronic transition will be from *p* band of N and Si to unoccupied Sm spin-up 4*f* states, what does not match with the experimentally observed transition from Sm 4*f* to La 5*d* states.

The calculated band gap of Sm^{II}-doped $LaSi_3N_5$ is 1.43 eV and the calculated electronic transition is from occupied Sm spin-up 4*f* states to La 5*d*, La 4*f*, or Sm 5*d* states, in good agreement with the experimentally observed electronic transitions from Sm *4f* states to La *5d* states.

ACKNOWLEDGEMENTS

This work was supported by the 7th FP Marie Curie Initial Training Network “FUNEA” (264873) and Slovak Grant Agency VEGA 2/0178/10. This publication is also the result of the project implementation: Effective control of production and consumption of energy from renewable sources (ITMS code 26240220028) supported by the Research & Development Operational Programme funded by the ERDF and the Center of Excellence for Functionalized Multiphase Materials (Fun-Mat).

PEVNOSŤ V ŠTVORBODOVOM OHYBE MATERIÁLOV Si_3N_4-7HM.%GNP PRIPRAVENÝCH RÔZNYMI METÓDAMI

BENDING STRENGTH OF Si_3N_4-7WT.%GNP PREPARED BY DIFFERENT PROCESSING ROUTES

Monika Kašiarová[1]*, Monika Michalková*[2]*, Peter Tatarko*[1]*, Pavol Šajgalík*[2]

[1]*Institute of Materials Research, Slovak Academy of Sciences, Watsonova 47, Košice*

[2]*Institute of Inorganic Chemistry, Slovak Academy of Sciences, Dúbravska cesta 9, Bratislava*

ABSTRACT

The bending strength of silicon nitride with the addition of 7 wt.% of graphene nanoplatelets (GNP) prepared by the different processing routes have been determined. The mean strength of the prepared composites varied for different processing routes from 400 MPa to 750 MPa. It has been shown that composites contain two kinds of the processing flaws – agglomerates of graphene platelets as well as the large grains of the silicon carbide. Taking into account the results of the fractographic analysis and bending strength of the composite prepared by the ultrasonic mixing of graphene and subsequent ball milling constitutes a promising composite for further investigation and optimization of the processing routes.

Keywords: *silicon nitride, graphene platelets, mechanical properties*

INTRODUCTION

Graphene is the atractive nanofiller among carbon based filler thanks to the mechanical, electrical and thermal properties. The positive influence of graphene platelets as a filler in different kind of polymeric materials has already been proved. During the last few years the addition of graphene platelets into the different ceramic and glass matrix has been extensively studied. However, there is a huge discrepancy in the published results concerning the influence of graphene multiplatelets on the mechanical properties of the ceramic composites. Some authors observed the significant improvement of properties others observed no or negligible improvement in mechanical properties.

EXPERIMENTAL MATERIALS AND METHODS

Si_3N_4-7wt.GNP were prepared by five different processing routes and compared with a monolithic silicon nitride. The processing routes can be briefly decribed as follows:

PBM planetary ball mill 4 h, 250 rpm, slurry dried in a rotary evaporator and powder sieved through 125 μm screen.

U-PBM GNPs dispersed in isopropanol by ultrasonification (200 W input power, frequency 20 kHz, amplitude 30 %, 5 min). Then silicon nitride with sintering additives were added and homogenized in planetary ball mill at speed 250 rpm for 4 hrs. Slurry was dried in a rotary evaporator and sieved through 125 μm screen.

U-BM GNPs were dispersed in isopropanol by ultrasonification. Silicon nitride with sintering additives was inserted and mixture was homogenized in ball mill for 24 hrs. Slurry was dried in a rotary evaporator and sieved through 125 μm screen.

U-A GNPs were dispersed in isopropanol by ultrasonification. Later on silicon nitride with sintering additives were inserted and mixture was homogenized in attritor at speed 250 rpm for 4 hrs. The slurry was dried in a rotary evaporator and the powder was sieved through 125 μm screen.

D-BM Homogenisation of Si_3N_4:Al_2O_3:Yb_2O_3 in attritor for 4 hod, 250 rpm, The slurry was dried in a rotary evaporator and the powder was sieved through 125 μm screen. GNPs were added into dried sieved mixture of silicon nitride with sintering aids and homogenized in ball mill for 24 hrs

Ref. SiN reference sample homogenized in attritor without graphene, were homogenized in isopropanol using attritor at speed 250 rpm for 4 hrs. The slurry was dried in a rotary evaporator and the powder was sieved through 125 μm screen.

The strength was estimated in four point bending test at the cross-head speed 0.5 mm/min. The distance of the outer and inner spans was 40and 20 mm, respectively. Fracture surface was investigated using SEM with EDX analyzer.

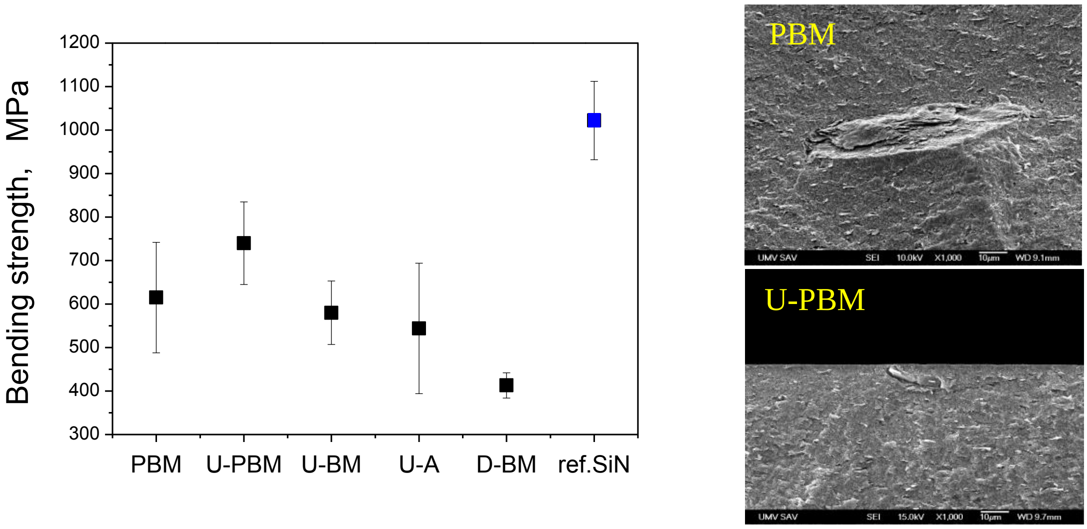

Fig. 1 Bending strength with the characteristic processing flaws

CONCLUSIONS

Material prepared by ultrasonic mixing of graphene and subsequent planetary ball milling has best bending strength with the very small processing flaws. Prolonged ball milling will be used to prevent agglomeration of graphene nanosheets and to decrease the thickness of graphene nanosheets.

ACKNOWLEDGEMENTS

This work was realized within the frame of the projects NanoCEXmat II: ITMS No: 26220120035; NanoCEXmat I: ITMS No: 26220120019; and CEKSIM: ITMS No: 26220120056; which are supported by the Operational Program “Research and Development” financed through European Regional Development Fund and project of APVV 0161-11.

PRÍPRAVA A FYZIKÁLNO-CHEMICKÉ VLASTNIOSTI SKIEL V SÚSTAVE Y_2O_3–Al_2O_3–ZrO_2

PREPARATION AND PHYSICO-CHEMICAL PROPERTIES OF GLASSES IN THE SYSTEM Y_2O_3–Al_2O_3–ZrO_2

R. Klement[1], A. Prnová[1], V. Hronský[2], B. Hruška[1] and D. Galusek[1]

[1] Vitrum Laugaricio – Centrum kompetencie pre výskum skla, spoločné pracovisko UACH SAV, TnUAD a FCHPT STU, Študentská 2, SK-91150 Trenčín

[2]Department of Physics, Faculty of Electrical Engineering and Informatics, Technical University of Košice, Park Komenského 2, SK-042 00 Košice, Slovakia

ABSTRACT

In recent decades, great challenges related to development of high performance materials with excellent high-temperature strength have been encountered. Because of the advantages in superior oxidation resistance, outstanding flexural strength, thermal stability and creep resistance at elevated temperatures, directionally solidified oxide ceramic eutectic in situ composites have attracted a lot of attention, and are considered to be the most promising structural materials for high-temperature structural applications such as turbine blades in oxidizing environments. This promotes a wide search and development of new eutectic oxide ceramics on a global scale. Among a series of single crystal oxides and oxide/oxide eutectics, directionally solidified Al_2O_3/YAG, YSZ/YAG (YSZ = Y_2O_3-stabilized ZrO_2), Al_2O_3/ZrO_2 and Al_2O_3–Y_2O_3–ZrO_2 eutectic ceramics have been demonstrated as the most promising candidates for a new generation of ultra-high temperature structural materials suitable for oxidative environments over a long period of time [1-3]. In the present study, we report on the physical-chemical properties of glasses in the system Y_2O_3–Al_2O_3–ZrO_2. These are studied from the point of view of their structure, crystallization and thermal properties, as promising starting materials which, under suitable temperature-pressure regime, can be compacted to bulk materials with eutectic microstructure, and excellent mechanical properties [4]. The glasses were prepared in the form of glass microspheres with composition derived from Y_2O_3–Al_2O_3 eutectic (76.8 mol. % Al_2O_3, 23.2 mol. % Y_2O_3) and modified by the addition of 5, 10, 15 and 20 mol. % of ZrO_2. The precursor powders for glass microspheres preparation were synthesized via Pechini sol-gel route.

The optical microscopy revealed spherical particles of prepared glasses with diameter up to 30 μm. However, closer inspection by SEM shows regular features (facets) at the surface of some microspheres indicating that some of them were at least partially crystalline, especially those with higher ZrO_2 contents. The composition of prepared glasses was verified by SEM-EDS: the measured values were found to be close to the theoretical (calculated) values. The powder XRD patterns of the glass microbeads are shown in Fig. 1A. Apart of broad amorphous background the XRD patterns of the samples AYZ15MSG and AYZ20MSG revealed also the presence of YAG ($Y_3Al_5O_{12}$) and YSZ phases. Samples AYZ5MSG and AYZ10MSG were found to be XRD amorphous. The DSC records of the glasses microbeads are shown in Fig. 1B. The glass transition temperature (T_g), onset of crystallization temperature (T_x), and the temperature at maxima of the exothermic crystallization peak (T_c) were estimated from DSC curves. The T_g of studied glasses was found to be in the range 865 – 870 °C. As shown in the Fig. 1B, two major crystallization peaks were observed in DSC records; the first sharp peak at temperature ~ 930 °C and the second one broader peak which position is composition dependent. As documented by HT XRD experiments, the first sharp peak found in the DSC curves of prepared glass microspheres with T_x at ~930 °C and T_c at 940 °C corresponds to crystallization of YSZ phase, except of the sample AYZ5MSG. The second crystallization peak, observed for the samples AYZ10MSG, AYZ15MSG and AYZ20MSG, which position is compositional dependent, corresponds to the crystallization of YAG phase, as documented by the results of HT XRD experiments. YAG was the only phase found to crystallize from the AYZ5MSG glass. The results of HT XRD by means of the temperature intervals of crystallization of individual phases are in excellent agreement with crystallization temperatures determined by DSC measurements. Detailed analysis of the HT XRD patterns of all studied systems, together with the results of the study of crystallization kinetics of one selected system AYZ15MSG, are presented.

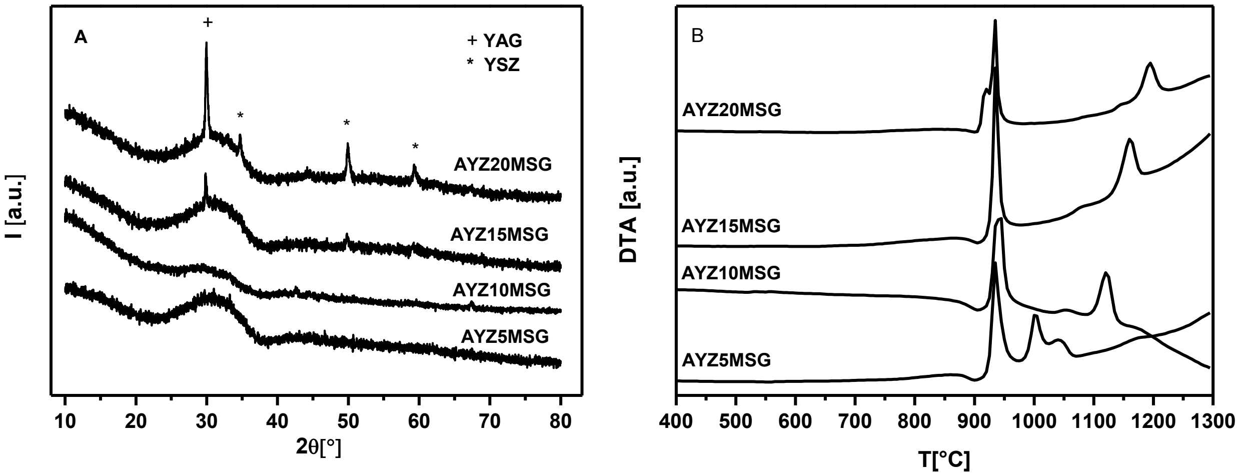

Fig.1 The XRD diffraction patterns of glass microbeads prepared from Pechini sol-gel method (A) and corresponding DSC traces of the glasses.

The structure of prepared glasses has been examined by ^{27}Al MAS NMR spectroscopy. The spectra of all studied AYZ glasses show very similar features and contain three broad lines observed at ~76 ppm, ~45 ppm and ~14 ppm, corresponding to four ($^{[4]}$Al), five ($^{[5]}$Al) and six-coordinated ($^{[6]}$Al) Al species, respectively. For the sample AYZ20, another signal of $^{[4]}$Al species at ~85 ppm was observed. The broad lines are due to the distribution of quadrupolar coupling and chemical shifts inherent to the structural disorder that is observed in glasses. The simulation of the NMR spectra (including quadrupolar broadening of the central lines) revealed that relative abundance (based on the integral intensity of spectral lines) of the $^{[4]}$Al, $^{[5]}$Al and $^{[6]}$Al species change with composition of the glasses and the predominant Al species are $^{[4]}$Al. With increasing content of ZrO_2 increases also the abundance of $^{[5]}$Al and $^{[6]}$Al species, while abundance of $^{[4]}$Al species decreases. This indicates that ZrO_2 behaves as glass modifying oxide that stabilizes the aluminate structure network.

Keywords: *Aluminate glasses, ZrO_2, thermal properties, crystallization kinetics, HT XRD*

ACKNOWLEDGEMENT

The financial support of this work by the bilateral project (Slovakia–Taiwan) SAS-NSC JRP 2012/14 is gratefully acknowledged. This work was carried out in the frame of the project „Centre of Excellence for Ceramics, Glass and Silicate Materials“, ITMS code 262 201 20056, based on the Operational Program Research and Development funded from the European Regional Development Fund.

REFERENCES

[1] Oelgardt C., Anderson J., Heinrich J.G., Messing G.L: Sintering, microstructure and mechanical properties of Al_2O_3–Y_2O_3–ZrO_2 (AYZ) eutectic composition ceramic, J. Eur. Ceram. Soc., 30, 649–656 (2010).

[2] Harada Y., Uekawa N., Kojima T., Kakegawa K.: Fabrication of $Y_3Al_5O_{12}$-Al_2O_3 eutectic materials having ultra fine microstructure, J. Eur. Ceram. Soc., 28, 235–240, (2008).

[3] Su H., Zhang J., Yu J., Liu L., Fu H.: Rapid solidification and fracture behavior of ternary metastable eutectic Al_2O_3/YAG/YSZ *in situ* composite ceramic, Mater. Sci. Eng. A, 528, 1967–1973, (2011).

[4] A. Prnová, D. Galusek, M. Hnatko, J. Kozánková, I. Vávra, Composites with eutectic microstructure by hot pressing of Al_2O_3–Y_2O_3 glass microspheres, Ceramics – Silikáty, 55 [3] 208-213 (2011)

VPLYV PRÍDAVKU H-BN NA MECHANICKÉ VLASTNOSTI A ODOLNOSŤ VOČI OPOTREBENIU BN/Si_3N_4 KOMPOZITOV

INFLUENCE OF H-BN CONTENT ON MECHANICAL PROPERTIES AND WEAR RESISTANCE OF BN/Si_3N_4 COMPOSITES

Alexandra Kovalčíková[1], Ján Balko[1], Csaba Balázsi[2], Ján Dusza[1], Pavol Hvizdoš[1]

1Institute of Materials Research, Slovak Academy of Sciences, Watsonova 47, 040 01 Košice, Slovakia

2Bay Zoltan Nonprofit Ltd for Applied Research, Institute for Materials Science and Technology, Budapest

ABSTRACT

Silicon nitride materials containing 1-5 wt % of hexagonal boron nitride were prepared by hot-isostatic pressing at 1700°C for 3h. Different type of BN powder (micro BN or nano BN) has been used as reinforcement material. Effect of BN content on microstructure, mechanical and tribological properties has been investigated. As expected, the increase of BN content resulted in a sharp decrease of hardness (from 14 to 7.5 GPa), Elastic modulus (from 240 to 170 MPa) and strength (from 600 MPa to 300 MPa) of BN/Si_3N_4 micro/microcoposites and BN/Si_3N_4 nano/microcomposites. In addition, the fracture toughness of BN/Si_3N_4 ceramics is similar to monolithic Si_3N_4 (in interval of 6.5-7 MPa.m$^{1/2}$). The friction coefficient slightly decrease in the case of BN/Si_3N_4 micro/microcoposites. An improvement of wear resistance (one order of magnitude) occurs when the BN was added to Si_3N_4 matrix.

Keywords: *BN/Si_3N_4 composite, microstructure, mechanical properties, wear resistance*

INTRODUCTION

Silicon nitride has very good combination of mechanical, physical, and chemical properties. The high strength, hardness, and toughness at room and elevated temperatures, the high thermal shock and wear resistance make it suitable for use in several structural and tribological applications. It is well known that h-BN offers a number of interesting properties such as lubrication action, low hardness and low friction coefficient. Hexagonal boron nitride has also excellent machinability due to a plate-like structure similar to that of graphite. To improve the machinability and tribological properties of Si_3N_4 ceramics at elevated temperatures, hexagonal boron nitride particles were introduced as second-phase dispersions into the Si_3N_4 matrix.

RESULTS

The microstructure of BN (1wt %) /Si_3N_4 nano/micro composite consisted mainly of elongated β-Si_3N_4 grains, equaixed β-Si_3N_4 grains, BN particles and intergranular phase. Different from the BN/Si_3N_4 micro/microcomposite, no large BN platelets or aggregates were found in the nanocomposites. The microstructure of BN (5 wt %) /Si_3N_4 micro/micro composite consisted of large h-BN platelets. The distribution of h-BN was quite uniform but the agglomeration of bundles of micro BN were still observed. Micro BN added samples had significantly larger porosity than reference monolithic sample and nano/microcomposite. As expected, the Vickers hardness, Elastic modulus and bending strength of the composites significantly decreased with increasing content of BN. The fracture toughness of BN/Si_3N_4 micro/microcomposites was slightly improved, mainly at 5 wt% BN addition, fig.2. The fracture toughness of nano/microcomposite was comparable with monolith. In our case the addition up to 5 wt% of BN had a positive effect on wear resistance of BN/Si_3N_4 composite ceramics, fig.3.

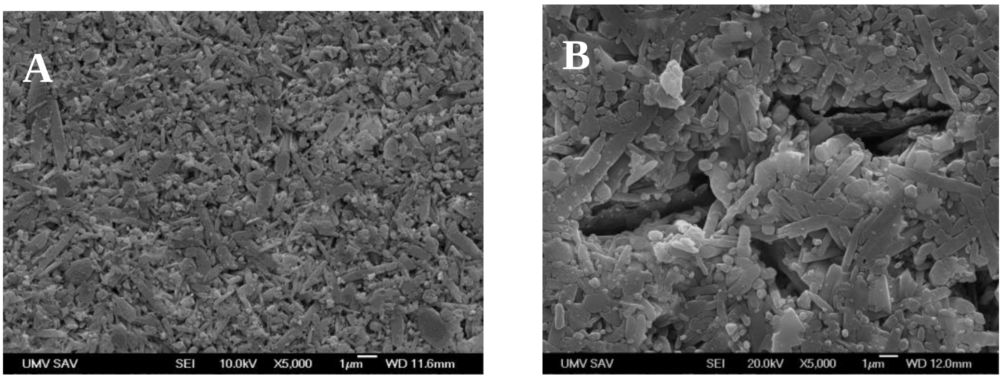

Fig.1 SEM micrographs of a) BN (1wt %) /Si_3N_4 nano/micro composite; b) BN (5wt %) /Si_3N_4 micro/micro composite

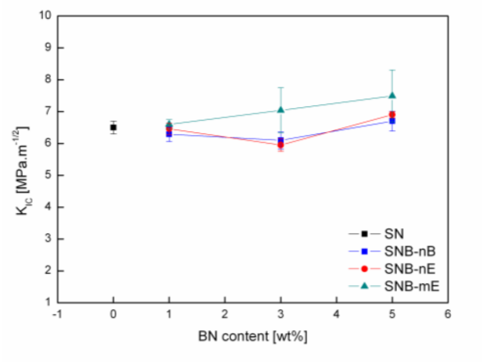

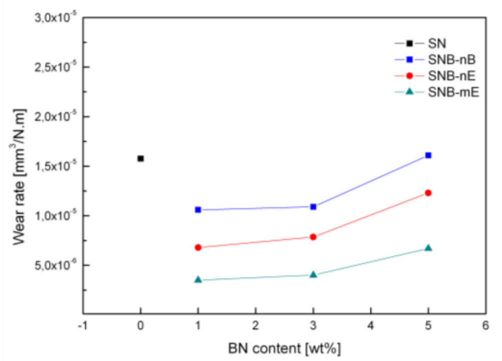

Fig.2 Coefficient of friction versus BN content of experimental materials
Fig.3 Specific wear rate versus BN content of experimental materials

CONCLUSION

The homogenous dispersion of BN particles into the matrix is probably an effective way to ensure the mechanical properties of BN/Si_3N_4 composite ceramics. The positive effect of BN on friction is accompanied by an increase in wear resistance only when low BN content (up to 5 wt %) is added to the Si_3N_4. The addition of small quantity of BN can increase the fracture toughness of Si_3N_4 ceramic matrix because different type of toughening mechanisms could be observed in these microstructures.

ACKNOWLEDGEMENTS

This work was realized within the frame of the projects NanoCEXmat II: ITMS No: 26220120035; NanoCEXmat I: ITMS No: 26220120019; and CEKSIM: ITMS No: 26220120056; which are supported by the Operational Program “Research and Development” financed through European Regional Development Fund and by projects APVV 0161-11, APVV-0500-10 and by LPP 0203-07.

VPLYV SPRACOVANIA NA LOMOVÚ HÚŽEVNATOSŤ Si_3N_4 + S GRAFÉNOVÝMI PLATNIČKAMI

INFLUENCE OF PROCESSING ON FRACTURE TOUGHNESS OF Si_3N_4 + GRAPHENE PLATELET COMPOSITES

Lenka Kvetková[a,] , *Annamária Duszová*[a], *Monika Kašiarová*[a], *Františka Dorčáková*[a],
Ján Dusza[a,b], *Csaba Balázsi*[c]

[a] *Institute of Materials Research, SAS, Watsonova 47, 04353 Košice, Slovak Republic*

[b] *Óbuda University, Donát Bánki Faculty of Mechanical and Safety Engineering, Budapest,*

[c] *Bay Zoltan Nonprofit Ltd for Applied Research, Institute for Materials Science and Technology, 1116 Budapest*

ABSTRACT

Silicon nitride + 1 wt% graphene platelet composites were prepared using various graphene platelets (GPLs) as a filler. Two different sintering routes were applied: the hot isostatic pressing (1700 ^{0}C/3h/20 MPa) and the gas pressure sintering (1700^{0}C/0h/2 MPa). In this work, an influence of the GPLs addition and of processing routes on the fracture mechanism of Si_3N_4+GPLs was investigated. In the both sintering routes, the main toughening mechanisms which originated from the presence of the graphene platelets are crack deflection, crack branching and crack bridging. These mechanisms are responsible for an increase of fracture toughness which is higher than that of monilitic Si_3N_4. The highest value of fracture toughness was obtained in case of the hot isostatic pressing.

Keywords: *HIP, GPS, graphene platelets, Si_3N_4*

INTRODUCTION

During the last few years new cost effective, high quality carbon based filamentous was developed in the form of graphene platelets (GPLs), also called graphene nanoplatelets (GNP), multilayer graphene nanosheets (MGN) or graphene nanosheets (GNS). These platelets demonstrates exceptional high thermal and electrical conductivity and an exceptional combination of mechanical properties **[1].** Number of authors have reported improved mechanical and functional properties in the case of these composites compared to the monolithic ceramics. Graphene, as a monolayer of sp2-hybridized carbon atom arranged in a two-dimensional lattice, has attracted tremendous attention in recent years owing to its exceptional mechanical, thermal and electrical properties. Graphene has been produced by several routes **[2],** including growth by chemical vapor deposition, micro-mechanical exfoliation of graphite, and growth on crystalline silicon carbide. These platelets usually contain several graphene layers in contrast to the mono-layered graphene. Nano-scaled graphene plates of several desired size ranges (e.g., length and width of approximately 0.05 to 10 microns and thickness of approximately 1 to 10 nm). There are up to now only a few reports used of graphene platelet additives to improve the mechanical properties of bulk silicon nitride ceramics. Walker et al **[3]** used spark plasma sintering for preparation of Si_3N_4 + GPLs composites with fracture toughness of 6.6 MPa.m$^{0.5}$ for the systems with 1.5 vol% of GPLs.

The aim of this work is to investigate the HIP and GPS processing route for the preparation of dense Si_3N_4 based ceramics at the addition of several types of graphene platelets and their effect on fracture toughness this way prepared composites.

EXPERIMENTAL PROCEDURES

The starting powders were: 90wt%Si_3N_4 (Ube, SN-ESP), 4wt%Al_2O_3 and 6wt%Y_2O_3 4 wt% Al_2O_3 (Alcoa, A16) and 6 wt% Y_2O_3 (H.C. Starck, grade C) to aid the sintering process. Polyethylenglycol (PEG) surfactants and deionized water were added to the powder mixture. These mixtures were milled in high efficient attritor mill (Union Process, type 01-HD/HDDM) equipped with zirconia agitator delta discs (volume of 1400 cm^3) and zirconia grinding media (diameter of 1 mm) in a 750 ml silicon nitride tank. Each batch contained zirconia as contamination from media and discs. This milling process has been performed whith high rotation speed 3000 rpm until 4.5 h. **[4].**

Four types of Grapnene platelets were used: **GPL – 1:** Multilayer graphene nanosheets prepared by mechanical milling method with average thickness of 14 nm and average particle diameter 3 µm; **[5]**; **GPL – 2:** Commercially available GNPs (Angstron Materials LLC, USA): exfoliated graphene nanoplatelets xGnP-M-5 with average thickness of 7 nm and average particle diameters of 5 µm, **GPL-3**: exfoliated graphene nanoplatelets xGnP-M-25 with average thickness of 7 nm and average particle diameters of 25 µm and a typical surface area of 120 to 150 m²/g **[6]**; and **GPL- 4**: nanographene platelets Angstron N006-010-P with average thickness of 15 nm and average particle diameters of 14 µm **[7]**. These types of GPLs are illustrated at **Fig.1.**

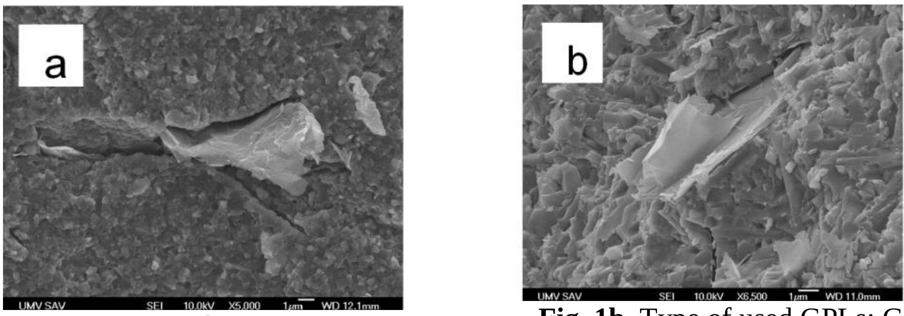

Fig. 1a Type of used GPLs: GPL-1: Multilayer graphene nanosheets

Fig. 1b Type of used GPLs: GPL-2: Exfol. graphene nanoplatelets xGnP-M-5

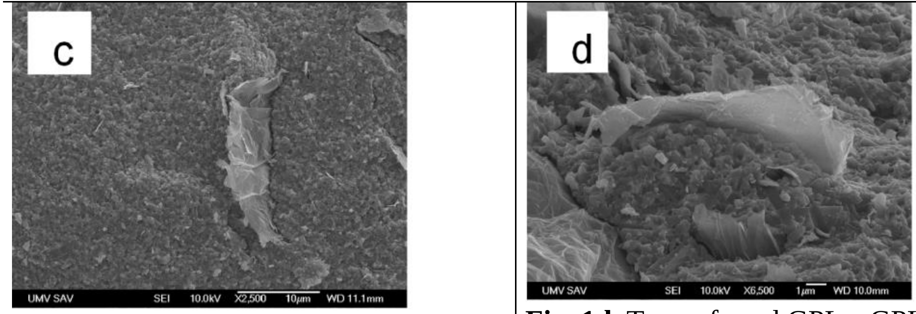

Fig. 1c Type of used GPLs: GPL-3: Exfol. graphene nanoplatelets xGnP-M-25

Fig. 1d Type of used GPLs: GPL-4: Nano graphene platelet Angstron N006-010-P

Fig. 1 Used Type of GPLs

Two different processing routes have been applied for the densification. Hot isostatic pressing (HIP) was performed at 1700°C at 20 MPa pressure of high purity nitrogen, with a 3 h holding time in BN embedding powder. Gas pressure sintering (GPS) was employed at 1700°C at 2 MPa pressure of high purity nitrogen, without holding time in BN embedding powder. The heating rate did not exceed 25°C/min.

The experimental materials were characterized by SEM (JSM – JEOL 7000F). Indentation fracture toughness testing was performed at loads of 147 N using a Vickers indenter (Leco Instruments), and the K_{IC} calculation was calculated using the Shetty equation (1) **[8]**.

$$KI_{CI}nd = 0.0899(H.P/4l)^{1/2} \qquad (1)$$

where H is the hardness, P is the indentation load and l = c - a is the length of the indentation crack.

RESULTS AND DISCUSSION

Characteristic fracture surface of the two monolithic materials is illustrated in **Fig. 2**.

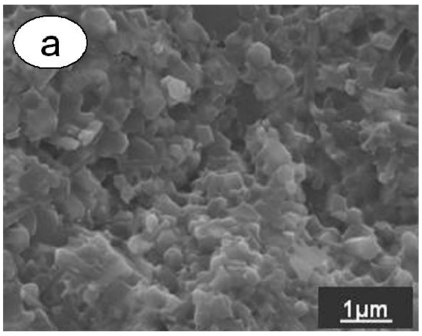

Fig 2a Fracture surface of Si_3N_4 - processed by GPS

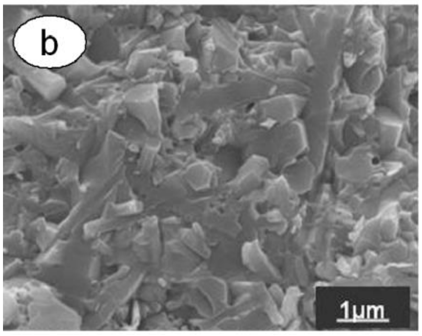

Fig.2b Fracture surface of Si_3N_4 - processed by HIP

The hardness and indentation fracture toughness of the investigated materials are listed in **Table 1.**

***Table 1** The hardness and indentation fracture toughness of the GPS investigated materials*

Composition of investigated materials [wt%]				**GPLs aditives**	**Hardness HV1 [GPa]**		**Fracture Toughness K_{Ic} [MPa.m$^{0.5}$]**	
Si_3N_4	**Al_2O_3**	**Y_2O_3**	**C**		**GPS**	**HIP**	**GPS**	**HIP**
90	4	6	0	-	16.2 ± 0.3	16.4 ± 0.4	6.3± 0.2	6.5 ± 0.2
90	4	6	1	GPL - 2	14.9 ± 0.5	14.6 ± 0.3	6.7 ± 0.4	7.8 ± 0.4
90	4	6	1	GPL - 3	14.7 ± 0.4	15.1 ± 0.3	6.1 ± 0.3	8.6 ± 0.2
90	4	6	1	GPL - 4	15.3 ± 0,2	14.6 ± 0.4	7.6 ± 0.2	8.9 ± 0.4
90	4	6	1	GPL - 1	16.3 ± 0.4	16,4 ± 0,4	8.5 ± 0.4	9,9 ± 0,4

Beside the system reinforced by multilayer graphene nanosheets GPL1 all composites exhibit lower hardness in comparison to the hardness of monolith. This is a result of the un-sufficient sintering and the present porosity around the graphene platelets. The density of the sintered materials measured by Archimedes method were 3,32 – 3,37 g/cm^3**[4]**. The GPS monolithic silicon nitride show slightly lower fracture toughness in comparison to the silicon nitride prepared by HIP. This is connected with the different microstructure of these systems. The differences in microstructure and properties of the sintered bodies, prepared by GPS and HIP, can be attributed to the dissimilar techniques as well as to the different sintering conditions. The monolithic Si_3N_4 and composites prepared by GPS exhibit smaller grain size in comparison to HIP materials with an average grain diameter/width of Si_3N_4 matrix grains of all composites approximately 0.2 µm. The average grain width of Si_3N_4 grains in HP composites is in the interval from 0.3 to 0.5 µm. The toughening mechanisms on the fracture line and fracture surface during the crack propagation was observed.

CONCLUSION

Graphene platelets added silicon nitride (GPL/Si_3N_4) composites with various GPLs have been prepared and the influence of the type of GPLs and processing on the fractography, toughening mechanisms and fracture toughness was studed.

- The matrix of the composites prepared by GPS consist of Si_3N_4 grains with smaller diameter and aspect ratio in comparison to the composite prepared by HIP.
- The indentation fracture toughness of the composites was in the range 6.69 – 9.92 MPam$^{0.5}$, which is significantly higher compared to the monolithic silicon nitride 6.9 and 6.8 MPam$^{0.5}$,

respectively.The highest value of K_{IC} was 9.92 $MPam^{0.5}$ in the case of composite reinforced by smallest multilayer graphene nanosheets, prepared by HIP. The composites prepared by GPS exhibit lower fracture toughness from 6.69 to 8.1 $MPam^{0.5}$.

REFERENCES

[1] G. Wang, J. Yang, J. Park, X. Gou, B. Wang, H. Liu, et al., J. Phys. Chem. 112, 819 - 825(2008)
[2] Y. Zhu, S. Murali, W. Cai, X. Li, J. W. Suk, J. R. Potts: Advanced Materials, Vol. 22, 2010, p. 3906-3924
[3] L. S. Walker, V. R. Marotto, M. A. Rafiee, N. Koratkar, E. L. Corral: Ceramic Composites, Vol. 5, 2011, No. 4, p. 3182–
[4] P. Kun, O. Tapaszto, F.Weber, Cs. Balaszi, Ceram. Int. 38, 211 (2012)
[5] P. Kun, F.Weber, Cs. Balaszi, Cent. Eur J. Chem 9, 47 – 51 (2011)
[6] http://www.xgsciences.com.
[7] http://angstronmaterials.com.
[8] D.K. Shetty, I.G. Wright, P.N. Mincer, A.H. Clauser, J.Mater. Sci. 20, 1873 (1985)

ACKNOWLEDGEMENT

This work was realized within the frame of the projects NanoCEXmat II: ITMS No: 26220120035; NanoCEXmat I: ITMS No: 26220120019; CEKSIM: ITMS No: 26220120056; and SVIP: ITMS No: 26220220053 which are supported by the Operational Program “Research and Development” financed through European Regional Development Fund and projects of APVV with number 0161-11, VEGA 2/0122/12 and CE SAS CLTP-MREC.

MODELOVANIE NAPÄTÍ V DENTÁLNOM IMPLANTÁTE A KOSTI

MODELING OF STRESS DISTRIBUTION IN DENTAL IMPLANT AND BONE

Dušan Németh[1], František Lofaj[1], Ján Kučera[2], Vladimír Ivančo[3]

[1]Institute of Materials Research, Slovak Academy of Sciences, Watsonova 47, 040 01 Košice, Slovak republic

[2]STONEK, s.r.o., Krivá 23, 040 01 Košice, Slovak republic

[3]Technical University of Košice, Faculty of Mechanical Engineering, Letná 9, 042 00 Košice, Slovak republic

ABSTRACT

The aim of this work is the modeling of the stress distribution in cortical and trabecular bone of model frontal part of mandible by FEM analysis using linear static methods applying monocortical and bicortical fixation of dental implant. Depending on the position of the screw thread with regard to the bone surface, three different cases were simulated: exactly on the bone surface, 1,5 mm above and 0,5 mm below the surface of the cortical bone. It was found out that the stress field in the cortical part and the implant are cobsiderably lower in the case of slightly recessed position in contrast with the above and normal position of the implant in both, monocortical and bicortical fixations. However, the bicortical fixation in this case generates slightly lower stress field in the bone and implant parts than in monocortical fixation. Monocortical fixation is otherwise slightly more favorable from the viewpoint of maximum stresses in the bone in the case of exact and above positions of the implant.

Keywords: *modelling, stress distribution, implants, bone, FEM analysis*

ÚVOD

Aplikácia implantátu v prednej časti dolnej sánky je problémom nielen chirurgickým, biochemickým, biofyzikálnym, ale tiež biomechanickým. Žuvacie sily, pôsobiace na zubné implantáty, môžu vyvolávať nežiaduci tlak v priľahlých kostiach, čoho následkom môže byť poškodenie okolitého kostného tkaniva a následné zlyhanie implantátu, prípadne poškodenie vlastného tela implantátu. Z toho hľadiska je dôležité poznať, aké napätia vznikajú pri zaťažení implantátov rôznej geometrie v kosti. Na rozloženie napätí v kosti a implantáte sa používajú metódy numerickej aproximácie konečných prvkov aplikované na samotný implantát, ako aj kortikálnu aj spongióznu kosť. Implantáty bývajú v kosti uchytené dvoma spôsobmi: monokortikálne alebo bikortikálne (obr.1). U mono-kortikálneho zaťaženia dochádza k spojeniu implantátu s hustou a pevnou kortikálnou kosťou len v oblasti krčku implantátu. Jeho dolná časť je uložená len v mäkšej a pórovitej spongióznej kosti. Takéto spojenie kladie vysoké nároky na prenos žuvacieho tlaku v kortikálnej kosti zvlášť pri vertikálnom zaťažení. Bikortikálne kotvenie, kedy je implantát uchytený do kortikálnej kosti aj v oblasti hrotu implantátu, predpokladá zvýšenie odolnosti voči vertikálnemu zaťaženiu a kvôli tomu aj proporcionálnejšie rozdelenie zaťaženia.

Cieľom danej práce je porovnanie rozloženia napätí v kortikálnej kosti pri mono a bikortikálnom fixovaní implantátu ako aj určenie vplyvu hĺbky zavŕtania implantátu vzhľadom na okraj kortikálnej kosti.

EXPERIMENT

MATERIÁL A METÓDA

Pre tento experiment sa použila metóda konečných prvkov (MKP) s lineárne statickou analýzou. Výpočtové modely sa vytvárali v programe Solidworks pre monokortikálne a bikortikálne upevnenie implantátu. Pri týchto upevneniach sa simulovali tri prípady vnorenia implantátu vzhľadom na kortikálnu kosť: situovanie závitu implantátu presne po okraj kosti, 1,5 mm nad úroveň a 0,5mm pod úroveň povrchu kortikálnej kosti. Výpočtové modely boli zostavené pre implantát, kortikálnu aj spongióznu kosť. Na modelovanie implantátu bol použitý reálny typ implantátu SVMB 3,0-14D (firma Martikan, SR). Tento implantát je špecifický tým, že sú na ňom vytvorené tri výrezy, aby dochádzalo k lepšiemu obrastaniu implantátu kosťou. Rozmerové charakteristiky pre jednotlivé časti boli nasledovné: dĺžka implantátu 17 mm, stúpanie závitu implantátu 1,25 mm, priemer implantátu 3 mm, hrúbka kortikálnej kosti po celom obvode bola 2 mm a výška kosti pre bikortikálne upevnenie 13,5 mm. V prípade monokortikálneho upevnenia bola výška kosti 14,5 mm, aby sa zabezpečilo upevnenie implantátu iba v hornej časti kortikálnej kosti. Materiálové charakteristiky implantátu a kosti potrebné pre MKP sú v tab. 1.

Tabuľka 1 Materiálové charakteristiky pre MKP.

	Kortikálna kosť	Spongiózna kosť	Implantát Ti-Al6-V4 Gr.5
Modul pružnosti E [MPa]	$13{,}7\times10^3$	$2{,}3\times10^3$	$1{,}14\times10^5$
Poissonov sučiniteľ μ [-]	0,3	0,3	0,3

Geometrické okrajové podmienky simulovali upevnenie kosti v prednej časti sánky. Fyzikálne okrajové podmienky definovali zaťažovanie implantátu vertikálne na sánku, kolmo na sánku a pozdĺž sánky. Ako sily pôsobiace v jednotlivých smeroch boli použité F_x=114,6N; F_y=17,1N; F_z=23,4 N, ktoré boli vybraté na základe literárnych zdrojov [2,3]. Zložky sily pôsobili 11 mm nad kosťou (obr. 2). Po určení všetkých potrebných parametrov nasledovalo vytvorenie siete konečných prvkov. Sieť bola vytvorená z 356734 tetrahedrálnych elementov a 483353 uzlov.

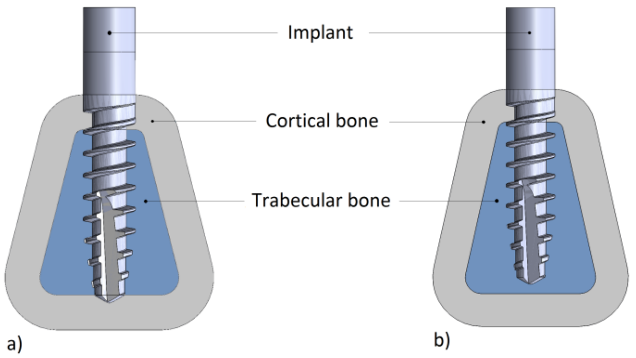

Obr. 1 Upevnenie implantátu a) bikortikálne b) monokortikálne.

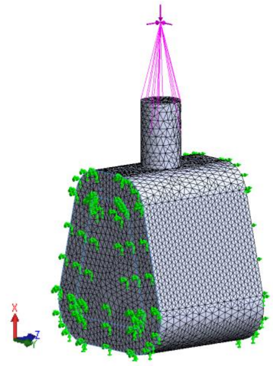

Obr. 2 Geometrické a fyzikálne okrajové podmienky

VÝSLEDKY

Na obr. 3 a obr. 4 je zobrazené koncentrácia napätí v implantáte a kosti v bi resp. monokortikálnom upevnení v prípade mierneho zapustenia implantátu 0,5 mm do kosti.

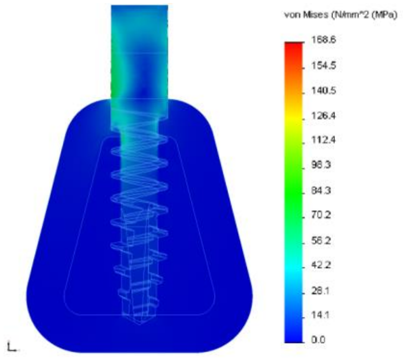

Obr. 3 Bikortikálneupevnenie implantátu do kortikálnej kosti

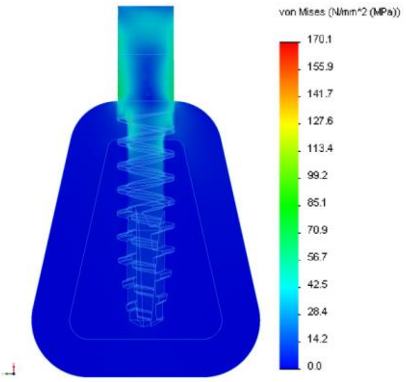

Obr. 4 Monokortikálne upevnenie implantátu do kortikálnej kosti.

Zo stupnice vidno, že rozdelenie napätí je v bikortikálnom prípade homogénnejšie a maximálne napätia sú nižšie, ako v prípade monokortikálneho upevnenia implantátu. Maximálne napätia bikortikálne upevneného implantátu boli σ_{max}=168,6 MPa zatiaľ čo v monokortikálnom prípade σ_{max}= 170,1 MPa. Koncentrácia týchto napätí v implantáte je detailne zobrazená na obr. 5 a obr. 6. Ako je vidieť, maximálne napätia sa koncentrujú v miestach, kde implantát vystupuje z kosti von. To je zapríčinené tým, že implantát sa v týchto miestach správa ako votknutý nosník.

Na obr. 7 je zobrazený priebeh napätí pozdĺž implantátu smerom k spodnej časti. Uzli boli vybraté na línií od miesta kde implantát vystupuje z kosti von po prvý zub smerom na dol, keďže v tejto oblasti bola koncentrácia napätí najväčšia.

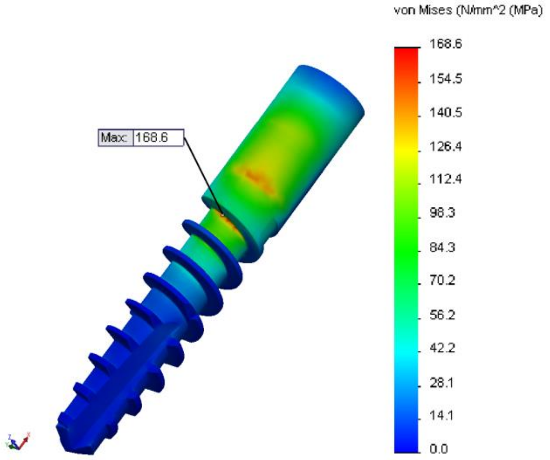

Obr. 5 Rozloženie napätí v implantáte pri bikortikálnom upevnení.

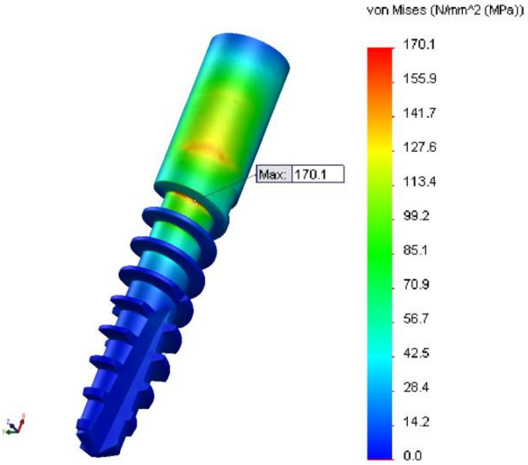

Obr. 6 Rozloženie napätí v implantáte pri monokortikálnom upevnení.

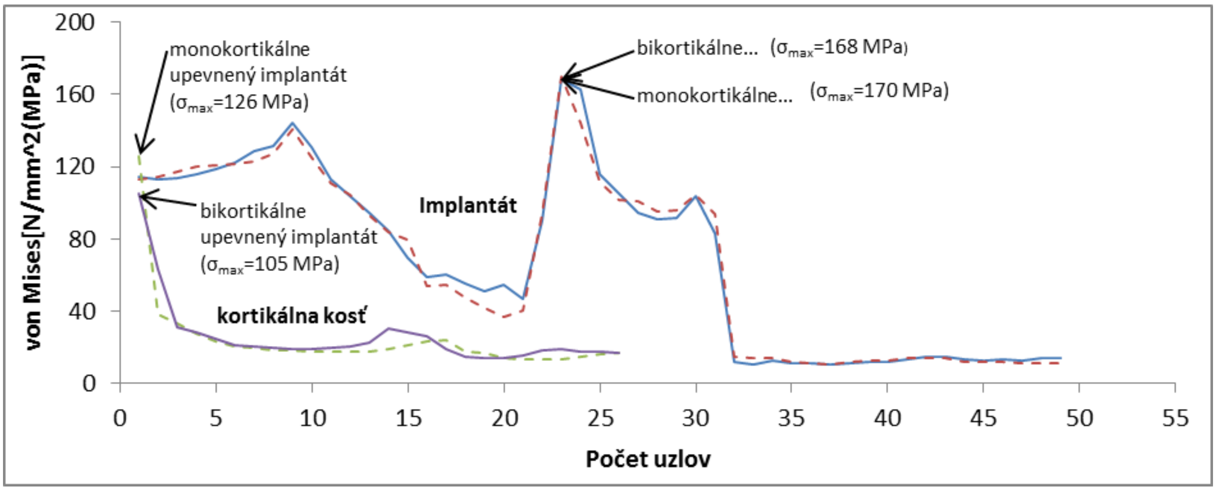

Obr. 7 Porovnanie priebehov napätí v implantáte a kortikálnej kosti pri bikortikálnom a monokortikálnom upevnení.

Hodnoty maximálnych napätí v kortikálnej kosti pri bikortikálnom upevnení boli σ_{max} = 105,2 MPa (obr. 8) a pri monokortikálnom σ_{max} = 126,1 MPa (obr. 9). Rozdiely v napätiach sú teda podstatne väčšie. Tak ako v prípade implantátu aj u kortikálnej kosti sa najväčšie napätia sústredili v hornej časti kosti. Rozloženie napätí pozdĺž línie maximálnych napätí sú porovnané na obr. 7.

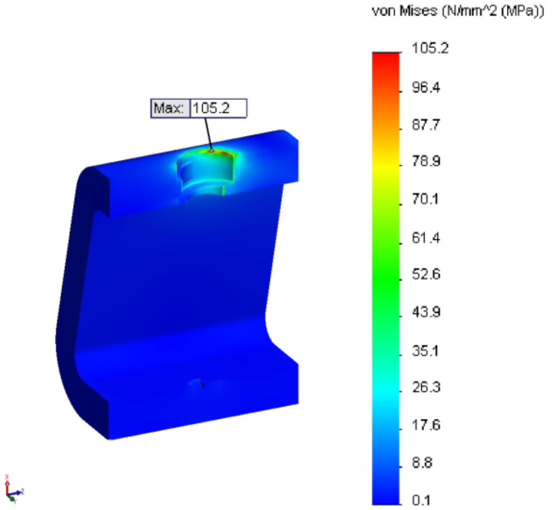

Obr. 8 Rozloženie napätí v kortikálnej kosti pri bikortikálnom upevnení.

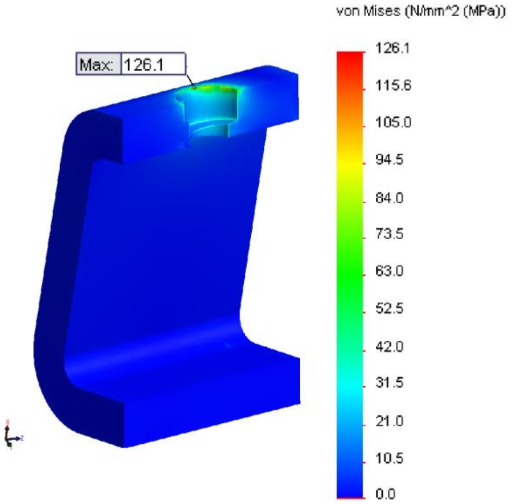

Obr. 9 Rozloženie napätí v kortikálnej kosti pri monokortikálnom upevnení.

Hodnoty maximálnych napätí v implantáte, kortikálnej a spongióznej kosti pre všetky študované prípady sú v tab. 2.Maximálne napätia v implantáte pri bikortikálnom upevnení sú menšie oproti monokortikálnemu, iba keď je krčok implantátu 1,5 mm nad povrchom a 0,5 mm pod povrchom kortikálnej kosti. U kortikálnej kosti sú napätia menšie pri bikortikálnom upevnení implantátu, ak zapustenie krčku implantátu je 0,5 mm pod povrch kortikálnej kosti. V prípade zapustenia krčku implantátu po okraj a 1,5 mm nad povrch kosti sú menšie napätia v kortikálnej kosti pri monokortikálnom upevnení implantátu. V spongióznej časti vznikajú napätia minimálne o rád nižšie, ako v kortikálnej kosti a implantáte, preto nie sú podstatné.

Tabuľka 2 Maximálne napätia v implantáte, kortikálnej a spongióznej kosti pre tri študované prípady vnorenia implantátu do kosti.

Bikortikálne upevnenie implantátu			
	Implantat σ_{max}[MPa]	Kortikalis σ_{max}[MPa]	Spongióza σ_{max}[MPa]
Implantát 0,5 mm pod povrch	168,6	105,2	8,2
Implantát 1,5 mm nad povrch	856,7	333,2	10,8
Situovanie závitu po okraj kosti	240,7	154,3	7
Monokortikálne upevnenie implantátu			
	Implantat σ_{max}[MPa]	Kortikalis σ_{max}[MPa]	Spongióza σ_{max}[MPa]
Implantát 0,5 mm podpovrch	170,1	126,1	7,7
Implantát 1,5 mm nad povrch	954,9	262,1	12,7
Situovanie závitu po okraj kosti	232,2	143,4	7,2

DISKUSIA

Tabuľka 2 v súlade s inými autormi [1] potvrdila, že vo väčšine prípadoch situovania implantátu v kortikálnej kosti pri použití monokortikálne uchyteného implantátu vznikajú menšie napätia, ako u bikortikálneho uchytenia implantátu. Nižšie napätia v kortikálnej kosti pri bikortikálnom uchytení boli zistené len pri miernom vnorení krčku implantátu 0,5 mm pod povrch kortikálnej kosti. Napätia namerané v implantáte boli pri bikortikálnom upevnení implantátu menšie v dvoch prípadoch, ale kritickou oblasťou pre porovnanie napätí nie je implantát ale kortikálna kosť. Z toho vyplýva, že napriek prvotným očakávaniam je z hľadiska maximálnych napätí v kortikálnej kosti vo väčšine študovaných prípadov vhodnejšie používať monokortikálne uchytenie implantátu.

ZÁVER

Rozdelenie napätí v implantáte a kosti ukazuje, že menšie napätia vznikajú v kortikálnej kosti pri použití implantátu zapusteného mierne pod povrch. Tento prípad zapustenia implantátu je vhodný používať pri monokortikálnom a bikortikálnom upevnení. Z hľadiska situovania závitu po okraj respektíve nad povrch je vhodnejšie používať monokortikálne upevnenie, pretože napätia sú menšie, ako u bikortikálneho upevnenia.

POĎAKOVANIE

Táto práca bola realizovaná s podporou projektov APVV-0520-10,VEGA 2/0108/11, NanoCEXmat II: ITMS No: 26220120035, NanoCEXmat I: ITMS No: 26220120019 a CEKSIM: ITMS No: 26220120056.

LITERATÚRA

[1] Himmlová, L., Goldmann, T., Kácovský, A.: Stability of bone bed crest of loaded implant - comparison with finite element models, Česká stomatologie 105 (3) 66-72 (2005).

[2] Himmlová, L., Dostálová, T., Kácovský, A., and Konvičková, S.:Influence of implant length and diameter on stress distribution: A finite element analysis,J. Prosthetic Dentistry, 91(1) 20-25 (2004).

[3] Dvořák, I., Hrubý, V., Kadlec, J., Pospíchal, M., Svoboda, E., Martikaň, A., Konečná, H., Sedlák, I.: Analýza zatížení kostní dřeně a kovového dentálniho implantátu, Akademia O.P.S Jún 2010, DIČ: CZ - 00216224.

ROZLIČNÉ INDENTAČNÉ PODMIENKY A ICH VPLYV NA HĹBKOVÉ PROFILY NANOTVRDOSTI TENKÝCH W-C POVLAKOV

DIFFERENT INDENTATION CONDITIONS AND THEIR INFLUENCE ON NANOHARDNESS DEPTH PROFILES OF THIN W-C COATINGS

Michal Novák[1,2], František Lofaj[1,2], Petra Hviščová[2]

[1] Slovenská technická univerzita v Bratislave, Materiálovotechnologická fakulta so sídlom v Trnave, Bottova 25, Trnava, Slovenská republika

[2]Slovenská akadémia vied, Ústav materiálového výskumu, Watsonova47, Košice, Slovenská republika

ABSTRACT

Nanohardness depth profiles from dynamic indentation analysis were studied with the aim to find the influence of different indentation parameters, such as loading/strain rate, sinus frequency and sinus amplitude on their shape and maximum nanohardness values. The experimental procedures were carried out using nanohardness tester G200 (Agilent Technologies) in dynamic CSM (Continuous stiffness measurement) mode. Firstly, series of single load indents in different penetration depths were carried out for obtaining reference nanohardness depth profile. Another series of experiments were performed using CSM mode and CSM mode upgraded for measurements of properties in thin films, respectively. The analyses were performed using different indentation conditions (sinus amplitude, frequency and strain rate). It was found out that the increase of strain rates causes apparent decrease of nanohardness values. Increase of sinus frequency causes the reduction of the maximum and widening of the corresponding plateau of nanohardness depth profile. In contrary, the increase of sinus amplitude causes the shift of the profile maximum to higher values.

Keywords: *nanoindentation, continuous stiffness measurement, frequency, amplitude, strain rate*

ÚVOD

Pri vývoji a aplikácii tenkých povlakov pre inžinierske aplikácie je kladený vysoký dôraz hlavne na ich odolnosť proti opotrebeniu, koróznu a oxidačnú odolnosť, ale aj tvrdosť a modul pružnosti. Pre meranie tvrdosti tenkých povlakov s hrúbkami v rozsahu stoviek nanometrov bola vyvinutá technika nanoindentácie, ktorá sa odlišuje od klasických metód merania tvrdosti, ktoré nemajú na takýchto tenkých vrstvách dostatočnú presnosť [1,2]. Prvú ucelenú teóriu o možnostiach merania tvrdosti veľmi tenkých vrstiev priniesli Dorner a Nix [2], ktorá viedla po dopracovaní Oliverom a Pharrom[3]k vzniku novej vedeckej oblasti – inštrumentovanej indentácie. V prípade merania tvrdosti tenkých povlakov na podložkách s odlišnou tvrdosťou metódami inštrumentovanejindentácie je kvôli oddeleniu vplyvu podložky vhodné používať dynamické indentačné skúšky, ktoré majú na maximálnu hodnotu záťaže ešte aplikovanú dodatočnú moduláciu so zadanou amplitúdou a frekvenciou [6]. Na rozdiel od indentácie s klasickým jednoduchým spôsobom zaťažovania je v tomto prípade z jedného merania získaný celkový hĺbkový profil tvrdosti a indentačného modulu [4-6]. Z hĺbkového profilu tvrdosti je možné oddeliť vplyv podložky na merané vlastnosti povlakov a určiť jeho skutočnú tvrdosť [6]. Základný priebeh zaťažovania sa robí dvomi rôznymi spôsobmi: s lineárnou rýchlosťou zaťažovania (linear loading rate – LLR), alebo v režime konštantnej rýchlosti deformácie (constant strain rate – CSR). Cieľom tejto štúdie je skúmať vplyv rozličných indentačných parametrov na vývoj hĺbkových profilov nanotvrdosti na tenkých povlakoch na báze W-C [7,8].

EXPERIMENTÁLNA ČASŤ

Výskum bol zameraný na vplyv režimu, rýchlosti zaťažovania/deformácie, amplitúdy a frekvencie počas dynamickej indentácie. Experimentálne meranie boli vykonané za použitia nanoindentora G200 od Agilent Technologies. Skúšky jednotlivých indentačných parametrov boli vykonané v troch rôznych režimoch zaťažovania, v statickom režime jednoduchej záťaže (single load

– SL) a v režimoch dynamickej indentácie (tzv. CSM – continuous stiffness measurement), resp. jeho špeciálneho režimu CSM určeného pre meranie tenkých povlakov [7]. Merania boli vykonané na tenkom povlaku na báze W-C pripraveného pomocou DC magnetrónového naprašovania na depozičnom zariadení Cryofox Discovery 500 (vzorka označená ako WC34) [8].Tabuľka 1 zobrazuje použité indentačné módy a popis jednotlivých experimentálnych parametrov.

Tabuľka 1. Podmienky indentačnej analýzy na vzorke WC34.

Indentačný režim	Parametre			
	Skratka	Rýchlosť	Amplitúda	Frekvencia
Single load	SL	1min. to max/1min. to min	-	-
CSM mode	CSM	0.01 – 0.2 s^{-1}	1 nm – 12 nm	10 – 80 Hz
CSM forthinfilms	CSM coatings	0.01 – 0.2 s^{-1}	1 nm – 12 nm	10 – 80 Hz

VÝSLEDKY A DISKUSIA

Referenčný hĺbkový profil nanotvrdosti bol získaný z analýzy v režime jednoduchého zaťažovania (single load - SL) zo série individuálnych vpichov v rôznych hĺbkach (od 20 nm do 900 nm). Meranie zo SL analýzy bolo následne overené meraním v dynamickom indentačnom režime (CSM a CSM pre tenké povlaky). Bolo zistené, že hodnoty tvrdosti, ako aj získané profily nanotvrdosti sa v rámci jednotlivých režimov odlišovali. V prípade analýzy v „single load“ boli namerané vyššie hodnoty nanotvrdosti v malých hĺbkach v porovnaní s obomi dynamickými režimami. V prípade analýzy v jednoduchom režime bol zaznamenaný aj vyšší rozptyl okolo strednej hodnoty nameranej nanotvrdosti. Namerané maximá sa však líšili aj v rámci jednotlivých sinusových režimov (obr.1). Bolo zistené, že použitie CSM režimu pre klasické materiály vykazuje mierne vyššie stredné hodnoty nanotvrdosti, ako to bolo v prípade CSM režimu upraveného pre tenké povlaky.

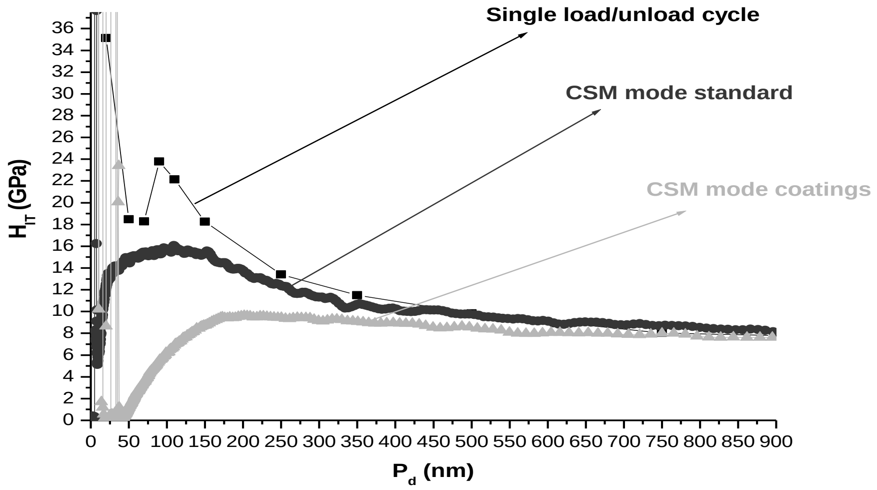

Obr. 1. Porovnanie hĺbkových profilov pri použití rôznych režimoch indentácie.

Obr. 2a znázorňujúci vplyv sinusovej amplitúdy preukázal, že so zvyšujúcou sa hĺbkovou amplitúdovou moduláciou dochádza k posunu hĺbkového profilu doprava a k umelému poklesu hodnôt nanotvrdosti. Bolo tiež zistené, že s narastajúcou amplitúdou dochádza k rozšíreniu plató profilu nanotvrdosti v oblasti zodpovedajúcej tvrdosti tenkého povlaku na mäkšej podložke. Vo väčších hĺbkach profily konvergovali k rovnakej hodnote, ktorá zodpovedá tvrdosti samotného podkladu. V prípade sledovania vplyvu sinusovej frekvencie bol zistený opačný priebeh vývoja profilov nanotvrdosti, ako to bolo v prípade amplitúdy. Závislosť vplyvu rýchlosti deformácie preukázala (obr.2b), že so zvyšujúcou sa rýchlosťou v rozsahu od 0.02 do 0.05 s-1 dochádzalo k poklesu nameraných maximálnych hodnôt nanotvrdosti a k umelému nárastu maximálnych hodnôt nanotvrdosti v prípade rýchlostí vyšších ako 0.07 s-1. V prípade nižších rýchlostí došlo aj k rozšíreniu plató na profiloch nanotvrdosti. V tomto prípade tiež bol pozorovaný výrazný rozptyl v hodnotách nanotvrdosti v oblastiach prislúchajúcich tvrdosti sklenej podložky.

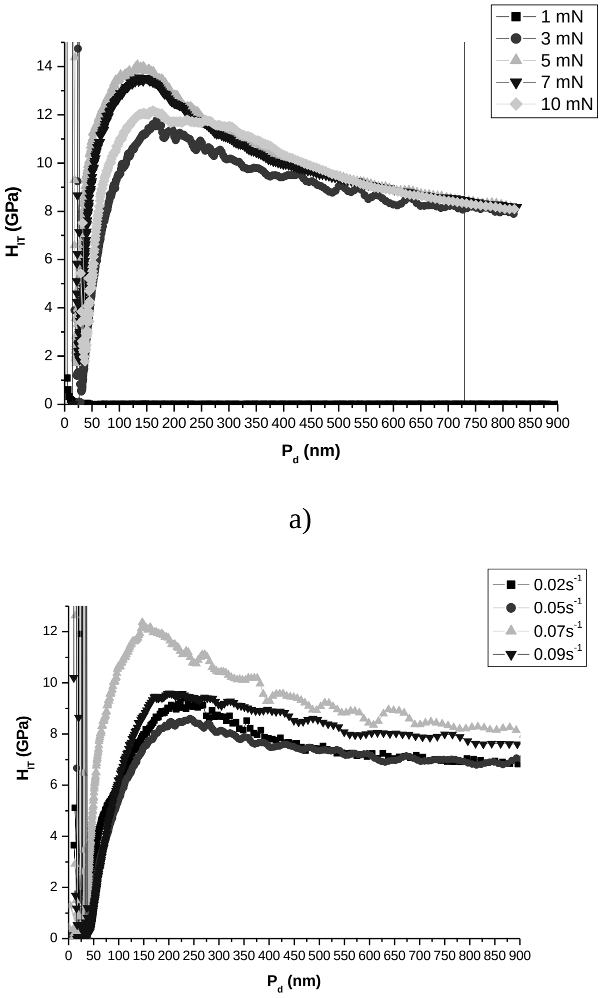

a)

b)

Obr. 2. Vplyv amplitúdy (a) a rýchlosti deformácie (b) na vývoj profilu nanotvrdosti v tenkom povlaku na báze W-C.

ZÁVER

Na základe pozorovania závislosti hĺbkových profilov tvrdosti pri rôznych módoch zaťažovania (jednoduchá záťaž, CSM a CSM pre tenké povlaky) boli zistené výrazné rozdiely. V prípade merania v dynamických režimoch sa maximálne hodnoty pohybovali v menších hĺbkach v nižších maximálnych hodnotách nanotvrdosti, ako v prípade hodnôt získaných z analýzy v režime jednoduchej záťaže. Analýza vplyvu frekvencie preukázala klesajúci trend v nameraných hodnotách nanotvrdosti s rozšírením plató v oblasti prislúchajúcej tvrdosti naneseného povlaku. Zvyšovanie sínusovej amplitúdy spôsobuje pokles nameraných hodnôt nanotvrdosti s postupným rozšírením a vyhladením plató v oblastiach zodpovedajúcim tvrdosti povlaku. Z meraní vplyvu rýchlosti deformácie bol pozorovaný mierny pokles nameraných maximálnych hodnôt nanotvrdosti: v prípade nízkych a stredných rýchlostí deformácie bolo pozorované rozšírenie oblasti plató prislúchajúceho nanotvrdosti povlaku. V prípade vyšších rýchlostí deformácie bol preukázaný opačný trend. Na základe uvedeného je pre meranie tenkých povlakov W-C typu odporúčaný sínusový (CSM) režim pre tenké filmy s rýchlosťou deformácie 0,05 s^{-1}, frekvenciou 45 Hz a amplitúdou 5 nm.

POĎAKOVANIE

Práca bola realizovaná za podpory projektov: NanoCEXmat II (ITMS č. 26220120035), NanoCEXmat I (ITMS č.26220120019) a CEKSIM(ITMS č. 26220120056), ktoré sú podporované z Operačného programu "Výskum a vývoj" financovaného prostredníctvom Európskeho regionálneho fondu pre podporu vývoja a projektov APVV č. 0520-10 a VEGA č. 2/0108/11.

LITERATÚRA

[1] PHARR,G.M., OLIVER, W.C. On the generality of the relationship among contact stiffness, contact area, and elastic modulus during indentation. J.Mater.Res.3, 1992, p.613 – 617.

[2] Available online :[cit. 2013-10-25] <http://www.perkinelmer.com/CMSResources/ Images/4474546GDE_IntroductionToDMA.pdf>

[3] Sinus mode guidelines, Information bulletin for manipulation with technical devices, CSM Instruments SA (Switzerland), 2010.

[4] Sinus mode equations, Sinus mode calculations principles. In CSM Instruments – online bulletin, CSM Instruments SA (Switzerland), 2010, p.18–20.

[5] HAY,J., AGEE,P., HERBERT,E. Continuous stiffness measurement during instrumented indentation testing. In Experimental techniques - Nanomechanical Characterization of Materials by Nanoindentation Series, 2010, p.86–94.

[6] XIAODONG,L., BHARAT,B. A review of nanoindentation continuous stiffness measurement technique and its applications In Materials Characterization vol.48, 2002, p.11–36.

[7] NOVÁK,M., LOFAJ,F., HVIŠČOVÁ,P. The influence of indentation conditions on nanohardness depth profiles of W-C based coatings In Local Mechanical Properties, 2013, In press.

[8] HVIŠČOVÁ, P., LOFAJ,F., NOVÁK,M. Nanohardness of CrN Coatings vs. Deposition Parameters In Local Mechanical Properties, 2013, In press.

MIKROŠTRUKTÚRA, MECHANICKÉ A FUNKČNÉ VLASTNOSTI A VYSOKOTEPLOTNÉ SPRÁVANIE Al_2O_3/SiC MIKRO/NANO KOMPOZITOV

MICROSTRUCTURE, MECHANICAL AND FUNCTIONAL PROPERTIES AND CREEP BEHAVIOR OF Al_2O_3/SiC MICRO/NANO COMPOSITES

Milan Parchovianský[1], *Dušan Galusek*[1], *Jaroslav Sedláček*[3], *Peter Švančárek*[1],

Monika Kašiarová[2], *Ján Dusza*[2], *Pavol Šajgalík*[3]

1Vitrum Laugaricio – Joint Glass Center of the IIC SAS, TnU AD, and FChFT STU,
Študentská 2, 911 50 Trenčín, Slovakia

2Institute of Materials Research, Slovak Academy of Sciences, Watsnova 47,
SK-043 53 Košice, Slovakia

3Institute of Inorganic Chemistry, Slovak Academy of Sciences, Dúbravská cesta 9,
SK-845 36, Bratislava, Slovakia

ABSTRACT

Al_2O_3/SiC micro/nano composites are much more resistant materials than monolithic alumina ceramics regarding some mechanical properties, functional properties and creep resistance. In this work the Al_2O_3/SiC micro/nano composites were fabricated by hot pressing at 1740 °C for 1h and 30 MPa in argon atmosphere. Various aspects of the hot pressed composites, including starting materials, microstructure, mechanical properties (hardness, fracture toughness, flexural strength), functional properties (thermal and electrical conductivity) and creep behaviour were studied. To clarify the role of particle size of SiC on the properties of composites two kinds of SiC powders with micron (200 nm) and nano-size (50 nm) were selected, together with the high purity Al_2O_3 powder with mean particle size of 150 nm. Different Al_2O_3/SiC compositions with SiC content in the range of 3 – 20 vol.% were prepared. The properties of the composites were compared to the monolithic Al_2O_3 reference. By XRD analysis only α-Al_2O_3 and β-SiC crystalline phases were detected before and after sintering. This is an important observation, because the persistence of the SiC phase in the final composite is necessary condition for the improvement of the mechanical and functional properties, and higher creep resistance of the Al_2O_3/SiC micro/nano composite. Significant attention was paid to investigation of the influence of the size of SiC nanoparticles (micro vs. nano) on the properties of composites prepared under identical conditions and containing equivalent volume fractions of the SiC particles. The flexural strength increased with increasing volume fraction of SiC particles. The maximum flexural strength (655 ± 90 MPa) was achieved for the composite containing 20 vol.% of micro SiC particles, which is more than twice as high as the strength of Al_2O_3 reference. Vickers hardness improved moderately, but the fracture toughness was lower when compared to the monolithic Al_2O_3. The observed improvement of mechanical properties (hardness, fracture strength) was mainly attributed to the refinement of the alumina matrix, grain boundary reinforcement, and the related change of fracture mode from intergranular in the alumina reference to transgranular in the composites. SEM analysis confirmed the transformation of fracture mode from intergranular in monolithic Al_2O_3 to transgranular in the composites. The creep behaviour at temperatures up to 1350 °C, and mechanical load of 200 MPa of the composites was also studied, and compared to the monolithic Al_2O_3 reference. The studied parameters include volume fraction, size, distribution of SiC particles, and the presence/absence of silica as the result of surface oxidation of SiC. To clarify the influence of silica, which is always present in the form of oxide layer at the surface of SiC particles, on creep resistance, the composites were also prepared from the SiC powder washed in HF in order to remove SiO_2 impurity. The Al_2O_3/SiC nanocomposites with 5 vol.% of SiO_2-free SiC, and with deliberate addition of 0.5, 1 and 5 wt.% of SiO_2 were also prepared. Tetraethylortosilicate was used as the source of SiO_2. However, the expected positive effect of SiO_2 removal on creep resistance of the composites was not confirmed. In the Al_2O_3/SiC nanocomposites the creep rate was influenced by the volume fraction of SiC particles and the size of alumina matrix grains. The creep resistance of Al_2O_3/SiC composites was significantly higher when compared to the creep resistance of the monolithic Al_2O_3. Particularly, the Al_2O_3/SiC nanocomposite with 10 vol.% of micro-SiC exhibited excellent creep resistance. The material was able to withstand the stress of 200 MPa at 1350 °C and 1400 °C for 150 h, while the monolithic Al_2O_3 reference failed already after 0.8 h at 75 MPa and 1350 °C. Long loading time before mechanical failure suggests diffusion controlled creep behaviour. The improvement of the creep resistance was attributed to pinning effect of the SiC particles at grain boundaries, which inhibited grain boundary sliding, and reduced the creep strain rate. Thermal and electrical conductivity were also modified in the composites, and increased with increasing volume fraction of SiC. The maximum value of thermal conductivity at room temperature was reached in the samples containing 20 vol.% of micro or nano SiC particles (38 W/m.K), while the value of the thermal conductivity of monolithic alumina was only 28 W/m.K. It was also found, that the thermal conductivity decreased with increasing temperature. This fact is most likely due to the fact that with increasing temperature increases the intensity oscillations of the crystal lattice, which then interact with the proliferation of phonons. The increasing of electrical conductivity by adding micro/nano SiC particles into Al_2O_3 matrix was more pronounced as in the case of thermal conductivity. Experimental results revealed that electrical conductivity increased with increasing volume fraction of SiC. The composite AS20c showed the highest value of electrical conductivity (4.05×10^{-2} S/m), whereas the electrical conductivity of monolithic Al_2O_3 was only 7.80×10^{-6} S/m. Concerning the Al_2O_3/SiC nanocomposites with the same volume fraction of SiC, but different particle size of SiC, no statistically significant deviation of electrical conductivity could be identified.

Keywords: *Al_2O_3/SiC micro/nano composites, mechanical properties, functional properties, creep*

ACKNOWLEDGMENT

The financial support of this work by the APVV grant LPP 0297-09 and the SAS-NSC-2010-02 Joint research bilateral project is gratefully acknowledged. This publication was created in the frame of the project "Centre of excellence for ceramics, glass, and silicate materials" ITMS code 262 201 20056, based on the Operational Program Research and Development funded from the European Regional Development Fund.

PHOTOLUMINISCENCE PROPERTIES OF $(ZnO)_{X-Z}(SiO_2)_Y:(MnO)_Z$ PREPARED BY DIRECT THERMAL SYNTHESIS

FOTOLUMUNISCENČNÉ VLASTNOSTI $(ZnO)_{X-Z}(SiO_2)_Y:(MnO)_Z$ PRIPRAVENÉHO PRIAMOU VYSOKOTEPLOTNOU SYNTÉZOU

Peter Švančárek, Robert Klement and Dušan Galusek

Vitrum Laugaricio - Joint Glass Center of the IIC SAS, TnUAD, and FChPT STU, 911 50 Trenčín, Slovak Republic

ABSTRACT

Willemite based compounds were prepared by thermal synthesis from mixed powders with different ratios of ZnO, SiO_2 and with addition of MnO_2 as optically active dopant. Using coarse grained, precipitated SiO_2 resulted in a heterogeneous product where unreacted SiO_2 was detected. Nevertheless strong photoluminescence in green (523nm) region of electromagnetic spectra was detected. The strongest excitation peak was observed at 277 nm and is attributed to the charge transfer transition of the Mn^{2+} ions.

Keywords: *willemite, Mn^{2+}-dopant, green emission, photoluminescence*

INTRODUCTION

High efficiency of light sources depends on high quantum efficiency of the phosphor. Willemite based manganese doped phosphor ($Zn_2SiO_4:Mn^{2+}$) is used due to its properties for longer than 180 years. Its chemical and thermal stability plays also important role why this phosphor is often selected as a phosphor of choice. X-Ray, UV light or electron irradiation are used as energy carriers to charge willemite crystal lattice, and Mn^{2+} ions, which are incorporated into the lattice as a substitute for small fraction of Zn^{2+} ions are used as photoluminescence activator for the green phosphor. They are widely used in plasma display panels, cathode ray tubes, oscilloscopes and fluorescent lamps [1].

Phosphors are prepared by various methods:

For preparation of thin films, laser deposition [2], spray pyrolysis [3] and dip-coating [4, 5] of the material intended as a carrier of the photoluminescent film, are used. Low temperature hydrothermal synthesis from aqueous solution at temperatures as low as 230 °C [6-8] is also possible, although the photoluminescence efficiency without further annealing is rather poor (about 11% of similar commercial photoluminescent [7]). Low luminescence efficiency was attributed to short crystal formation times [9].

For preparation of bulk fluorescent materials, sol-gel techniques [10, 11] and direct thermal synthesis [1, 11] are used. High temperature (1000 - 1400 °C) is often required to obtain ordered willemite structure even in the case when the phosphor is prepared by sol-gel methods or hydrothermal synthesis.

In order to improve the emission characteristics of current willemite based phosphors, compositional variations of ZnO, SiO_2 and MnO_2 were examined. According to literature, MnO_2 is reduced to MnO at temperatures higher than 1000°C, regardless of the furnace atmosphere [11]. This is important because the light emission occurs due to non-radiative energy transfer from the host lattice of Zn_2SiO_4 through formation of electron-hole pairs, which recombine at the luminescent centers (Mn^{2+}) and give visible luminescence [1]. In the present paper we report on the preparation and luminescence properties of Mn^{2+} doped zinc silicate as a green light emitting phosphors.

EXPERIMENTAL

Three sets of luminescent materials were prepared by mixing and annealing the powders of ZnO, SiO_2 and MnO_2 at the compositions corresponding to $Zn_{2-x}SiO_4$ - $xMnO_2$, $Zn_{1-x}SiO_3$ - $xMnO_2$, and $Zn_{1-x}Si_2O_5$ - $xMnO_2$, where $x = 0.01$, 0.03 and 0.05. All chemicals used were of analytical grade. The coarse grained SiO_2 (AFT – Bratislava, precipitated) and fine grained powders of ZnO (AFT – Bratislava, 99.5 %, average grain size 300 nm) and MnO_2 (ACROS ORGANICS, 99 %, average grain size 1 μm) were milled and homogenized together in vibratory mill for 30 minutes. Obtained mixture of fine powders was calcined at 1300°C for 2 h in air. After calcination second milling (and homogenization) took place to obtain fine powder of average grain size about 10 μm. For the SEM analysis (JEOL JSM-7600 Thermal FE SEM) the powder was cast into phenolic conductive compound and polished by diamond polishing disc. Both the emission and excitation fluorescence spectra were measured by Fluorolog 3 (FL3-21, Horiba) fluorescence spectrometer. The phase composition was determined using powder X-ray diffraction (PANalytical Empyrean Series 2 X-ray diffractometer).

RESULTS AND DISCUSSION

The SEM examination of the powder revealed that even after 2 hours of annealing the solid state reaction was not completed and chemically and structurally homogenous powder was not formed (Fig.1).

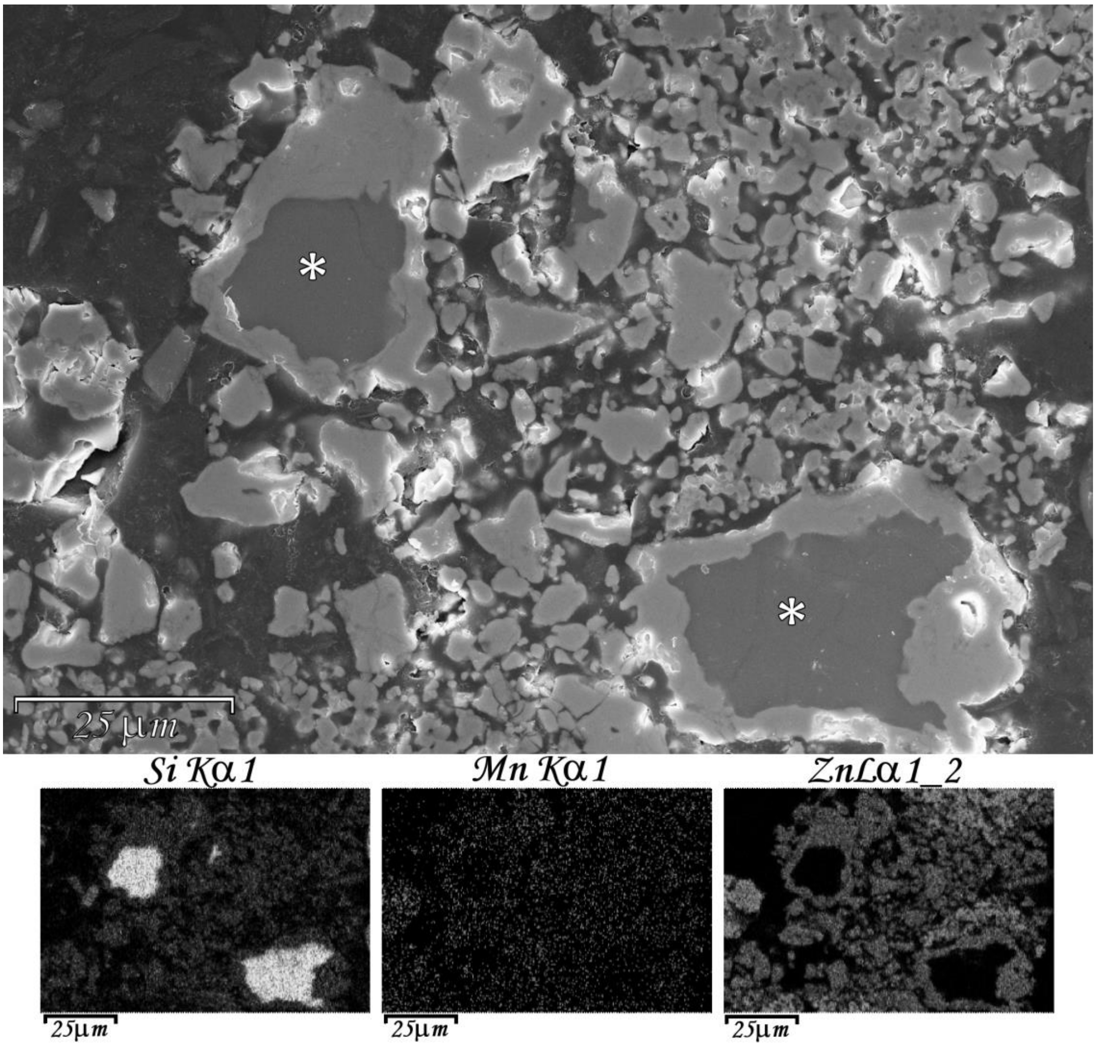

Fig. 1. Map of elements in Zn_2SiO_4 : 5at% Mn^{2+}. * Unreacted SiO_2 core of large silica particles.

Larger particles contained a core of pure SiO_2 surrounded by rim containing SiO_2, ZnO and MnO_2. For completion of the diffusion process longer time of annealing will be needed, because higher annealing temperatures would lead to undesirable melting of the system. Irrespective of the composition, the X-ray powder diffraction patterns show the presence of willemite (Zn_2SiO_4) as a major phase, unreacted ZnO, and traces of SiO_2.

The excitation and emission spectra of all Mn^{2+}-doped phosphors were similar. Figure 2 shows the excitation and emission spectra of $Zn_{1.97}Mn_{0.03}SiO_4$ (λ_{em} = 523 nm, λ_{exc} = 277 nm). The strongest excitation peak was observed at 277 nm and is attributed to the charge transfer transition of the Mn^{2+} ions. Under sample excitation at 277 nm intense broadband emission at 523 nm was observed, which is due to a *d*-level spin-forbidden transition of Mn^{2+} ion ($^4T_{1g}$ - $^6A_{1g}$). The mechanism involved in the generation of a green emission from $Zn_2SiO_4:Mn^{2+}$ under UV excitation is well understood, and can be described as follows [**Error! Bookmark not defined.**]: the electron from the Mn^{2+} ground state $^6A_{1g}$ is excited to the conduction band (CB) of willemite by UV photons, and the free electrons in the CB can relax to the $^4T_{1g}$ excited state of Mn^{2+} through non-radiative processes, which is then followed by radiative transitions from the $^4T_{1g}$ excited state to the $^6A_{1g}$ ground state giving green emission. The emission intensities for all studied phosphors are depicted in Fig. 3.

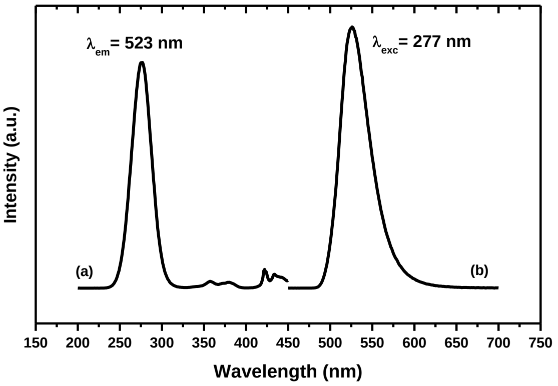

Fig. 2. Excitation and emission spectra of $Zn_{1.97}Mn_{0.03}SiO_4$ (λ_{em} = 523 nm, λ_{exc} = 277 nm).

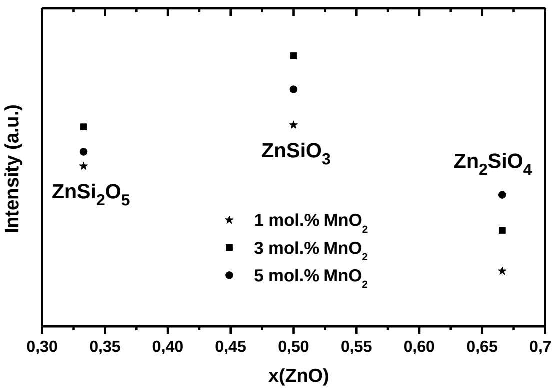

Fig. 3. Corrected emission intensities of studied phosphors at λ_{exc} = 277 nm.

The highest emission intensity was found for the phosphor of starting composition of $ZnSiO_3:Mn^{2+}$. The concentration quenching effect, which often occurs in the $ZnSiO_3:Mn^{2+}$ and $ZnSi_2O_5:Mn^{2+}$ phosphors, was not observed in the $Zn_2SiO_4:Mn^{2+}$ system in given Mn^{2+} concentration range.

ACKNOWLEDGEMENTS

The financial support of this work by the bilateral project (Slovakia–Taiwan) SAS-NSC JRP 2012/14 is gratefully acknowledged. This work was carried out in the frame of the project „Centre of Excellence for Ceramics, Glass and Silicate Materials“, ITMS code 262 201 20056, based on the Operational Program Research and Development funded from the European Regional Development Fund.

REFERENCES

[1] Y. Hao, Y. Wang: Luminescent properties of Zn_2SiO_4 :Mn^{2+} phosphors under UV, VUV and CR excitation, Journal of luminescence 122-123 (2007) 1006-1008.

[2] P. Thiyagarajan, M. Kottaisamy, M.S. Ramachandra Rao: Structural and luminescence properties of pulsed laser deposited green-emitting Zn_2SiO_4:Mn phosphor thin films, Scripta Materialia, Volume 57, Issue 5, (2007) 433-436

[3] Y. C. Kang, S. B. Park: Zn_2SiO_4:Mn phosphor particles prepared by spray pyrolysis using a filter expansion aerosol generator, Original Research Article Materials Research Bulletin, Volume 35, Issue 7, (2000) 1143-1151

[4] J. Lin, D. U. Sänger, M. Mennig, K. Bärner: Sol–gel synthesis and characterization of Zn_2SiO_4:Mn phosphor films, Materials Science and Engineering B64 (1999) 73–78

[5] R. Selomulya, S. Ski, K. Pita, C.H. Kam, Q.Y. Zhang, S. Buddhudu: Luminescence properties of $Zn_2SiO_4:Mn^{2+}$thin-films by a sol-gel process, Materials Science and Engineering B100 (2003) 136-141

[6] T. J. Lou, J. H. Zeng, X. D. Lou, H. L. Fu, Ye Feng Wang, Rui Li Ma, Lin Jian Tong, Ya Li Chen: A facile synthesis to Zn_2SiO_4:Mn^{2+} phosphor with controllable size and morphology at low temperature, Journal of Colloid and Interface Science 314 (2007) 510–513

[7] S. W. Lu, T. Copeland, B. I. Lee, W. Tong, B. K. Wagner, W. Park, F. Zhang: Synthesis and luminescent properties of Mn^{2+} doped Zn_2SiO_4 phosphors by a hydrothermal method, Journal of Physics and Chemistry of Solids 62 (2001) 777-781

[8] H. Wang, Y. Ma, G. Yi, D. Chen: Synthesis of Mn-doped Zn_2SiO_4 rodlike nanoparticles through hydrothermal method, Materials Chemistry and Physics 82 (2003) 414–418

[9] M. Takesue, H. Hayashi, R. L. Smith Jr., Thermal and chemical methods for producing zinc silicate (willemite): A review, Progress in Crystal Growth and Characterization of Materials 55 (2009) 98-124

[10] T. H. Cho, H. J. Chang: Preparation and characterizations of Zn_2SiO_4:Mn green phosphors, Ceramics International 29 (2003) 611–618

[11] C. C. Diao, C. F. Yang: Synthesis of high efficiency Zn_2SiO_4 :Mn^{2+} green phosphors using nanoparticles, Ceramics International 36 (2010) 1653-1657.

PRÍPRAVA OBRÁBATEĽNÝCH KOMPOZITOV NA BÁZE Si_3N_4 S PRÍDAVKOM POLYMÉRNYCH PREKURZOROV AKO SPEKACÍCH PRÍSAD

PREPARATION OF MACHINABLE SILICON NITRIDE-BASED COMPOSITES WITH PRECERAMIC POLYMERS AS SINTERING ADDITIVES

Michal Vetrecin, Zoltán Lenčéš, Pavol Šajgalík

Institute of Inorganic Chemistry, Slovak Academy of Sciences, Dúbravská cesta 9, 84536 Bratislava, Slovakia

ABSTRACT

Conventional sintering additives (MgO, Al_2O_3, Y_2O_3) used for the preparation of Si_3N_4-based ceramic materials by pressureless sintering or hot-pressing were replaced in this work by SiAlOC polymer precursors. The green bodies were prepared by uniaxial pressing and/or cold isostatic pressing (CIP) from three kinds of powder compositions with the addition of 23.3, 30 and 40 wt.% of SiAlOC to the Si_3N_4 matrix. Samples were crosslinked and/or pyrolysed in quartz tube furnace to 1100 °C with a controlled flowing atmosphere of argon. The machinability test shown us that it is easier to machine crosslinked samples as pyrolyzed and samples prepared by mixed pressing method shown us best machinability. The machined samples were pressureless sintered at 1750 °C for 1 hour in mixed atmosphere of nitrogen and carbon monooxide. The sintered samples were characterized in terms of density, phase composition and microstructure.

Key words: *silicon nitride, machinability, SiAlOC, SiAlON*

ÚVOD

Keramické kompozity nitridu kremičitého majú nízku hustotu a tepelnú rozťažnosť v porovnaní s kovmi, majú aj vysokú pevnosť a odolnosť voči tepelným šokom. Tieto kompozity sa pripravujú hutné (napr. rezné nástroje na obrábanie kovov) ako aj pórovité materiály (filtre plynov alebo kvapalín). Vo väčšine prípadov sú pripravované spekaním v prítomnosti kvapalnej fázy, ktorá vzniká v procese zhutňovania. Kvapalná fáza je obyčajne tvorená eutektickou taveninou ktorá vzniká z oxidu kramičitého (hlavná nečistota vo východiskovom Si_3N_4 prášku) a z iného oxidu použitého ako prídavok spekania.

V predloženej práci sme nahradili konvenčne používané prídavky spekamnia (MgO, Al_2O_3, Y_2O_3) polymérnymi spekacími polymérmi, ktoré pri teplotách nad 1000 °C vytvárajú kvapalnú fázu, ktorá podobne ako konvenčné spekacie prísady urýchľujú spekanie. Podľa druhu použitých polymérnych prekurzorov môžeme ovplyvňovať chemické zloženie na hranici zŕn počas procesu zhutnenia a tak ovplyvniť nielen výsledné vlastnosti materiálu, ale aj jeho vlastnosti v procese ich polymerizácie prekurzorov.

Pre prípravu kompozitov nitridu kremičitého bol použitý hliníkom modifikovaný SiOC polymérny prekurzor s cieľom urýchliť proces spekania a modifikovať chemické zloženie na hranici zŕn. Výhodou tohto postupu je nielen potenciálne zníženie teploty spekania, ale predovšetkým fakt, že po zosieťovaní polyméru na hraniciach zŕn je možné pripraviť teleso, ktoré má dostatočnú pevnosť a húževnatosť na mechanické opracovávanie. Týmto by bolo možné pripravovať keramické výrobky sústružením, bez významných nárokov na ich finálne opracovanie po spekaní.

EXPERIMENT

Na prípravu kompozitov nitridu kremičitého bol použitý prášok nidridu kremičitého (SN-E10, UBE Industries, Ltd., Tokyo, Japan) s veľkosťou zŕn 0,5 μm a vysokým obsahom α fázy (α pomer > 95 %). Ako spekacia prísada bol použitý SiAlOC polyméry prekurzor. Tento polyméry prekurzor bol pripravený modifikáciou polymetylsilsesquioxánu (Wacker-Belsil™ PMS, MK;$(CH_3\text{–}SiO_{3/2})_x$) Alumatránom ($Al(OCH_2CH_2)_3N$) s obsahom 23,6 hm.%. MK polymér a Alumatrán boli rozpustené v izopropanele, zmiešané a miešané 12 hodín za vzniku gélu, ktorý sa po odparení izopropanolu sušil pri izbovej teplote 48 hodín. Vysušený SiAlOC bol mletý v planetovom mlyne PM100 30 minút. Pripravili sa 3 zmesy nitridu kremičitého a SiAlOC s 23, 30 a 40 hm.% obsahom polymerného prekurzoru (tabuľka 1).

Tabuľka 1 Obsah SiAlOC v zmesi SND23, SND30 a SND40.

	SiAlOC [hm. %]	SiAlOC [obj. %]
SND23	23	51.5
SND30	30	60.0
SND40	40	70

Z týchto zmesí boli pripravené výlisky jednoosovým lisovaním (UC), izostatickým lisovaním (CIP) a použitím oboch lisovacích metód (UC). Tieto výlisky boli tepelne upravené pri teplotách 300, 500 a 1100 °C v rúrovej peci v atmosfére argónu. Cieľom bolo zistiť ich vlastnosti v procese polymerizácie a možnosti ich opracovania.

Tabuľka 2 Zobrazenie voriek po jednotlivých krokov tepelného spracovania 300, 500 a 1100 °C a následnom mechanickom opracovaní jednotlivých vzoriek.

SND23 SND30 SND40		***SND23 SND30 SND40***
	*UC* *300 °C*	
	UC *500 °C*	
	UC *1100 °C*	

Takto tepelne upravené výlisky boli mechanicky opracované na sústruhu. Po mechanickom opracovaní boli vzorky beztlakovo spekané pri teplote 1750 °C 1 hodinu v zmiešanej atmosfére dusíka a oxidu uhoľnatého. U spekaných vzoriek bola meraná hustota archimedovou metódou a sledovaná mikroštruktúra na polaziročnom a elektrónovom mikroskope (SEM).

Graf 1 Hustota SND23, SND30 a SND40 podľa použitej metódy lysovania.

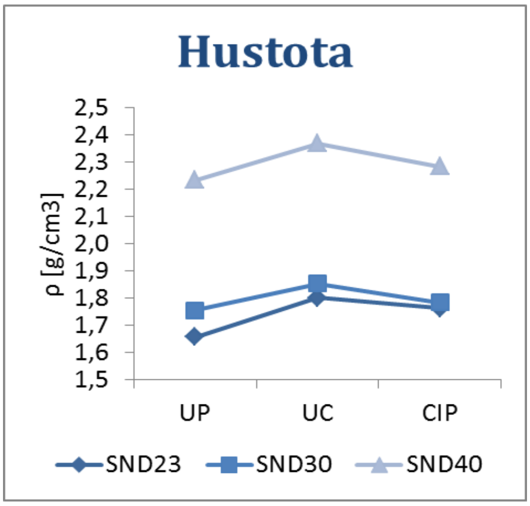

ZÁVER

Najľahšie opracovateľné vzorky boli s obsahom 30 hm.% polymérneho prekurzoru. Pri nižšom obsahu spekacej prísady dochádza k nedostatočnému spevneniu a nižšiemu obsahu polymérnej sieťe, ktorá drží zrná Si_3N_4 pohromade po tepelnej úprave do 1100 °C a pri mechanickom opracovaní dochádza k odštepovaniu kusov vzorky (tabuľka 2), prípadne k poškodeniu v držiaku sústruhu. Vzorky s vyšším obsahom polymérneho prekurzoru vytvárajú polymérnu sieť s vyššou pevnosťou a mechanické opracovanie s oceľovými nožmi je náročnejšie pri použití rovnakého tlaku, prípadne dochádza k odštepovaniu kusov zo vzorky (tabuľka 2). Všetky vzorky boli dobre opracovateľné po šiastočnom alebo úplnom zosieťovaní (300 až 500 °C), po úplnej pyrolýže je vytvorená polymérna amorfná siešť a vo všetkých prípadoch dochádza k odštepovaniu kusov vzorky. Pri použití nízkeho obsahu polymérneho prekurzoru, do 30 hm.%, je možné pripraviť mechanicky opracovateľné produkty s otvorenou pórovitosťou (viac ako 90% z celkovej pórovitosti). Veľkosť pórov sa pohybuje do 20 µm. Vzorky s vyšším obsahom polymérneho prekurzoru, 40 hm.%, počas pyrolýzy majú vyššiu tenteciu praskať v dôsledku nižšej otvorenej pôrovitosťi. Počas spekania vytvárajú viac kvapalnej fázy a dochádza k väčšiemu zmrašteniu a zhutneniu, čím sa dosiahne omnoho vyššia hustota (graf x) v porovnaní so vzorkami s nižším obsahom polymérneho prekurzoru. Počas spekania dochádzalo k minimálnemu rastu zŕn s prevažnou veľkosťou do 500 nm, čo bolo dokázané zo zábarov pomocou skenovacej elektrónovej mikroskopie (SEM, obr. 1).

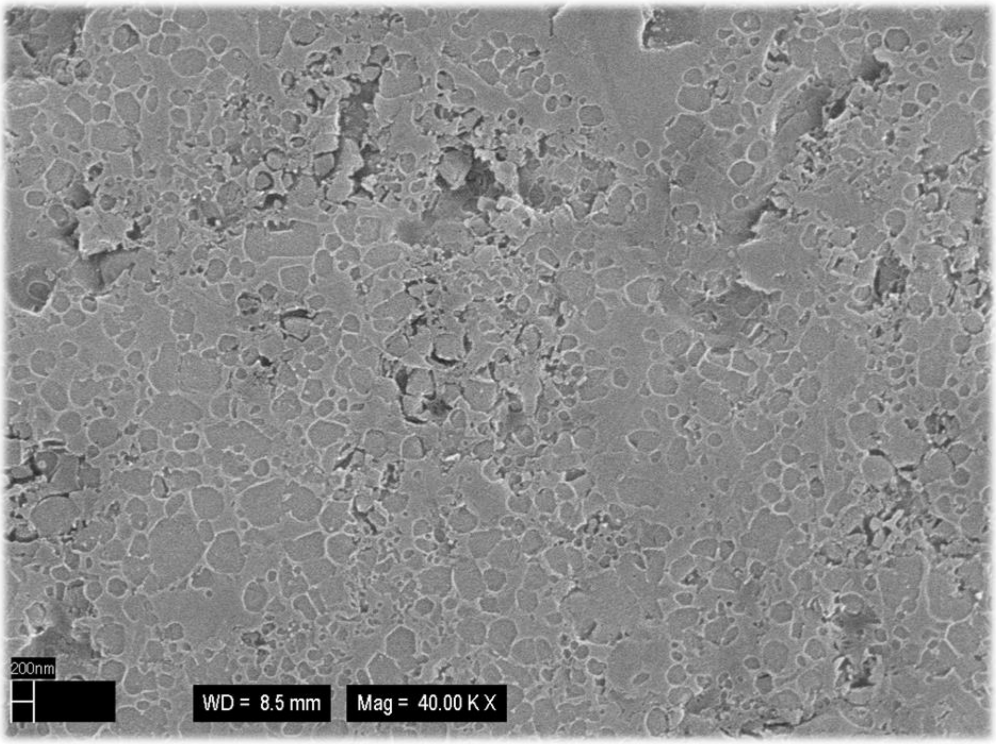

Obr. 1 Mikroštruktúra voľne spekaného jednoosovo lysovaného a cipovaného SND40.

POĎAKOVANIE

Táto práca bola podporovaná DAAD projektom s číslom 50725208 a Kompetenčným centrom pre nové materiály, pokročilé technológie a energetiku (ITMS 26240220073).

MIKROŠTRUKTÚRA A MECHANICKÉ VLASTNOSTI BIOMATERIÁLOV NA BÁZE NITRIDU KREMIČITÉHO

MICROSTRUCTURE AND MECHANICAL PROPERTIES OF SILICON NITRIDE BASED BIOMATERIALS

Zuzana Vilčeková[a], *Monika Kašiarová*[a], *Magdaléna Domanická*[b], *Pavol Šajgalík*[b]

[a]*Institute of materials research, SAS, 47 Watsonova, 040 01 Košice, Slovakia*
[b]*Institute of inorganic chemistry, SAS, 9 Dúbravská cesta, 845 36 Bratislava, Slovakia*

ABSTRACT

Microstructure and mechanical properties, particularly Young's modulus, hardness and compressive strength of silicon nitride based biomaterials were studied in this work. Silicon nitride samples were prepared using polyurethane foam replication method to obtain appropriate cellular structure for bio-application. This method is based on infiltration of silicon nitride slurry into the polyurethane sponge. The aim of this work is to present different ways for the preparation of these materials and study their mechanical properties. Measurements of hardness and Young's modulus were performed using instrumented indentation with Berkovich diamond indenter. Two types of the polyurethane foams were used with average pore size 0.48 mm and 0.62 mm. The effects both of structures, temperature of pre-sintering, volume fraction of Si_3N_4 powder and number of the infiltrations on the local mechanical properties were investigated and compared with human trabecular bone.

Keywords: *silicon nitride, biomaterials, polyurethane foam, human trabecular bone*

ÚVOD

Biomateriály patria medzi materiály, ktoré sú vďaka svojim netoxickým a biokompatibilným vlastnostiam určené najmä pre použitie v ľudskom tele. Dodnes ešte nebol vyvinutý dokonalý kostný implantát, ktorý by svojimi vlastnosťami zodpovedal vlastnostiam ľudskej kosti. Všetky existujúce biomateriály, používané ako kostné náhrady, majú tendenciu v priebehu času sa opotrebovávať alebo uvoľňovať. Ako sa predlžuje dĺžka života, tak sa zvyšuje aj počet nevyhnutných revíznych operácií. Interakcie medzi implantovaným umelým materiálom a živými tkanivami v organizme sú veľmi zložité a menia sa v závislosti od druhu použitého materiálu a rovnako od druhu cieľového tkaniva v tele. Aj napriek tomu, že princípy procesov, ktoré sa odohrávajú na rozhraní biomateriálu a tkaniva sú známe, podrobnosti a detaily sú ešte stále do istej miery nejasné [1].

Keramické materiály ako Si_3N_4 sa vyznačujú veľmi dobrými mechanickými vlastnosťami, čo im umožňuje využitie v rôznych multifunkčných aplikáciách. Nitrid kremičitý má nízku hustotu a s ňou súvisiacu hmotnosť, vysokú tvrdosť a pevnosť, má výbornú odolnosť proti korózii a tepelným šokom a v porovnaní s hydroxyapatitom má aj vyššiu lomovú húževnatosť. Si_3N_4 sa taktiež vyznačuje dobrou oteruvzdornosťou a necytotoxicitou, z čoho vyplýva aj jeho bioinertnosť. Vďaka týmto výborným vlastnostiam môže mať nitrid kremičitý široké využitie v bioaplikáciách, napríklad na výrobu umelých náhrad kostí, zubných implantátov alebo biocementov [2, 3].

Hlavným cieľom tejto práce bola príprava a charakterizácia vhodného pórovitého biomateriálu na báze nitridu kremičitého, ktorý by sa svojimi vlastnosťami čo najviac podobal ľudskej trabekulárnej kosti a následne ho využiť v bioaplikáciach, napr. ako umelé náhrady kostí.

EXPERIMENT

Experimentálny materiál bol pripravený replikačnou metódou v ÚACh SAV, Bratislava. Táto metóda je založená na infiltrácii suspenzie Si_3N_4 do polyuretánovej (PU) špongie, pričom boli použité dva typy PU špongií so strednou veľkosťou pórov 0,48 mm a 0,62 mm. Vzorky s označením 1 boli pripravené infiltráciou suspenzie s obsahom 40 obj.% Si_3N_4 do PU špongie, následne bola špongia vypálená pri 600°C a vzorky boli predspekané pri teplote 1000°C po dobu 30 minút. Po kalcinácii boli znova infiltrované suspenziou s obsahom 15 obj.% Si_3N_4 a 5 hm.% SiO_2 a spekané pri teplote 1200°C v ochrannej dusíkovej atmosfére. Vzorky s označením 2 boli pripravené rovnakým postupom ako vzorky s označením 1, avšak boli predspekané pri teplote 1100°C počas 1 hodiny. Vzorky s označením 3 boli pripravené rovnakým spôsobom ako vzorky s označením 2, s tým rozdielom, že suspenzia použitá pri druhej infiltrácii obsahovala 25 obj.% Si_3N_4 a 5 hm.% SiO_2. Vzorky označené 2i boli infiltrované dvakrát a vzorky označené 3i boli infiltrované trikrát. Označenia 48 a 62 symbolizujú veľkosť pórov v použitých polyuretánových penách.

Vzorky mali tvar kvádra s rozmermi 50x20x15 mm^3. K dispozícii bolo aj niekoľko vzoriek ľudskej trabekulárnej kosti s rozmermi 10x10x20 mm^3. Všetky študované vzorky boli brúsené a leštené použitím SiC papierov so zrnitosťou 500, 800, 1200, 2500 a vody. Príklady mikroštruktúr študovaných vzoriek sú uvedené na obr. 1.

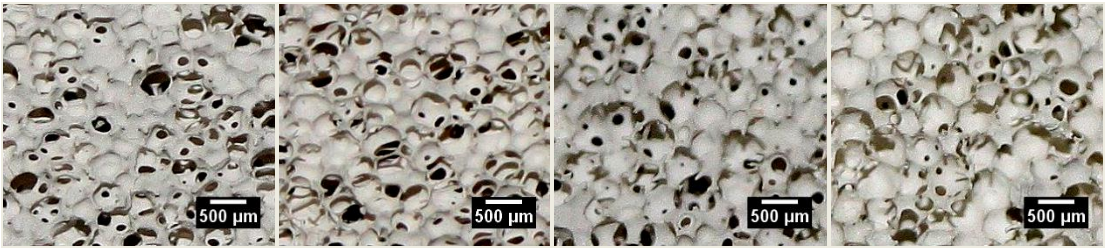

Obr. 1. Charakteristické mikroštruktúry študovaných vzoriek.

Na meranie mechanických vlastností boli použité inštrumentovaná indentácia a skúška v tlaku. Nanoindentáciou bol nameraný modul pružnosti a tvrdosť vzoriek. Merania boli uskutočnené na mikronanotvrdomeri G200 od firmy Agilent Technologies. Z meraní boli získané typické zaťažujúco-odľahčujúce krivky, z ktorých boli metódou Olivera&Phara [4] vypočítané hodnoty tvrdostí a modulov pružnosti. Pri meraniach bol použitý Berkovichov diamantový indentor, maximálna zaťažujúca sila bola 100 mN, rýchlosť zaťažovania a odľahčovania bola 200 mN/min a výdrž v maximálnom zaťažení bola 10s, aby sa zamedzilo vzniku visko-elastického toku, ktorý sa vyskytuje pri nanoindentácii kostí. Testom v tlaku boli namerané hodnoty pevností jednotlivých vzoriek. Merania boli uskutočnené na prístroji od firmy LLOYD Instruments. Posuv priečnika v priebehu meraní bol 1 mm/min a vzorky mali rozmery 10x10x15 mm^3. Výsledky nameraných hodnôt sú uvedené v tabuľke 1.

Tabuľka 1. Mechanické vlastnosti študovaných vzoriek.

Vzorky	Tvrdosť (GPa)	Modul pružnosti (GPa)	Pevnosť v tlaku (MPa)
kosť	0,59 ± 0,08	14,5 ± 0,85	4,87 ± 1,31
1-3i-48	0,58 ± 0,13	12,0 ± 2,23	1,07 ± 0,13
2-3i-48	1,30 ± 0,24	18,2 ± 4,09	1,27 ± 0,15
1-3i-62	0,77 ± 0,30	16,2 ± 3,88	0,81 ± 0,43
2-3i-62	0,90 ± 0,29	18,8 ± 4,09	1,05 ± 0,24
3-3i-62	1,15 ± 0,13	21,8 ± 1,35	2,09 ± 0,42
2-2i-48	0,40 ± 0,09	11,7 ± 1,80	0,25 ± 0,09
1-2i-62	0,75 ± 0,14	14,6 ± 2,57	0,49 ± 0,16
2-2i-62	0,85 ± 0,46	15,3 ± 4,62	0,82 ± 0,20
3-2i-62	1,47 ± 0,21	25,2 ± 2,43	0,97 ± 0,24

ZÁVER

Z nameraných výsledkov je možné usúdiť, že s nárastom teploty predspekania sa zvyšuje tvrdosť, modul pružnosti a rovnako aj pevnosť študovaných vzoriek. Hodnoty rastú aj so zvýšením obj.% Si_3N_4 po dvojnásobnej a trojnásobnej infiltrácii. Výsledky taktiež ukázali, že PU špongia s veľkosťou pórov 0,48 mm má lepšie mechanické vlastnosti ako špongia s 0,62 mm pórmi a že viacnásobná infiltrácia zvyšuje hodnoty meraných mechanických vlastností. Na záver možno zhodnotiť, že na prípravu vzoriek je vhodnejšia polyuretánová pena s 0,48 mm pórmi, trojitá infiltrácia a teplota predspekania 1100°C. Ďalej možno skonštatovať, že 40% obsah Si_3N_4 a 5% prídavok SiO_2 do suspenzie je postačujúci, nakoľko so zvyšujúcim obsahom tuhej frakcie v suspenzii sa zhoršujú výsledné mechanické vlastnosti pórovitých keramických materiálov.

POĎAKOVANIE

Táto práca bola realizovaná s podporou projektov APVV-0500-10, NanoCEXmat II: ITMS No: 26220120035, NanoCEXmat I: ITMS No: 26220120019 a CEKSIM: ITMS No: 26220120056.

LITERATÚRA

[1] Muhonen, V.: Bone-Biomaterial Interface: The effects of surface modified NiTi shape memory alloy on bone cells and tissue, Acta Univ. Oul., D 974, (2008).
[2] Pánek, Z., Figusch, V., Haviar, M., Ličko, T., Šajgalík, P., Dusza, J.: Konštrukčná keramika, R&D Print, Bratislava (1992).
[3] Ebenstein, D. M., Pruitt, L. A.: Nanoindentation of biological materials, Nanotoday, 1, 26-33 (2006).
[4] Oliver, W. C., Pharr, G. M.: An improved technique for determining hardness and elastic modulus using load and displacement sensing indentation experiments, J. Mater. Res., 7, 1564-1583 (1992).

INDEX AUTOROV

ISBN 978-80-971499-4-9